



**HAL**  
open science

# Dynamics of Janus colloids interacting with giant lipid vesicles

Vaibhav Sharma

► **To cite this version:**

Vaibhav Sharma. Dynamics of Janus colloids interacting with giant lipid vesicles. Physics [physics]. Université de Strasbourg, 2021. English. NNT : 2021STRAE028 . tel-03664749

**HAL Id: tel-03664749**

**<https://theses.hal.science/tel-03664749>**

Submitted on 11 May 2022

**HAL** is a multi-disciplinary open access archive for the deposit and dissemination of scientific research documents, whether they are published or not. The documents may come from teaching and research institutions in France or abroad, or from public or private research centers.

L'archive ouverte pluridisciplinaire **HAL**, est destinée au dépôt et à la diffusion de documents scientifiques de niveau recherche, publiés ou non, émanant des établissements d'enseignement et de recherche français ou étrangers, des laboratoires publics ou privés.

## ÉCOLE DOCTORALE PHYSIQUE ET CHIMIE-PHYSIQUE INSTITUT CHARLES SADRON (ICS, UPR 22)

# THÈSE

 présentée par :

## Vaibhav SHARMA

soutenue le : 3<sup>rd</sup> December 2021

pour obtenir le grade de : **Docteur de l'université de Strasbourg**

Discipline/ Spécialité : Physics

### *Dynamics of Janus colloids interacting with Giant Lipid Vesicles*

**THÈSE dirigée par :**

**Dr. STOCCO Antonio**

**Dr. MARQUES Carlos**

Chargé de recherche, Université de Strasbourg

Directeur de recherche, Université de Strasbourg

**RAPPORTEURS :**

**Pr. DIMOVA Rumiana**

**Pr. BICKEL Thomas**

Professeur, Max Planck Institute of Colloids and Interfaces

Professeur, Université de Bordeaux

---

**AUTRES MEMBRES DU JURY :**

**Pr. CHARITAT Thierry**

**Dr. RAFAI Salima**

Professeur, Université de Strasbourg

Chargé de recherche, Université de Grenoble

To my Family and specially my little newpew.

## Acknowledgements

There are so many special individuals who had graciously lent their helping hand during my PhD journey. This period of my PhD has been the most valuable and educational time of my life and helped me being not only a better scientist but also a better person.

I would like to thank Antonio Stocco, my thesis supervisor for not only believing in me but also supporting me at every point. I still remember being interviewed for the position and since then I have only learned and admired Antonio's knowledge and his patience. I must also acknowledge his efforts and recommendations in making this project a reality and his insights in keeping me on the right path not only in the view of the experimental progress but taking the time and patience to explain me the details of the study.

Carlos Marques my co-supervisor, for the regular discussions and insight on every aspect of the subject. His contributions have been invaluable during the thesis. It was his insights and motivations that kept the momentum going during the PhD.

I would also like to extend my gratitude towards the whole MCUBE team, Fabrice Thalmann, our team lead and the person who introduced me to statistical physics in my masters, Pierre Muller for his invaluable suggestions and prompt correction on this manuscript, Marc Basler for his expertise on experimental system (and to buy me origin), Tatiana Schmatko and Andre Schroder for their support during the last three years and last but not the least Thierry Charitat not only for being the my Jury but also for all his help which started even during my masters phase. I would like express my appreciation and gratitude to Florent Fessler for his contribution to this manuscript



I would also like to thank Wiebke Drenckhan, and Manish Kaushal with whom it all started during my Masters phase and I learnt the actual meaning of working in a lab.

Due credit and my gratitude to the administrative staff of ICS specially Odile and Nadia, who were always patient, kind and helped me navigate through the french administrative system (no complains), and the University of Strasbourg that funded my research work.

My PhD doesn't just belong to me but also to a group of very special people and without their support this would not have been possible. First, my family, my mom and dad who sacrificed a lot for my education and have always supported my every decision good or bad. My elder brother, my best friend who has been with me every step guiding me and growing up with you were the moments I still cherish. My sister-in-law for who I have the utmost respect and of course my little nephew Kabeer.

Secondly, my friends, my super family away from home. I would have never been able to do it without all of you. Othmene Benazieb, and Eulalie Lafarge, sharing an office with you I couldn't have asked for anyone better. The time we spent in and outside of F141 would always remind me to smile and live life to the fullest. Anastasiia Shpiruk (o Bozhe), my partner in crime, these years have been crazy, couldn't have and wouldn't, spend it with anyone else. Fedir Demydiuk, Imen(e) Ben djemaa and Nicolas Capit and Jean Muller your help and wisdom can only be surpassed by your kindness and positivity, Thank you for the time we had spent with each other I will always cherish those moments. Geevarghese George and Siddharth Saraswati (the Indians in Kehl) who would've thought we would come this far, It all started with the small room in Kehl with pizza weekends. Senor Nelson Ricardo Avila Rovelo thank you for being a supportive room mate. And last but not the least Marie Sebastien, I cannot appreciate more how much you supported me, your patience and kindness these past months helped me get through the tough times.

---

# Contents

List of Figures	ix
List of Tables	xix
Glossary	xxi
Préface	xxiii
<b>1 State of the art</b>	<b>1</b>
1.1 Introduction to active matter and biomimetic membranes . . . . .	2
1.2 Janus Colloids . . . . .	3
1.2.1 Properties and self-propulsion . . . . .	4
1.3 Giant Unilamellar Vesicles, GUV . . . . .	6
1.3.1 Lipids : self-assembling amphiphilic molecules . . . . .	6
1.4 Janus colloids close to a solid wall . . . . .	8
1.5 Active Janus colloids in the presence of obstacles . . . . .	11
1.6 Wrapping of spherical colloids by GUVs . . . . .	14
1.7 Thesis outline . . . . .	16
<b>2 Materials &amp; methods</b>	<b>17</b>
2.1 Janus colloid fabrication . . . . .	18
2.1.1 Analysis and characterisation of Janus colloids . . . . .	20
2.1.1.1 Platinum layer thickness by light reflectivity . . . . .	20
2.1.1.2 SEM Analysis . . . . .	21
2.2 GUV formation . . . . .	23
2.2.1 Gel Assisted Swelling . . . . .	25
2.2.2 The Electroformation/Electroswelling method . . . . .	28

## CONTENTS

---

2.3	Interaction between Janus colloids and GUVs . . . . .	29
2.3.1	Spontaneous interaction of Janus colloids and GUVs . . . . .	30
2.3.2	Force driven interaction between Janus colloids and GUVs . . . . .	31
2.4	Image Analysis and tracking . . . . .	31
2.4.1	Motion tracking for Janus colloids . . . . .	31
2.4.1.1	Tracking of Janus orientation . . . . .	34
2.4.2	Vesicle Size and position . . . . .	35
2.5	Optical tweezer . . . . .	36
2.5.1	Setup . . . . .	36
2.5.2	Calibration . . . . .	37
2.5.3	Particle manipulation . . . . .	39
<b>3</b>	<b>Particle motion close to a solid wall in- and out- of thermal equilibrium</b>	<b>41</b>
3.1	Thermal Brownian trajectories of Janus colloids . . . . .	42
3.1.1	Particle translational diffusion . . . . .	43
3.1.2	In-plane and out-of-plane particle rotational diffusion . . . . .	46
3.1.2.1	In-plane rotational diffusion close to the solid-liquid interface . . . . .	48
3.1.2.2	Out-of-plane rotational diffusion close to the solid-liquid interface . . . . .	49
3.1.3	Comparison between experiments and hydrodynamic models . . . . .	51
3.2	Active motion of isolated Janus colloids . . . . .	52
3.2.1	Particle self-propulsion velocities . . . . .	53
3.2.2	Janus colloid orientation in active motion . . . . .	57
3.3	Comparing rotational diffusion in active and passive motion . . . . .	60
3.4	Conclusion . . . . .	61
<b>4</b>	<b>Janus colloids in GUV neighbourhood</b>	<b>63</b>
4.1	Brownian motion of a Janus colloid near a vesicle . . . . .	64
4.2	Active motion in a diluted regime close to a GUV . . . . .	66
4.2.1	Capture in persistent orbital motion . . . . .	67
4.2.2	Orbital time statistics . . . . .	71
4.2.3	Characterization of orbital motion . . . . .	73

4.2.4	Velocity comparison between orbital and free motion . . . . .	75
4.3	Particle rotation dynamics in orbital motion . . . . .	76
4.4	Force transfer between vesicle and particle . . . . .	77
4.4.1	Torque transfer in the system . . . . .	78
4.5	Conclusion . . . . .	79
<b>5</b>	<b>Janus colloid engulfment by GUV membranes</b>	<b>81</b>
5.1	Overview . . . . .	82
5.2	Particle engulfment by a membrane: theoretical background . . . . .	83
5.3	Force driven interaction for Janus colloid engulfment by GUV . . . . .	84
5.3.1	Centrifugation . . . . .	84
5.3.2	Optical Tweezers study on the interaction between a bare colloid and a GUV . . . . .	87
5.4	Tuning membrane and particle properties to trigger engulfment . . . . .	91
5.5	Particle rotational dynamics in the engulfment regime . . . . .	96
5.5.1	Rotational dynamics of engulfed MF-Pt colloids by GUVs . . . . .	96
5.5.2	$D_{R,\perp}$ and $D_{Tr,\parallel}$ in the engulfed regime . . . . .	100
5.6	Conclusion . . . . .	103
<b>6</b>	<b>Towards active dynamics of engulfed Janus colloids by GUVs</b>	<b>105</b>
6.1	Overview . . . . .	106
6.2	Transport of GUVs by engulfed active Janus colloids . . . . .	106
6.3	Quenching of active motion due to the partial engulfment state . . . . .	108
6.4	Future experimental investigations . . . . .	111
6.5	Final Conclusions . . . . .	112
	<b>References</b>	<b>115</b>
	<b>Resumé en Français</b>	<b>121</b>
	<b>List of Symbols</b>	<b>135</b>
	<b>Appendix</b>	<b>137</b>

## CONTENTS

---

# List of Figures

- 1.1 Overview of possible Janus particle architecture. Image taken from [22] 4
- 1.2 Schematic representations of a phospholipid and different structures obtained by self-assembly: (A) Phospholipid molecule, (B) Lipid Bilayer and (C) Giant Unilamellar Vesicle (GUV). . . . . 7
- 1.3 (A) Schematic of a spherical Janus particle with radius  $R_P$ , separated by a distance  $h$  from the nearby solid boundary. (B) Ratio of the rolling rotational drag close to a solid wall and in bulk as a function of the normalized gap distance. Image reproduced from [62]. . . . . 9
- 1.4 (A) Schematic representation of a Janus colloid close to a solid wall. The gap distance  $h$  is obtained from the measured translational diffusion coefficient of the colloid. (B)(C) show the effect of salt concentration ( $C_{NaCl}$ ) on a Janus colloid with  $R_P \approx 1.3 \mu\text{m}$ . (B) shows the translational diffusion coefficient and gap distance in passive Brownian conditions as a function of  $C_{NaCl}$ , where the lines show the theoretical predictions based on gravity and electrostatic balancing [64, 65]. (C) shows the diffusion coefficient and gap distance as a function of  $C_{NaCl}$  for a Janus colloid moving actively at 10%  $\text{H}_2\text{O}_2$ . Image taken from [63]. . . . . 10
- 1.5 (a) If an active colloid moving on a solid plane interacts with a vertical interface, it quenches a degree of freedom of the rotational motion (green arrow). (b) Three solid interfaces are able to quench the particle rotation locking the colloid into a set trajectory. Image Taken from [66] . . . . . 11

## LIST OF FIGURES

---

- 1.6 (A) A spherical Janus colloid swimming towards a passive obstacle of radius 5, 10, 15, and 20 times the particle size  $R_P$ . The critical obstacle size predicted for orbital trapping was  $R_C \approx 15R_P$ . (B) Basin of attraction  $h^*$  denotes the critical initial distance from the colloid above which the particle escapes, and below which entrapment ensues. (C) Flow field around a pusher particle near an obstacle. Image taken from [75] . . . . . 13
- 1.7 (A,B) Cross-section sections of confocal image stacks of a GUV sedimented on a PEG-DA hydrogel, which exhibits obvious thermal fluctuations in the presence of 0.65% weight percent PEG in the solution. The length of the scale bars is 10  $\mu\text{m}$ . (C) Schematic of the experimental system, and hypothesized mechanism for reduced depletion interactions against a hydrogel. (D,E) Confocal images of 1.1  $\mu\text{m}$  PS particles (green) and POPC membranes (red). The inside and outside of the GUV are indicated by i and o respectively. The particle in (D) with 0.24 wt% PEG100K does not deform the membrane. The membrane wraps the particle in (E) at 0.53 wt% PEG100K. The scale bar is 2  $\mu\text{m}$  in length. (F) Phase diagram based on the particle radius and amount of PEG depletant in the system. Numbers next to each data point indicate the number of membrane-particle pairs that were probed in each condition, Image taken from [83]. . . . . 15
- 2.1 Top row: schemes showing fabrication of  $\text{SiO}_2$ -Pt Janus colloids. (A)(B) Array of  $\text{SiO}_2$  colloids on a silicon wafer before and after platinum deposition. (C) Colloids in solution, with Janus boundary perpendicular to the substrate. Bottom row: bright-field microscopy images for colloids in a solution (D) bare colloids, (E) after platinum deposition and (F)  $\text{SiO}_2$ -Pt particles in a solution after being detached from the substrate. . . . . 19
- 2.2 (A) Bright-field microscopy image of  $R_P \approx 1 \mu\text{m}$  MF colloids existing in clusters after solvent drying. Janus boundary for MF-Pt colloids is unnoticeable in bright-field microscopy, (B) Fluorescent microscopy image of an MF-Pt colloid with the darker partial Pt coating. (C) Binary image of MF-Pt colloid after applying threshold limits. . . . . 20



## LIST OF FIGURES

---

2.3 Laser-light reflectivity curve to measure platinum thickness at different spots on a silicon wafer substrate. . . . .	<b>21</b>
2.4 SEM images of (A) SiO <sub>2</sub> -Pt, (B) MF-Pt Janus colloids with darker bare side and brighter Pt coating. . . . .	<b>22</b>
2.5 SEM images of (A) SiO <sub>2</sub> colloids showing shadowing effect due to clustering of particles. (B) Image showing the wavy and bumpy morphology of the Janus boundary, (C) MF-Pt colloids exhibiting nano-roughness and inhomogeneities. . . . .	<b>22</b>
2.6 Mechanism for formation of inhomogeneities in platinum coating during metal sputtering process. . . . .	<b>23</b>
2.7 Schematic illustrating three steps during swelling of lipid bilayer: (A) dried lipid bilayers on a substrate, (B) beginning of hydration and self assembly of vesicles, (C) swollen vesicles detaching from the bilayer. . .	<b>24</b>
2.8 Image of a home made PTFE plate with 4 × 3 grid of wells for vesicle growth. Each well is 12 mm wide and 10 mm deep. . . . .	<b>25</b>
2.9 Radius size distribution histogram curve for GUVs where the solid line is a fit yielding average size of $R_{GUV} = 11 \pm 5 \mu\text{m}$ . . . . .	<b>27</b>
2.10 Image of a home made PTFE electroformation cap with platinum electrodes. The gap between the electrodes was about 2.5 mm. . . . .	<b>28</b>
2.11 Image of a self adhesive Silicon isolator well (volume of 150 $\mu\text{L}$ ) on a glass slide for microscopy where particle-GUV contact is only by sedimentation due to gravity. . . . .	<b>30</b>
2.12 Schematic for force driven interaction between GUVs and Janus colloids. Particles are sedimented to the bottom of the centrifugation tube and the vesicles are added and brought in contact with different force of centrifugation ( $F_c$ ). . . . .	<b>31</b>
2.13 Tracking COM of a SiO <sub>2</sub> -Pt colloid using <i>Blender</i> .(A) Marker following the centre of the particle with the red and blue worms indicating the position of the particle in the previous and next 50 frames of the trajectory.(B) Precise position of the marker on the colloid. . . . .	<b>32</b>

## LIST OF FIGURES

---

- 2.14 Center of mass trajectory for self propelled MF-Pt ( $R_P \approx 1 \mu\text{m}$ ) and SiO<sub>2</sub>-Pt ( $R_P \approx 2 \mu\text{m}$ ) colloids in 2% H<sub>2</sub>O<sub>2</sub>, sedimented close to the bottom of the sample cell, where the solid square and triangle indicate the beginning and the end of the trajectory respectively. . . . . 33
- 2.15 (A) Fluorescent image of an MF-Pt colloid in bulk where the darker side is platinum coating. (B) After adjusting threshold the bare MF side is selected (in red) for conversion into black pixels. (C) Binary image after fitting an ellipse (yellow line) on the bare side of the colloid to track the orientation. . . . . 34
- 2.16 (A) Fluorescent image of GUVs prepared using gel formation method. (B) Tracking vesicle size and position after fitting a circle (green) on the vesicle periphery using HOUGH circle algorithm. . . . . 35
- 2.17 Scheme of modular optical tweezer setup (Thorlabs, United States) . . . 36
- 2.18 *MSD* curves corresponding to an MF colloid ( $R_P \approx 1 \mu\text{m}$ ) in Brownian and optically trapped conditions trapped with 50, 100, 150 mA laser power. The symbols are the experimental *MSDs* and the solid line is the theoretical fit corresponding to equation 2.1. At short time scales the *MSD* is diffusive while at long time scales it reaches a plateau due to trap confinement. The stronger the trap is the smaller is the value of the plateau. . . . . 38
- 2.19 Manipulation of SiO<sub>2</sub> bare colloid in X and Z direction using optical tweezer. The trapped particle is denoted by yellow plus sign and the movement can be clearly observed using the free reference colloids around the trapped particle. . . . . 39
- 3.1 Brownian trajectories for SiO<sub>2</sub>-Pt (left) and MF-Pt (right) Janus colloids sedimented close to a solid-liquid interface (observation time = 5 s). . . 43
- 3.2 Mean squared displacement (*MSD*) curve as a function of lag time  $\Delta t$  for SiO<sub>2</sub>-Pt ( $R_P \approx 2 \mu\text{m}$ ) and MF-Pt ( $R_P \approx 1 \mu\text{m}$ ) Janus particles in Brownian motion where the solid line indicates a linear fit over the curve. 44
- 3.3 Normalized gap height  $h/R_P$  as a function of Translational diffusion ( $D_{Tr,\parallel}$ ), comparison of experimental data with theoretical prediction [60, 104] close to an interface. . . . . 46

3.4 Schematic representation of the rotation of a Janus sphere about its axis: (A) out-of-plane (perpendicular) rotation defined by $\beta$ , (B) In-plane (parallel) rotation with respect to the solid-liquid interface, $\varphi$ is the angle between the Janus boundary and the Y-axis of the laboratory frame (XY plane). . . . .	47
3.5 Comparison between the orientation angle $\varphi$ for a ( $R_P \approx 1 \mu\text{m}$ ) MF-Pt Janus particle freely diffusing close to the solid-liquid interface and for a Janus particle stuck on the substrate. . . . .	48
3.6 Comparison between the orientation angle $\beta$ for a ( $R_P \approx 1 \mu\text{m}$ ) MF-Pt Janus freely diffusing close to the solid-liquid interface and for a Janus particle stuck on the substrate. . . . .	50
3.7 Mean Squared Angular displacement for the out-of-plane rotation of various MF-Pt colloids close to the interface where the solid lines are the linear fits of the experimental data (equation 3.4). . . . .	51
3.8 Rotational diffusion coefficient ( $D_{R,\perp}$ ) vs Translational diffusion coefficient ( $D_{Tr,\parallel}$ ). Comparison between experimental results and theoretical prediction for MF-Pt colloids close to a single wall. The solid line shows the theoretical predictions for the diffusion coefficients at different $R_P$ , while the dashed lines depict the predictions for normalized gap distance ( $\frac{h}{R_P}$ ). . . . .	52
3.9 Velocity autocorrelation function as a function of lag time $\Delta t$ for active $\text{SiO}_2\text{-Pt}$ ( $R_P \approx 2 \mu\text{m}$ ) and MF-Pt ( $R_P \approx 1 \mu\text{m}$ ) Janus particles. Corresponding trajectories are shown in Figure 2.14. . . . .	54
3.10 $MSD$ as a function of lag time $\Delta t$ for Janus colloids in active vs passive condition. The solid line fits the data with equation 3.7. The inset shows the parabolic behaviour of the $MSD$ curve for active Janus colloid. . . . .	56
3.11 Top view sketches of: (A) an ideal Janus colloid with a linear propulsion velocity $V$ . (B) A non-ideal Janus colloid with a linear active velocity $V$ , and angular velocity $\omega$ . . . . .	57
3.12 In-plane and out-of-plane rotation angle of an MF-Pt colloid in active condition close on the interface. . . . .	58

## LIST OF FIGURES

---

3.13	<i>MSAD</i> as a function of lagtime ( $\Delta t$ ) for in- and out-of-plane rotation of an active MF-Pt Janus colloid. The solid line fits the data linearly for $\Delta t \ll 4D_{Tr}/V^2 = \text{ca. } 0.4 \text{ s}$ . . . . .	59
3.14	Comparison between the out-of-plane angle $\beta$ of MF-Pt colloid in active and passive conditions. . . . .	60
3.15	Mean squared angular displacement curve for out-of-plane rotation of MF-Pt colloid in active and passive conditions. . . . .	61
4.1	Brownian trajectories for SiO <sub>2</sub> -Pt (left) and MF-Pt (right) Janus colloids close to a GUV near the solid-liquid interface. . . . .	65
4.2	Mean Squared Displacement curve as a function of lag time $\Delta t$ for Janus colloids ( <i>left</i> ) SiO <sub>2</sub> -Pt and ( <i>right</i> ) MF-Pt, in Brownian translation motion near a GUV, where the solid line indicates a quadratic fit over the curve. . . . .	66
4.3	Size distribution curve for GUV before and after addition of 2% H <sub>2</sub> O <sub>2</sub> . The average size of the GUV close to interface was observed to be almost the same $R_{GUV} \approx 11 \pm 6 \mu\text{m}$ before and after adding H <sub>2</sub> O <sub>2</sub> . . . . .	67
4.4	(A) Centre of mass trajectory of an active colloid of radius $R_P \approx 2 \mu\text{m}$ interacting with a GUV. Time lapse images of the interaction between an active particle and a GUV are shown in the insets. . . . .	68
4.5	Sketch of the experimental geometry: a Janus colloid orbiting a GUV along the substrate. $\Delta z$ is the difference between the focal plane of the GUV and the particle equator. $R_O$ is the radius of the orbital trajectory (see also Figure 4.6). . . . .	69
4.6	Centre of mass trajectories of active Janus colloids ( $R_P \approx 1$ and $2 \mu\text{m}$ ) around GUVs of different sizes. The range of observation time is 30–788 seconds. Clockwise (CW) and counterclockwise (CCW) directions are also reported close to the trajectories. . . . .	70
4.7	Normalized counts of orbital times of $R_P \approx 1$ & $2 \mu\text{m}$ particles rotating around GUVs. The red curves are exponential functions $\sim \exp(-t_{orb}/t^*)$ . A log-linear representation of the data is shown in the inset. . . . .	72
4.8	(A) Trajectory of a $R_P \approx 2 \mu\text{m}$ active colloid orbiting around two GUVs and performing a "free" motion in between. (B) Velocity autocorrelation functions as a function of lag time $\Delta t$ for the trajectory shown in (A). . . . .	73

## LIST OF FIGURES

---

4.9	Orbital speed of $R_P \approx 1$ and $2 \mu\text{m}$ active colloids as a function of the speed far from the orbit. . . . .	75
4.10	(A) $\varphi - \theta$ as a function of the experimental time for a $R_P \approx 2 \mu\text{m}$ active colloid orbiting a GUV. (B) Mean squared angular displacement $\langle \Delta(\varphi - \theta)^2 \rangle$ as a function of the lag time. Solid line is a fit of equation 4.2 to the data. In the inset, a sketch of a Janus particle (P) orbiting around a GUV together with the polar location angle $\theta$ and the orientation angle $\varphi$ in the GUV frame are displayed. . . . .	77
4.11	Time lapse images of an $R_P \approx 2 \mu\text{m}$ active colloid rotating in a CCW direction (yellow arrow) but not translating and interacting with a GUV, which is both revolving around the Janus colloid and rotating in a CW direction (red arrow). Arrow arc length shows the rotation around its own axis between two frames (time is given on the top of the image). . .	78
5.1	States of engulfment in a colloid-GUV system. . . . .	82
5.2	Illustration for wrapping geometry of a spherical colloid by a membrane. Image reproduced from [121] . . . . .	84
5.3	Force of centrifugation as a function of vesicle radius ( $R_{GUV}$ ) for different relative centrifugal force, RCF. . . . .	85
5.4	States of engulfment in a colloid-GUV system. (A) Schematic of GUV interacting with a Janus colloid under the force of centrifugation ( $10^{-11}$ - $10^{-9}$ N), (B) schematic for free, engulfed and membrane rupture regimes. (C) Brightfield (+ Fluorescence) microscopy image of $\text{SiO}_2\text{-Pt}$ ( <i>Left Column</i> ) and $\text{MF-Pt}$ ( <i>Right Column</i> ) Janus colloid in various regimes after centrifugation. . . . .	86
5.5	( <i>Left to Right</i> ) Contact regimes of $\text{SiO}_2$ ( $R_P \approx 2 \mu\text{m}$ ) shown in dashed yellow approaching a floppy GUV, deforms the vesicle with the force provided by optical tweezer, and then is fully engulfed by the vesicle. . .	87
5.6	( <i>Left to Right</i> ) Contact regimes of $\text{SiO}_2$ ( $R_P \approx 1 \mu\text{m}$ ) shown in yellow approaching a floppy GUV, deforms the vesicle with the force provided by optical tweezer, and then is fully engulfed by the vesicle. . . . .	89
5.7	Force curve as a function of time (t) during the engulfment for a $\text{SiO}_2$ colloid $R_P \approx 1 \mu\text{m}$ by a POPC GUV $R_{GUV} \approx 25 \mu\text{m}$ . . . . .	90

## LIST OF FIGURES

---

5.8	(Left to Right) SiO <sub>2</sub> ( $R_P \approx 2 \mu\text{m}$ ) colloid fully engulfed by a POPC GUV. Trapped colloid drags the GUV along with its path after manipulation with optical tweezer. The pear shaped geometry of the GUV is due to the drag it encounters while it is being pulled by the colloid. . . . .	91
5.9	Bright field images of SiO <sub>2</sub> -Pt Janus colloid persistently adhered to a GUV. . . . .	93
5.10	(A) SiO <sub>2</sub> -Pt Janus colloid under fluorescence microscopy after rupturing POPC GUVs and becoming fluorescent. (B) Intensity profile for the images in (A). . . . .	94
5.11	A montage SiO <sub>2</sub> -Pt Janus colloid persistently adhered/partially engulfed by DOPC GUV. . . . .	94
5.12	Fluorescence microscopy of MF-Pt Janus colloid splitting GUVs. The brighter spot stuck between membrane cleavage (highlighted in yellow) are the Janus colloids. . . . .	96
5.13	A montage of the MF-Pt Janus colloid in various regimes, where the difference in the particle rotation between the free and engulfed regimes can be inspected visually in Fluorescence microscopy. . . . .	97
5.14	Out-of-plane rotational angle as a function of time for MF-Pt Janus colloids in free, stuck as well as engulfed regime . . . . .	98
5.15	<i>MSAD</i> as a function of the lag time for MF-Pt Janus colloids in free, engulfed and stuck regimes. The plateau for the engulfed colloids signifies confinement due to engulfment. . . . .	99
5.16	Schematic showing the partial engulfment of an MF-Pt colloid ( $R_P \approx 1 \mu\text{m}$ ) by a GUV, where $\beta^*$ is a characteristic out-plane-rotation angle. For better visualisation the membrane thickness is not to scale, as the actual membrane thickness is only 5 - 6 nm. . . . .	100
5.17	$D_{R,\perp}$ as a function of $D_{T,\parallel}$ for MF-Pt colloids in free and engulfed regimes. The gray area is the limit of $D_{R,\perp}$ measurement. . . . .	101
6.1	SiO <sub>2</sub> -Pt Janus colloid actively transporting a POPC GUV. In yellow is the trajectory of the colloid and the GUV is highlighted in blue (dashed). Note that particle-GUV at 30, 75, and 130 s are superimposed images for visualisation purpose. . . . .	107

**LIST OF FIGURES**

---

6.2 MF-Pt Janus colloid actively transporting a DOPC GUV. In yellow is the trajectory of the colloid and the GUV is highlighted in blue (dashed). Note that particle-GUV at 30, 52, and 83 s are superimposed images for visualisation purpose. . . . . **108**

6.3 (A) Images showing an engulfed MF-Pt colloid changing orientation for  $t>0$  due to the addition of  $H_2O_2$ , pulling the GUV membrane and returning to the bottom of the GUV. The colloid is highlighted in yellow and the GUV in blue. (B) Schematic representation of the transient behaviour for the colloid migration shown in (A). The solid arrow denotes the propulsion direction while the dashed arrow denoted the rotational direction. Images after the addition of  $H_2O_2$  ( $t>0$ ) appear darker due to the formation of Oxygen bubbles in the cell. . . . . **110**

6.4 RICM + brightfield microscopy image of a floppy POPC vesicle where the blue (dashed) line represents the periphery of the vesicle while the yellow (dashed) line signifies the segment of the membrane touching the substrate. For a floppy membrane the footprint radius of the vesicle was observed to be up to  $3/4R_{GUV}$ . . . . . **110**

6.5 MF-Pt Janus colloid engulfed by POPC GUV resulting in a ballistic motion of the colloid repelling optical the trap, colloid migrating back to the bottom region of lower membrane tension. The position of the trap is indicated a red plus, the colloid is highlighted in dashed yellow and the GUV is highlighted in dashed blue. . . . . **111**

A4 Orbital time versus orbital radius for  $R_P \approx 1$  and  $2 \mu m$  active colloids. **142**

A5 RICM image of a POPC vesicle where the dashed yellow is the equator of the vesicle while the dashed blue line shows the area in contact with the substrate. . . . . **143**

## LIST OF FIGURES

---



# List of Tables

2.1	Physical properties of SiO <sub>2</sub> and MF colloids . . . . .	18
2.2	Actual radius SiO <sub>2</sub> -Pt and MF-Pt Janus colloids. . . . .	21
2.3	Properties of POPC and DOPC lipids. . . . .	24
3.1	Range of active and angular velocities for SiO <sub>2</sub> -Pt and MF-Pt Janus colloids in a free trajectory. . . . .	56
5.1	Effect of centrifugal force on POPC and DOPC GUVs interacting with SiO <sub>2</sub> -Pt Janus colloids, where (●) signifies observed events. . . . .	92
5.2	Effect of centrifugal force on POPC and DOPC GUVs interacting with MF-Pt Janus colloids, where (●) signifies observed events. . . . .	95

## GLOSSARY

---

# Glossary

<b>Ag-Pt</b>	Silver-Platinum	<b>MSD</b>	Mean squaree displacement
<b>COM</b>	centre of mass	<b>PBS</b>	Phosphate-Buffered Saline
<b>DMPC</b>	1,2-dimyristoyl-sn-glycero-3-phosphocholine	<b>PEG</b>	polyethylene glycol)
<b>DOPC</b>	1,2-dioleoyl-sn-glycero-3-phosphocholine	<b>PEG-DA</b>	poly(ethylene glycol) diacrylat
<b>fps</b>	frames per second	<b>POPC</b>	1-palmitoyl-2-oleoyl-glycero-3-phosphocholine
<b>GUV</b>	Giant Unilamellar Vesicles	<b>PS-Pt</b>	Polystyrene-Platinum
<b>H<sub>2</sub>O<sub>2</sub></b>	hydrogen peroxide	<b>PTFE</b>	polytetrafluoroethylene
<b>MF-Pt</b>	MelamineFluoride-Platinum	<b>PVA</b>	polyvinyl alcohol
<b>MSAD</b>	Mean squared angular displacement	<b>RCF</b>	Relative centrifugal Force
		<b>RICM</b>	Reflection Interference Contrast Microscopy
		<b>SEM</b>	Scanning electronic microscopy
		<b>SiO<sub>2</sub>-Pt</b>	Silica-Platinum
		<b>SOPC</b>	1-stearoyl-2-oleoyl-sn-glycero-3-phosphocholine
		<b>TPM-Pt</b>	3-(trimethoxysilyl)propyl methacrylate

## GLOSSARY

---

# Préface

De nombreux processus importants, tels que les infections microbiennes, la toxicité des nanomatériaux et l'administration interne de médicaments, dépendent de l'interaction entre les systèmes actifs et les membranes biologiques. L'étude de la matière active est une nouvelle discipline dans laquelle la physique de la matière molle est liée à l'étude des particules qui peuvent prendre et utiliser l'énergie de leur environnement pour générer un mouvement systématique et autonome. De nombreux systèmes biologiques et vivants tels que les bactéries, les oiseaux ou les humains sont de bons exemples de tels systèmes actifs. Inspirés par les systèmes biologiques, divers nageurs artificiels de différentes échelles ont été synthétisés, produisant des exemples faciles de micro-nageurs. Un exemple de ce type de système est constitué par les colloïdes de Janus, qui sont capables de produire un mouvement amélioré sans aucune intervention extérieure et, par extension, d'imiter la fonctionnalité des systèmes vivants actifs. En parlant d'imiter les systèmes vivants, j'en viens à la deuxième composante de cette étude, les vésicules unilamellaires géantes. Ces vésicules, de quelques microns de long, suivent le paradigme de base d'une cellule vivante et ont ouvert de nouvelles possibilités pour comprendre le fonctionnement d'une cellule vivante.

Le travail présenté dans cette thèse a été réalisé dans l'équipe Physique des Membranes et Matière Molle ( $M^3$ ) de l'Institut Charles Sadron à Strasbourg. L'équipe étudie le comportement global de la membrane cellulaire ainsi que ses propriétés physiques. Je suis également satisfait du fait que j'ai eu l'opportunité de tester toutes les idées que j'avais sur mon sujet durant cette période.

Dans ce travail de thèse, nous utilisons des vésicules unilamellaires géantes (GUV), un système modèle artificiel conçu pour imiter les caractéristiques physiques de la membrane cellulaire avec une composition contrôlée, et nous tentons de démontrer comment

## 0. PRÉFACE

---

les colloïdes artificiels autpropulsés interagissent avec la membrane. Bien que de nombreuses études antérieures se soient concentrées sur les colloïdes de Janus et les GUV en tant qu'éléments individuels, aucun progrès significatif n'a été signalé sur l'assemblage GUV-colloïde.

Le plus grand défi auquel j'ai été confronté était d'avoir à réfléchir à de nouvelles idées de travail qui n'avaient pas été utilisées auparavant pour un tel système. Cela a mis la barre plus haut pour mesurer mes propres progrès, tout en indiquant des directions avec lesquelles je n'étais pas toujours d'accord et en tirant des conclusions que je ne pouvais pas toujours valider. Cependant, les progrès que j'ai pu faire au cours de la période de la thèse semblent avoir valu tous mes efforts. Les nouvelles perspectives découvertes au cours de cette thèse serviront, je l'espère, de base à de futures discussions sur la nouvelle direction qui a émergé à la suite de l'ensemble Janus-GUV. En raison de la nature unique de cette thèse, combinant la matière molle et la biophysique, j'ai pu interagir avec des personnes de différents domaines et acquérir un aperçu de deux domaines de recherche très différents et dynamiques. Des interactions telles que celles-ci ont été mutuellement bénéfiques et ont eu un impact significatif sur le contenu de mon travail, comme décrit tout au long de ce manuscrit.

# Chapter 1

## State of the art

## 1. STATE OF THE ART

---

### 1.1 Introduction to active matter and biomimetic membranes

Living or artificial active matter systems show original dynamics when they interact with other objects like passive particles, interfaces, or membranes. First coined by Ramaswamy in 2004 [1], the term active matter is used to describe systems in which each component consumes energy at a local level. Therefore, active matter components (active particles) are out of thermal equilibrium, which affects their individual and collective behaviors. In a broad definition, active matter is classified into biological or artificial active matter (e.g. bacteria, viruses, nanocars [2], microswimmers/ Janus colloids [3]). Artificial self-propelled colloids are an important class of active matter systems. They can both absorb energy from an external source or consume chemical fuels to produce work and move in an autonomous way [4]. Such artificial active colloids can transport small cargos [5, 6, 7, 8] or can be guided by passive objects, performing simple tasks that could be implemented in more complex systems.

An example of such complex systems is a cell membrane. In fact, the cell membranes perform a variety of functions, by acting as a separation barrier, to control selective permeability for specific components such as water and gases. Many important processes, such as microbial infections, drug delivery, and nanomaterial toxicity [9], are influenced by interactions between active matter such as viruses, bacteria, or artificial active colloids and biological membranes, which are related to endocytosis, translocation and adsorption of living and artificial colloids in membranes. In biological cell membranes, many passive and active (fuel-consuming) mechanisms [10] occur during the recruitment of a particle inside the cell. Such mechanisms are often coupled together and are far from being understood today as shown by the COVID-19 pandemic [11]. The ideal scenario would be to empty a biological cell interior while controlling the composition of the resulting skeleton of lipids, membrane proteins, and other non-lipid components. We would be able to gain a better understanding of the biophysics of these membranes as well as the precise pathways that they regulate [12]. However, for the time being, we are unable to do so. Instead, biomimetic membranes can be used to better understand the working of cell membranes and their transport mechanisms, which is essential for the development of research into effective drug delivery systems and biosensors, among other things.



Such biomimetic membranes emulate the structure and/or transport mechanisms in biological membranes. Giant lipid vesicles [13, 14, 15, 16, 17, 18] are one of the many model membrane systems that have been used to resolve the structure of membranes and characterize them in the laboratory. Other types of model membranes include lipid monolayers at the air–water interface, solid-supported bilayers, black lipid membranes, and bilayer stacks [12].

## 1.2 Janus Colloids

Named after the two-faced Roman god, Janus colloids possess at least two different "faces" or surfaces differing in their physicochemical properties. Described as promising experimental Soft Matter systems [19], Janus colloids have come a long way in terms of experimental design: shape, size as well as composition. Recent progress in the field of Janus particles has focused on particle sizes in the colloidal domain, which are much larger than molecules but small enough to be subjected to Brownian diffusion. In the current literature, Janus colloids are available in different shapes (see Figure 1.1) as well as different surface domains including, different electric charge [20], and polarity [19, 21]. It has been predicted [22] and experimentally demonstrated that Janus colloids possess surface activities, or the ability to lower the interfacial tension at fluid interfaces, higher than the ones of bare colloids [23, 24]. The shape of Janus colloids may significantly affect the interfacial tension of fluid interfaces, as the shape changes from sphere to disc and rod [25] (see Figure 1.1). The size versatility of Janus colloids (few nm to tens of  $\mu\text{m}$ ) also brings further advantages as active carriers, or smart catalysts moving in a concentration gradient.

## 1. STATE OF THE ART

---

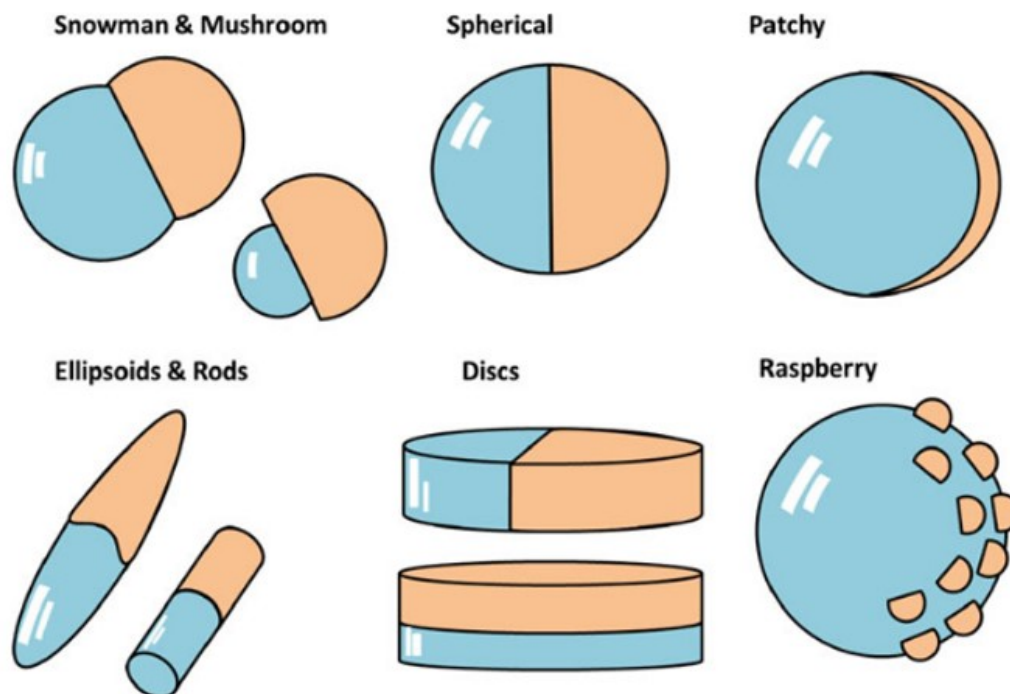


**Figure 1.1:** Overview of possible Janus particle architecture. Image taken from [22]

In general, Janus colloids can be grouped according to their composition, into 3 categories: polymeric (based on soft systems), inorganic (based on hard systems) and polymeric-inorganic compositions (based on hybrid systems) [26, 27, 28, 29]. Inorganic and polymeric-inorganic systems have gathered much attention due to the features of well-defined size, ease of processing, flexibility, and environmentally responsive properties like mechanical, magnetic, and photoelectric properties [27, 28, 30, 31, 32], along with the flexible nature of the polymer backbone (in the case of polymeric-inorganic hybrid systems). SiO<sub>2</sub>-Pt (Silica-Platinum), Ag-Pt (Silver-Platinum), MF-Pt (Melamine Fluoride-Platinum), and PS-Pt (Polystyrene-Platinum) are a few examples of inorganic and polymeric-inorganic Janus colloids.

### 1.2.1 Properties and self-propulsion

In this section, we list some important properties related to Janus colloids. Two remarkable features of Janus particles are: (i) to be able to respond to external fields

(in passive conditions); and (ii) in the presence of external or internal fuel sources, to perform the autonomous self-propelled motion, i.e. becoming "active" particles.

- **Magnetophoresis/electrophoresis** : In terms of responsiveness, manipulation of Janus colloids can be achieved under the application of a magnetic or electric field gradient. The magnetic field can either be generated by a permanent magnet or an electromagnet [33, 34]. Manipulation with a magnetic or electric field can result in the self-assembly of Janus colloids into multiple chains or supra structures. [33, 35, 36].
- **Self-thermophoresis** : Janus colloids may become active and show self-propulsion by absorbing light at the metal-coated side of the Janus particle. Absorption creates a local temperature gradient around the particle which in turn drives the particle [37]. The mechanism of such propulsion has been corroborated by observing the thermal slip flow field around a Janus colloid [37, 38, 39, 40]. Introduction of temperature gradients have been observed to have an ill effect on biological systems close to the induced temperature gradient [41]
- **Self-diffusiophoresis** : One of the most used mechanisms to achieve autonomous particle propulsion is due to a concentration gradient built by the particle as a result of a chemical reaction on one particle face. An example is the reaction of  $\text{H}_2\text{O}_2$  on Platinum, which is decomposed in  $\text{O}_2$  and  $\text{H}_2\text{O}$  [5]. Several self-propelled particles are now described in the literature. Wang *et al.* [42], for instance, fabricated different Janus systems by depositing Iridium on one side of silica particles and using hydrazine as fuel.  $\text{N}_2$ ,  $\text{H}_2$  and  $\text{NH}_3$  molecules are generated at the Iridium surface, which creates a concentration gradient around the particle, driving the autonomous motion. Such persistent motion can be used to achieve unique operational functions, such as particle cargo applications [42, 43].

For platinum coated Janus colloids, the mechanism of self-propulsion using  $\text{H}_2\text{O}_2$  has been debated in the scientific community. A large number of publications have been considering self-diffusiophoresis [44, 45]. According to Golestanian *et al.* [46], the simultaneous depletion of reactants and generation of products creates concentration gradients across the surface of the body, due to the diffusion of reactants from the bulk

## 1. STATE OF THE ART

---

to the catalytic surface giving rise to a lateral slip in the fluid across the surface of the particle generating propulsion whose velocity is inversely proportional to the radius of the colloid  $V \propto R_p^{-1}$ . However, some experiments show different behaviours that can not be described by self-diffusiophoresis and other proposed mechanisms include nano-bubble detachment [47] and self-electrophoresis have been discussed [3, 48, 49, 50].

### 1.3 Giant Unilamellar Vesicles, GUV

Biological cells typically have the size of 1 - 100  $\mu\text{m}$  which makes them visible under an optical microscope. The desire to create cell-like models for fundamental science spurred the interest towards creating giant unilamellar vesicles (GUVs). Vesicles are typically classified according to multilamellarity as well as their size. Small unilamellar vesicles (SUVs) are a few tens of nanometers in size, while large unilamellar vesicles (LUVs) are in the hundred nanometer range. Compared to SUVs and LUVs, GUVs are 10–1000 times larger. Which makes it easier to employ GUVs for optical microscopy studies and makes them a handy tool for directly displaying the response of the membrane on a cell-size scale [12].

#### 1.3.1 Lipids : self-assembling amphiphilic molecules

Lipids are the key elements of the cell membrane thanks to their amphiphilic properties. Two types of molecular groups, hydrophilic and hydrophobic groups, join together to form lipids. Hydrophilic groups are polar molecules that are soluble in aqueous solvents, in contrast, hydrophobic groups are typically lengthy carbon chains or oils that are insoluble in aqueous solvents. Due to the cohabitation of these groups in the same molecule, a molecular stress is created, in which one group attempts to escape from water while the other group attempts to seek it [51]. Amphiphilic lipid molecules self-assemble into supramolecular structures when brought in contact with an aqueous solution. At very low concentrations, lipids may self-assemble as a monolayer at an interface (solid-liquid or gas-liquid interfaces). Above a critical micellar concentration, however, lipids self-assemble in the bulk as spherical micelles, liposomes or bilayers according to the lipid packing parameter.

When sheets of lipid bilayers (see Figure 1.2(B)) are hydrated in an aqueous solution, the outermost bilayer deforms and closes into vesicles to shield free edges from water

(see Figure 1.2(C)), and under the right conditions yields vesicles up to 10-100  $\mu\text{m}$  in size. Among various lipid molecules, phospholipids are the primary constituents that make up a cell membrane, among other non-lipid molecules (e.g. proteins). The precise lipid composition of the cell membrane can vary significantly from one organelle to another, as well as from one type of living being to another. It is difficult to determine the exact composition of the membranes of organelles, but several articles describe the heterogeneity of the membranes of organelles [52]. The structure of a phospholipid contains a head group and two tail chains (see Figure 1.2(A)), two of the most common phospholipid head groups, are phosphatidylcholine (PC) and phosphatidylethanolamine (PE). Similarly, the tail groups of phospholipids can be classified according to their chain lengths and the number of unsaturations. Details on the physical and physicochemical properties of phospholipids can be found in the literature [12, 14, 53]. Briefly, lipid membranes can be characterized by: (i) **membrane tension** ( $\sigma$ ), which is the force per unit length acting on a cross-section of a membrane. (ii) **Bending modulus** ( $\kappa_b$ ), is a mechanical macroscopic constant that describes the tendency of membrane to resist to bending. (iii) **Mean curvature** ( $c$ ) derived from the principle curvatures ( $c_1$  &  $c_2$ ) that characterizes the shape of the membrane at each point in space. and (iv) **spontaneous curvature** ( $m$ ), which is related to the asymmetry existing between the inner and outer leaflets in the bilayer and results in a spontaneous tendency of a free membrane to bend.  $m$  is classified as negative (inward bending) or positive (outward bending) considering a vesicle geometry.

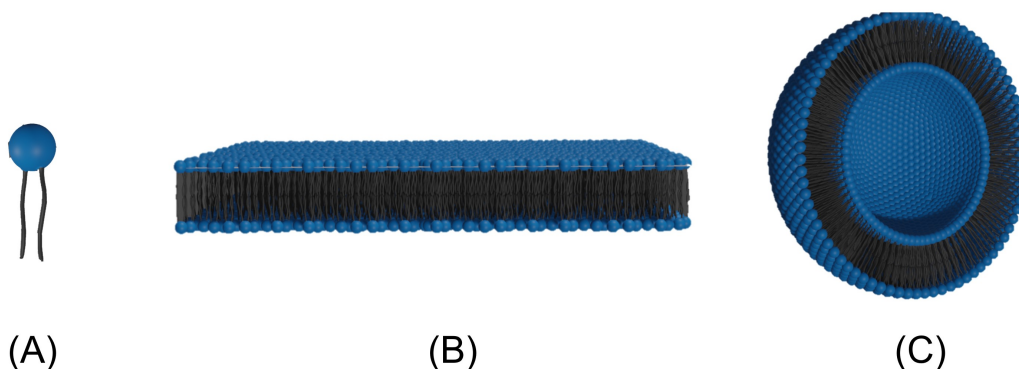


**Figure 1.2:** Schematic representations of a phospholipid and different structures obtained by self-assembly: (A) Phospholipid molecule, (B) Lipid Bilayer and (C) Giant Unilamellar Vesicle (GUV).

### 1.4 Janus colloids close to a solid wall

When a passive Janus colloid approaches a solid boundary, translational ( $D_{Tr} = \frac{k_B T}{\zeta_{Tr}}$ , where  $k_B T$  is the thermal agitation energy) and rotational diffusion ( $D_R = \frac{k_B T}{\zeta_R}$ ) coefficients of the spherical particle decrease due to an increase in the hydrodynamic drag force both in the direction perpendicular and parallel to the wall [54, 55]. In the low Reynolds number limit, far from a boundary, the drag coefficients for translational and rotational motion take the Stokes values of  $\zeta_{Tr,b} = 6\pi\eta R_P$  and  $\zeta_{R,b} = 8\pi\eta R_P^3$  respectively. In passive microrheology, Stokes drags are used to determine the exact viscosity  $\eta$  of the medium knowing the particle size. However, within a typical microfluidic or biological system, the effect of a confining wall leads to an increase in the hydrodynamic drag experienced by the spherical particle. The increased translational hydrodynamic drag for the motion of a spherical particle close to a wall has been extensively investigated both from a theoretical and an experimental point of view [56, 57, 58]. Note that both the translational and rotational mobility is reduced due to the wall hindrance. However, particle rotational drag experiments close to a solid wall are scarce. In the approach to solving simple Stokes [59] equations in the presence of solid boundaries, Faxén [60] proposed a wall correction factor for the slowing down of translational and rotational diffusion, which were further developed by Happel and Brenner [61], under the hypothesis that there is no relative motion at the fluid-solid interface, i.e., no-slip condition, provided an analytical expression in the form of an infinite series to account for another correction term for motion normal to the solid surface. Goldman *et al.* [62] investigated the slow viscous motion of a sphere in a quiescent viscous fluid in the near-wall region, using an asymptotic solution of the Stokes equation to analyze the rotational and translational motion close to the wall. In Figure 1.3(A) the gap distance  $h$ , defined as the separation between the solid wall and the pole of the colloid, plays a critical role in evaluating the hindered Brownian diffusion as with decreasing  $h$  the hydrodynamics of the colloid becomes more complex (see later in Chapter 3). The ratio of rotational drag close and far away (approaching bulk) from the solid wall as a function of normalized gap height is shown in Figure 1.3(B). For gap distance  $h/R_P = 10^{-3}$ , the out-of-plane rotational drag (rolling)  $\zeta_{R,\perp}$  is 3 times higher as compared to drag in the bulk.

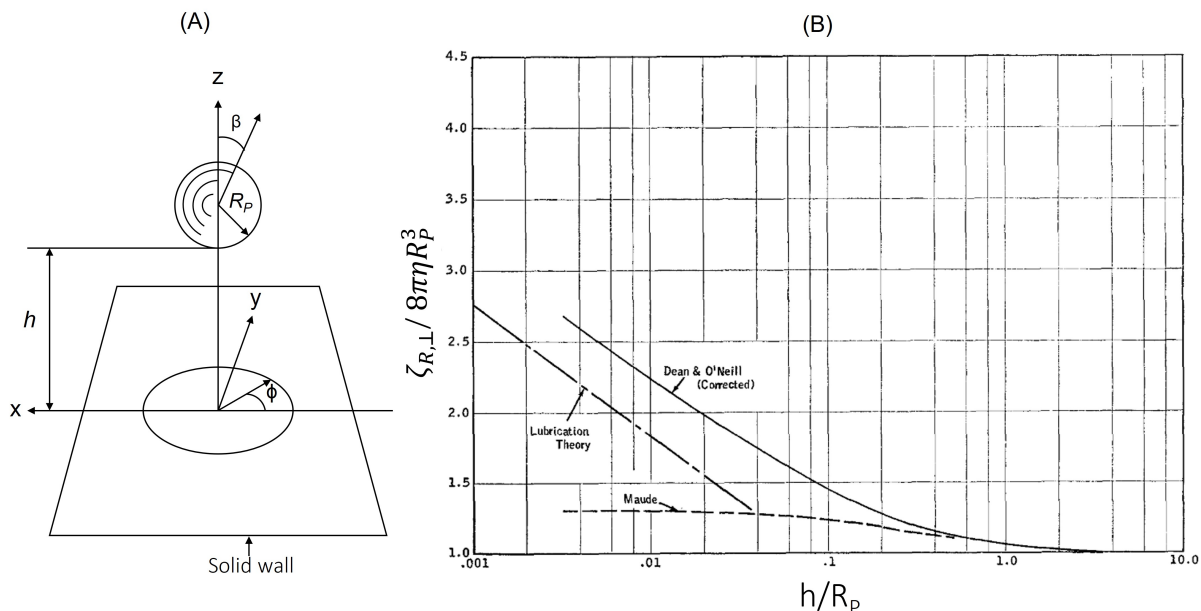


**Figure 1.3:** (A) Schematic of a spherical Janus particle with radius  $R_p$ , separated by a distance  $h$  from the nearby solid boundary. (B) Ratio of the rolling rotational drag close to a solid wall and in bulk as a function of the normalized gap distance. Image reproduced from [62].

Ketzetzi *et al.* [63] in a recent article, used the translational diffusion coefficient of Janus colloids close to a glass substrate to obtain the gap distance  $h$  by considering the above mentioned hydrodynamic predictions and by assuming a unique size of the colloids. They used 3-(trimethoxysilyl)propyl methacrylate colloids, partially coated with platinum (TPM-Pt,  $R_p \approx 1.35 \mu\text{m}$ ) in passive conditions and found that  $h$  can vary from ca.  $1 \mu\text{m}$  to  $250 \text{ nm}$  if the ion concentration is increased. These gap distances can be explained as equilibrium positions by a balance of gravity attraction and electrostatic double-layer repulsion between the colloid and the substrate. Surprisingly, the same Janus colloids in active conditions (see Figure 1.4(B)), tend to maintain a constant gap distance of  $h = 0.25 \pm 0.06 \mu\text{m}$  (see Figure 1.4(C)) at a concentration of up to 10%  $\text{H}_2\text{O}_2$  propellant. Even with any change in the ion concentration (NaCl), zeta potential or particle size seems to have no effect on the gap distance between the active Janus colloids and the solid wall.

## 1. STATE OF THE ART

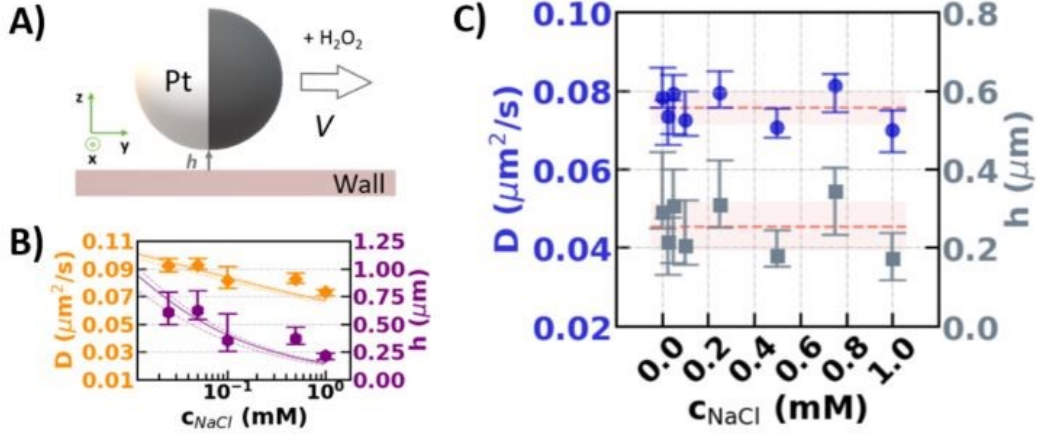


**Figure 1.4:** (A) Schematic representation of a Janus colloid close to a solid wall. The gap distance  $h$  is obtained from the measured translational diffusion coefficient of the colloid. (B)(C) show the effect of salt concentration ( $C_{NaCl}$ ) on a Janus colloid with  $R_P \approx 1.3 \mu m$ . (B) shows the translational diffusion coefficient and gap distance in passive Brownian conditions as a function of  $C_{NaCl}$ , where the lines show the theoretical predictions based on gravity and electrostatic balancing [64, 65]. (C) shows the diffusion coefficient and gap distance as a function of  $C_{NaCl}$  for a Janus colloid moving actively at 10%  $H_2O_2$ . Image taken from [63].

For a self-propelled catalytic colloid, the propulsion direction is usually away from the catalytic site, and in the short time limit, the motion of the particle is ballistic. Brownian rotational diffusion causes the change of the colloid orientation, resulting in randomization of the self-propelled direction for long times. An interesting phenomenon in which self-motile colloids interact with their physical environment is exploited in the view of reducing rotational randomness and producing longer lasting directional trajectories. According to Das *et al.* [66], self-propelled Janus colloids close to a solid-liquid interface have a far greater persistence in the active directional motion parallel to the interface if compared to active particles far from the interface. The presence of a solid wall can in fact confine the Brownian rotational diffusion in active conditions as depicted in Figure 1.5.



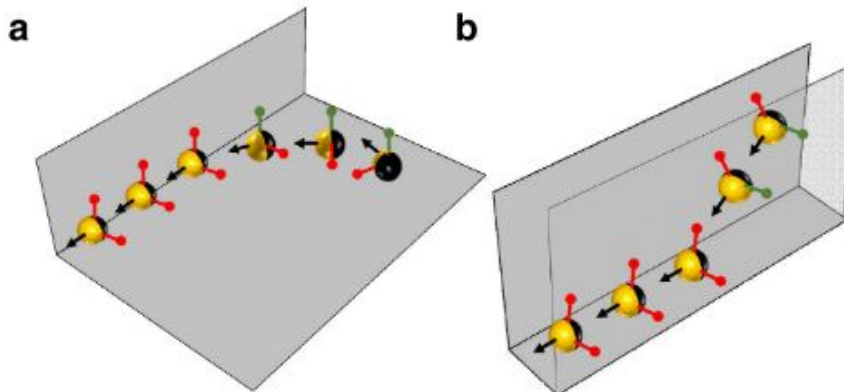


**Figure 1.5:** (a) If an active colloid moving on a solid plane interacts with a vertical interface, it quenches a degree of freedom of the rotational motion (green arrow). (b) Three solid interfaces are able to quench the particle rotation locking the colloid into a set trajectory. Image Taken from [66]

Other strategies including the use of a magnetic field, gravity [67, 68], fluid interfaces [69] as well as passive objects [70, 71] have been used to steer the active motion of self-propelled colloids and to bias the propulsion direction.

### 1.5 Active Janus colloids in the presence of obstacles

Some recent studies reported on the dynamics of active Janus colloids interacting with passive obstacles [70, 71]. Takagi *et al.* [70] carried out experiments in the presence of spherical passive obstacles, where active rod-shaped colloids were reported to be bound in orbital trajectories around obstacles. They described several observations pointing to quite general phenomena of orbital motion occurring for different obstacle sizes and material properties. Short-range hydrodynamic and steric interactions were used to model the trapping dynamics. They also reported no force or torque transfer between the particle and the spherical obstacle in this experimental system during orbital motion. Similar experimental observations were reported by Brown *et al.* [50] for active spherical Janus colloids moving in a 2D colloid crystal.

Far-field hydrodynamic models have been developed to describe the dynamics of self-propelled particles moving close to a wall and interacting with solid or fluid obstacles in the bulk [72, 73]. When using these models, only the fluid flow far (a fraction

## 1. STATE OF THE ART

---

of the body length) from the self-propelled particle is described, along with an obstacle particle repulsion, which ensures that the particle does not penetrate inside the obstacle. Lauga *et al.* [74] laid out theoretical models to describe the orbital trap and the factors facilitating their geometric capture and escape from the orbital dynamics. From a purely hydrodynamic viewpoint, self-propelled Janus colloids can be described as "pusher" squirmers. Far-field hydrodynamic models have been developed to describe the dynamics of self-propelled particles moving close to a wall and interacting with solid or fluid obstacles in the bulk [73, 74]. Flow field generated by a "pusher" microswimmer is directed outward on the front and back of the colloid, while an inward fluid flow is generated on the sides (around the Janus boundary), which leads to an attraction between the swimmer and an obstacle located on the side, see Figure 1.6(C). A critical size  $R_C$  of the obstacle was predicted to capture the active colloid in a persistent orbital motion if  $R_C > 15R_P$  (see Figure 1.6(A)). A basin of attraction ( $h^*$ ) (i.e., the domain in space over which the particle is eventually captured by the obstacle) was also described within this far-field hydrodynamic model, see Figure 1.6(B). The length of the basin of attraction is comparable to the particle size, and depends also on the obstacle dimension. Particle Brownian diffusion was also taken into account to describe the particle escape dynamics from the obstacle orbits [72, 73].

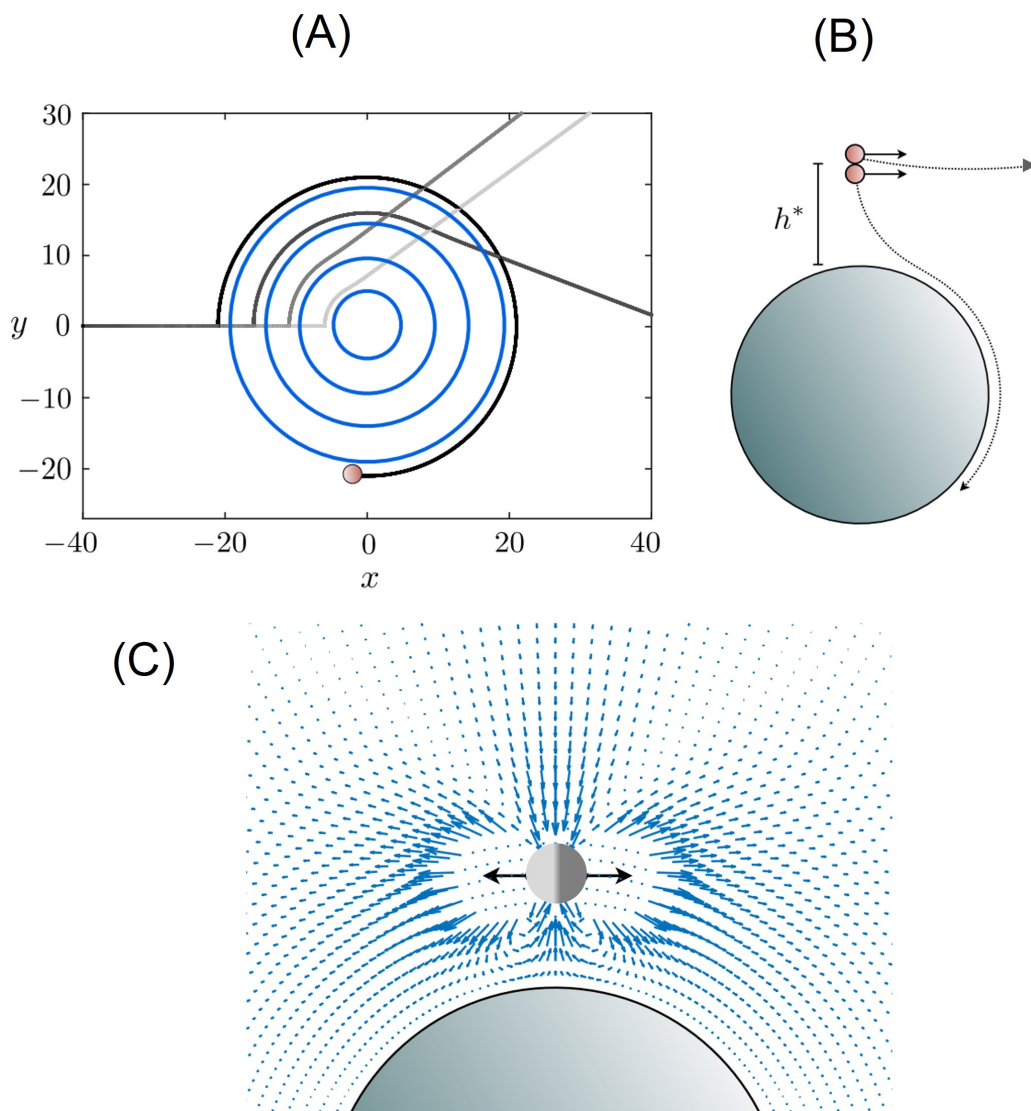


**Figure 1.6:** (A) A spherical Janus colloid swimming towards a passive obstacle of radius 5, 10, 15, and 20 times the particle size  $R_P$ . The critical obstacle size predicted for orbital trapping was  $R_C \approx 15R_P$ . (B) Basin of attraction  $h^*$  denotes the critical initial distance from the colloid above which the particle escapes, and below which entrapment ensues. (C) Flow field around a pusher particle near an obstacle. Image taken from [75]

For active particles encapsulated inside membranes or elastic compartments, a number of emerging dynamics have been numerically investigated. Paoluzzi *et al.* [76] and Daddi-Moussa-Ider *et al.* [77] used numerical simulations to investigate the shape changes and spontaneous migration of a flexible vesicle filled with active particles.

## 1. STATE OF THE ART

---

Changes in the vesicle shape from circular to elongated with a decrease in the number of encapsulated particles were reported. Active particle accumulation in the high curvature regions of the membrane was also reported. Recently, Rao *et al.* [78] used DOPC vesicles and active spherical PS-Pt colloids ( $R_P = 1 \mu\text{m}$ ) to experimentally demonstrate the large shape deformations in GUVs caused by active particles.

### 1.6 Wrapping of spherical colloids by GUVs

Pioneering experimental investigations on the spontaneous interaction between bare colloids and GUVs were performed by Dietrich *et al.* [79], using DMPC and SOPC GUVs interacting with micron-sized latex beads. A theoretical model based on the balance between adhesion and stretching of the GUV was also proposed to describe the experimental results. Shigyou *et al.* [80] on the other hand, used centrifugation forces to drive partial and complete wrapping of particles by lipid vesicles. They used DOPC GUVs and polystyrene colloids of different sizes. Complete engulfment of colloids was observed for colloids with  $R_P = 100 \text{ nm}$ , while for  $R_P = 200 - 800 \text{ nm}$  partial engulfment was observed. The translational diffusion of the colloids immersed in the membrane was found to agree with the DADL model [81] for spherical particles moving within a viscous membrane of surface shear viscosity  $\eta_s = 2 \times 10^{-9} \text{ Pa.s.m}$  [82].

Dufresne *et al.* [83] recently investigated the wrapping of micron-sized particles by GUVs showing low membrane tensions and weak reversible adhesion. Membrane-particle interaction was continuously tuned using the depletion attraction by polyethylene glycol (PEG) with a molecular weight of  $105 \text{ g.mol}^{-1}$ . PS colloids possessing  $R_P = 0.54 - 1.03 \mu\text{m}$  and POPC GUVs were investigated. As a function of the PEG concentration, activated wrapping and spontaneous wrapping was observed for colloids of different sizes. Spontaneous wrapping describes the particle engulfment by GUVs in the absence of any external forces. Activated wrapping instead was achieved upon the application of an optical trapping force on the particle to promote contact with the membrane. Figure 1.7(A,B) shows a GUV with low membrane tension (floppy GUV). The solid substrate was coated with poly(ethylene glycol) diacrylate (PEG-DA) to reduce membrane adhesion with the substrate. Figure 1.7(D) shows confocal microscopy images of a fluorescent polystyrene particle  $R_P = 0.5 \mu\text{m}$  in close proximity to a fluorescently labeled GUV. The particle is 'unwrapped,' meaning that the particle's center

## 1.6 Wrapping of spherical colloids by GUVs

of mass remains outside the convex hull of the GUV and that there is no significant membrane deformation occurs. Figure 1.7(E), on the other hand, depicts a particle that has been 'wrapped.' Not only has the particle been dragged to the other side of the membrane's convex hull, but the membrane has also been severely deformed and now covers a significant portion of the particle's surface area. At high concentrations of PEG, spontaneous wrapping of colloids was also reported.

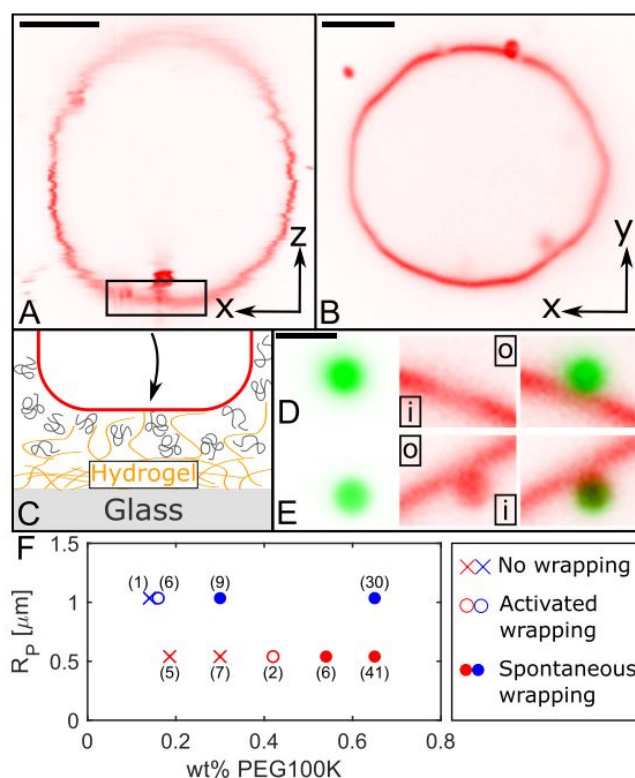


**Figure 1.7:** (A,B) Cross-section sections of confocal image stacks of a GUV sedimented on a PEG-DA hydrogel, which exhibits obvious thermal fluctuations in the presence of 0.65% weight percent PEG in the solution. The length of the scale bars is 10 μm. (C) Schematic of the experimental system, and hypothesized mechanism for reduced depletion interactions against a hydrogel. (D,E) Confocal images of 1.1 μm PS particles (green) and POPC membranes (red). The inside and outside of the GUV are indicated by i and o respectively. The particle in (D) with 0.24 wt% PEG100K does not deform the membrane. The membrane wraps the particle in (E) at 0.53 wt% PEG100K. The scale bar is 2 μm in length. (F) Phase diagram based on the particle radius and amount of PEG depletant in the system. Numbers next to each data point indicate the number of membrane-particle pairs that were probed in each condition, Image taken from [83].

## 1. STATE OF THE ART

---

Note that until now the engulfment studies have been limited to bare colloids and engulfment of Janus colloids by GUVs has not been experimentally investigated. Moreover, recent theoretical studies provide new insights into the dynamics of engulfment of bare and Janus particles by GUVs [9, 84]. Not only the particle size but also the membrane spontaneous curvature  $m$  are predicted to play crucial roles in particle engulfment by GUVs [9]. Free (non-engulfed), partial and complete engulfed states are predicted to occur in experimental conditions accessible to optical microscopy: micron-sized particles and GUVs. Note that the partial engulfment of bare particles is expected only in a narrow range of experimental parameters [9]. Janus colloids possessing two faces with tunable adhesion strengths may offer an additional opportunity to investigate the particle engulfment state diagram. Finally, for a Janus colloid partially engulfed by a GUV (showing differences in the mean membrane curvature), a curvature induced force is predicted to act on the Janus particle, which tends to move the colloid towards the lower membrane curvature regions (if the particle was originally in the outer phase of the GUV) [85].

### 1.7 Thesis outline

In **chapter 2**, we lay out the fundamental information of the components involved in this thesis, along with the design and details of the experimental procedures such as the fabrication of Janus colloids and GUVs as well as their characterization.

Experimental results for motion of Janus colloid close to a solid boundary, in- and out-of thermal equilibrium are reported in **chapter 3**. The spontaneous interaction dynamics of Janus colloids with GUVs are investigated in **chapter 4** in both passive and active conditions.

In **chapter 5** the engulfment of passive Janus colloids by GUVs is investigated using external forces. The effect of engulfment/wrapping of Janus colloids on the active motion is discussed in **chapter 6** along with future perspectives and the final conclusion of the thesis.

## Chapter 2

# Materials & methods

## 2. MATERIALS & METHODS

---

This chapter aims at describing the materials and procedures involved in the fabrication and characterisation of Janus colloids and GUVs. The first half of the chapter covers the fabrication of the components while the second half is dedicated to describing the experimental design and characterization.

Various microscopic techniques were used to characterize colloids and GUVs. While the procedures for the sample preparation, image acquisition and analysis will be addressed later in the chapter, the findings will be described in the following chapters.

### 2.1 Janus colloid fabrication

Spherical beads of Silica and Melamine Resin (purchased from Microparticles GmbH - Germany) were used in our experimental systems because of their higher density allowing purely two-dimensional motion sustained at the solid-liquid interface. The spherical geometry of the colloids yields simplicity in the fabrication of Janus colloids with a platinum hemisphere. We used two different sizes of microspheres, Silica (SiO<sub>2</sub>-R) colloids with a radius of  $R_P \approx 2 \mu\text{m}$  and fluorescent Melamine resin (MF-FluoOrange) with  $R_P \approx 1 \mu\text{m}$  radius with Excitation/Emission wavelength at 560 nm/584 nm respectively. To fabricate Janus colloids, we employed the technique of metal sputtering deposition method to deposit a thin solid film of platinum onto the colloids [86]. To prepare a colloidal suspension, first, bare colloids were diluted in ethanol to achieve a 0.2% concentration by volume from a 50 mg/mL stock solution.

Particle	Nominal Radius $\mu\text{m}$	Standard deviation	Density $\text{g}/\text{cm}^3$	Refractive Index
SiO <sub>2</sub> -R	2.15	0.065	1.85	1.47
MF-R	1.245	0.05	1.51	1.68

**Table 2.1:** Physical properties of SiO<sub>2</sub> and MF colloids

To begin, a monolayer of either silica or MF colloids was prepared on a 6" diameter silicon wafer (Figure 2.1(A)) using the drop casting method: drops of already prepared particle suspension were regularly deposited with a 100  $\mu\text{L}$  pipette, utilizing 6 mL of the particle suspension to achieve maximum monolayer coverage on the wafer. Because of capillary forces caused by solvent evaporation, particles may exist in small clusters rather than being evenly dispersed (Figure 2.2(A)).



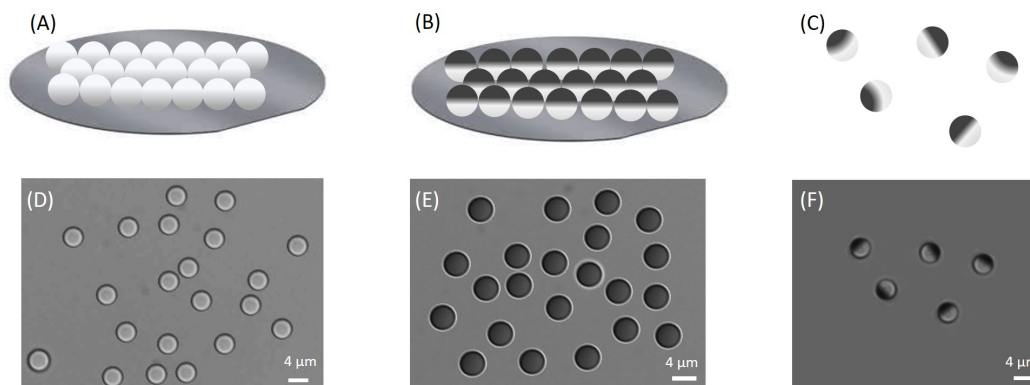


**Figure 2.1:** Top row: schemes showing fabrication of  $\text{SiO}_2\text{-Pt}$  Janus colloids. (A)(B) Array of  $\text{SiO}_2$  colloids on a silicon wafer before and after platinum deposition. (C) Colloids in solution, with Janus boundary perpendicular to the substrate. Bottom row: bright-field microscopy images for colloids in a solution (D) bare colloids, (E) after platinum deposition and (F)  $\text{SiO}_2\text{-Pt}$  particles in a solution after being detached from the substrate.

Following that, by using vacuum metal sputtering (Edward Auto 306 evaporator), a thin platinum layer was deposited on the substrate (Figure 2.1(B)). As seen in Figure 2.1(F) under bright-field microscopy, platinum layer appears darker than the bare face of the  $\text{SiO}_2\text{-Pt}$  colloid, which can be attributed to the difference in the refractive index of platinum and silica. However, for smaller MF-Pt colloids, a clear difference between the platinum layer and bare part was impossible to observe under bright-field microscopy as seen in Figure 2.2(A). To distinguish between the pristine and platinum coated sides of MF-Pt particles, fluorescence microscopy was employed (Figure 2.2(B)) where the bare part appears brighter while the platinum hemisphere appears darker.

The binary image in Figure 2.2(C) for the colloids was created using ImageJ's thresholding technique, in which each pixel is replaced by a black or white pixel depending on a preset threshold. The use of a binary image thresholding technique results in a simple tool for identifying Pt-coated face and particle orientation during active and passive Brownian motion of the colloids. This technique will be discussed in detail in the latter part of the chapter.

## 2. MATERIALS & METHODS

---

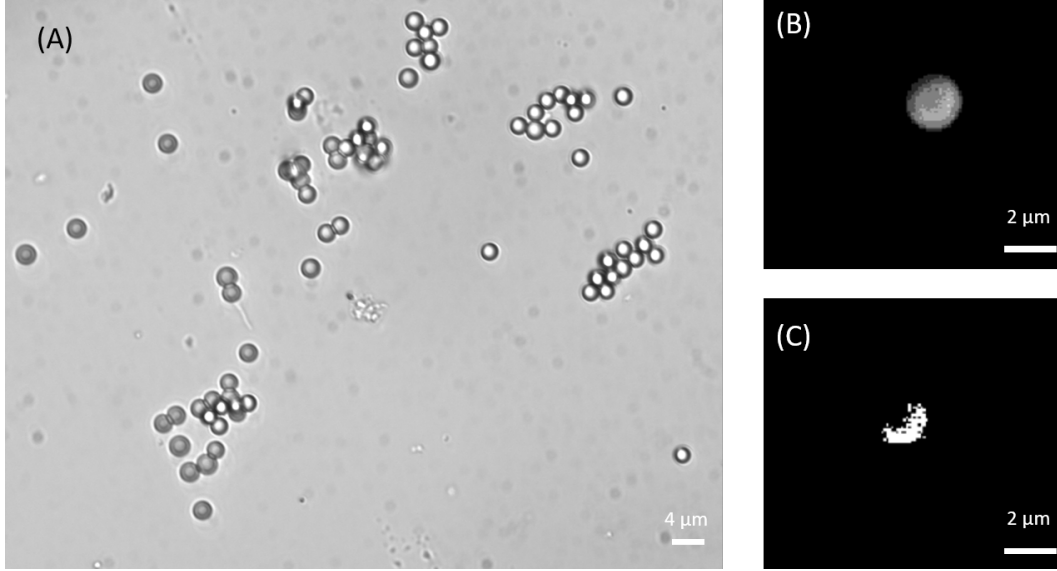


**Figure 2.2:** (A) Bright-field microscopy image of  $R_P \approx 1 \mu\text{m}$  MF colloids existing in clusters after solvent drying. Janus boundary for MF-Pt colloids is unnoticeable in bright-field microscopy, (B) Fluorescent microscopy image of an MF-Pt colloid with the darker partial Pt coating. (C) Binary image of MF-Pt colloid after applying threshold limits.

### 2.1.1 Analysis and characterisation of Janus colloids

#### 2.1.1.1 Platinum layer thickness by light reflectivity

To determine the thickness of the platinum layer deposited on the particles by physical vapour deposition, we carried out light reflectivity using a Multiskop Ellipsometer (Optrel, Germany). First, a quarter of a 6 inch silicon wafer disk was masked with another wafer without using any adhesive material that could leave a residue after removal. After which, a thin coating of the same amount of platinum as employed in the fabrication of Janus colloids was sputtered with the vapour deposition process (section 2.1). Following deposition, the mask is removed from the wafer, exposing the immaculate surface beneath. The wafer is then examined using light reflectivity at various spots on both the Pt-coated and untreated regions. Fresnel equation for polarized light intensity ( $I_P$ ) as a function of the incident angle ( $\phi$ ) was used to fit the reflectivity curve plotted in Figure 2.3 to obtain the thickness of the deposited platinum which was found to be  $6 \pm 1 \text{ nm}$ .

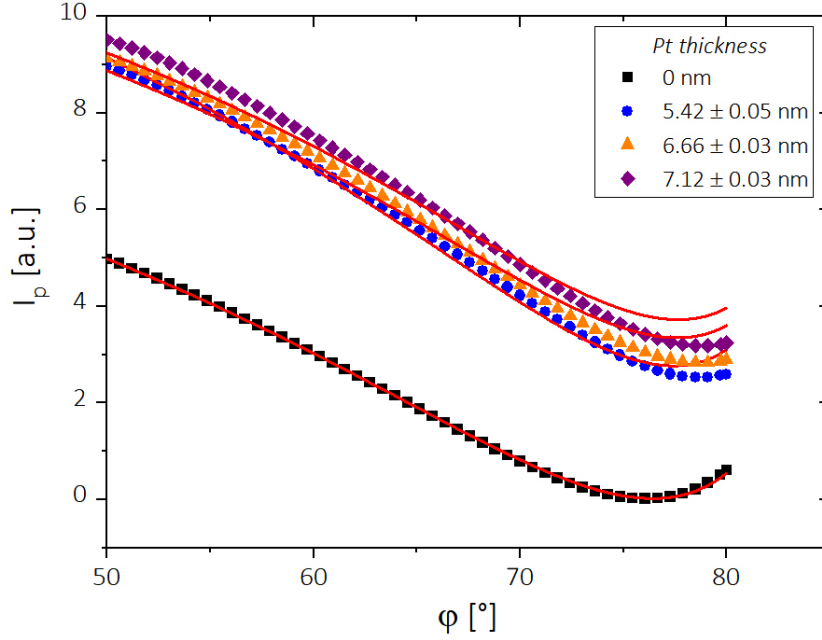


**Figure 2.3:** Laser-light reflectivity curve to measure platinum thickness at different spots on a silicon wafer substrate.

### 2.1.1.2 SEM Analysis

Scanning electronic microscopy (SU 8010 Ultra High-Resolution Field Emission SEM) was used to get the actual particle size distribution (see Table 2.2) as well as to obtain finer details on the deposited Pt layer. When compared to bare SiO<sub>2</sub> beads, Janus colloids display two unique zones (Figure 2.4(A),(B)). Here the bright areas correspond to the Pt-covered region. This is because the SEM image is constructed from secondary electrons generated by atoms excited by the electron beam, and the intensity of secondary electron emission is greater for materials with a higher atomic number.

Janus colloid	Nominal radius $\mu\text{m}$	Actual radius ( $\mu\text{m}$ ) $R_P = \bar{R}_P \pm \delta \bar{R}_P$
SiO <sub>2</sub> -Pt	$\approx 2$	$1.96 \pm 0.05$
MF-Pt	$\approx 1$	$1.29 \pm 0.06$

**Table 2.2:** Actual radius SiO<sub>2</sub>-Pt and MF-Pt Janus colloids.

## 2. MATERIALS & METHODS

---

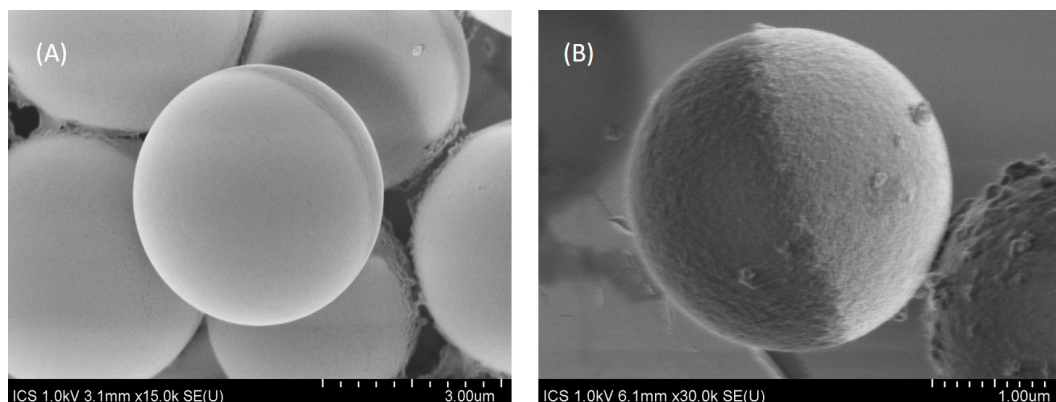


**Figure 2.4:** SEM images of (A) SiO<sub>2</sub>-Pt, (B) MF-Pt Janus colloids with darker bare side and brighter Pt coating.

Taking a look closer at the SEM images (Figure 2.5), the line where the deposited platinum and the pristine face of the colloids meet, referred to as Janus boundary, often exhibits a wavy and bumpy morphology instead of a homogeneous construction. The topology of the Pt coating on the surface of polymeric MF colloids exhibits grainy nano-roughness which can be attributed to the sputtering process when metal atoms are deposited by electron beam sputtering onto a rugged substrate, the atoms do not arrive uniformly to surface at the same moment. The surface roughness could also be attributed to the random fluctuations which are inherent in the process. It was also reported that a peak in surface roughness of up to 10 nm thickness was detected in sputtered Au films [87].

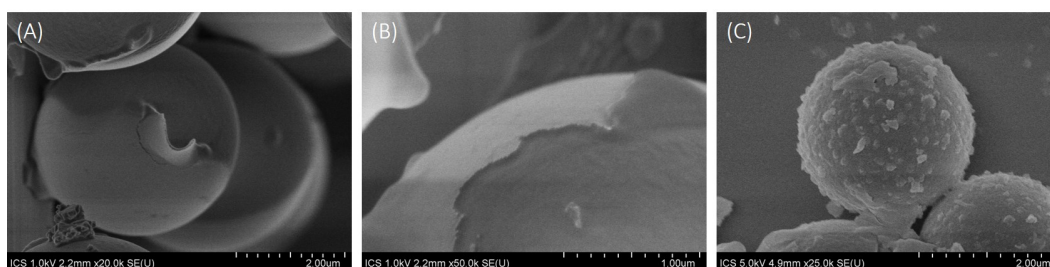


**Figure 2.5:** SEM images of (A) SiO<sub>2</sub> colloids showing shadowing effect due to clustering of particles. (B) Image showing the wavy and bumpy morphology of the Janus boundary, (C) MF-Pt colloids exhibiting nano-roughness and inhomogeneities.

The bumpy and wave-like appearance of the Pt-cap Janus boundary can be associated to re-emission and shadowing effects due to extra adjacent particles during the

Pt deposition process. Shadowing can be caused by obliquely incident Pt atoms preferentially depositing on the surface "hills" resulting in a long-range geometrical effect [88]. At the same time, bouncing non-sticking atoms can rebound off hills and deposit on a "valley", which is known as the re-emission effect. As seen in Figure 2.6, when a colloid is located on the substrate away from the cluster and in an isolated region, the re-emission effect induces a homogeneous Pt coating which might span more than a hemispherical pattern on the colloid. In our experiment, as mentioned in the previous section, the drop coating process leads to the evaporation of the solvent, giving rise to aggregation of the colloids on the surface [89] and when the colloidal particles exist in such a closely packed aggregate, the neighbouring beads act as shields which prevent the sputtered atoms of platinum to be deposited into the "valley" which leads to an uneven curved Pt-cap Janus boundary (Figure 2.5).

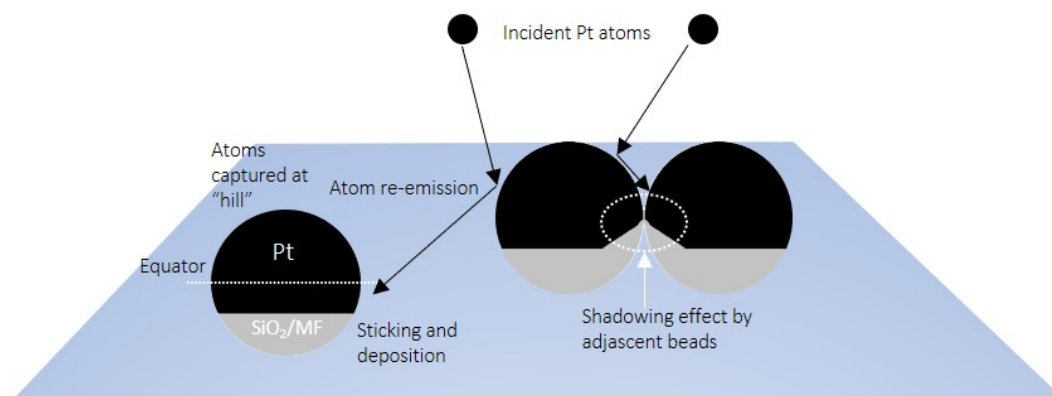


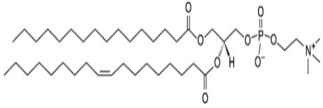
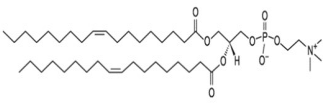
**Figure 2.6:** Mechanism for formation of inhomogeneities in platinum coating during metal sputtering process.

## 2.2 GUV formation

The main phospholipids used in this work were POPC (1-palmitoyl-2-oleoyl-sn-glycero-3-phosphocholine) and DOPC (1,2-dioleoyl-sn-glycero-3-phosphocholine) acquired from Avanti polar lipids-USA and were received in dried form (Table 2.3). The dried lipids were dissolved in chloroform (HPLC grade from Sigma Aldrich, MO-USA) at a concentration of 10 mg/mL to make the stock solutions. For the experiments, a 1 mg/mL lipid solution was prepared and labelled with nitrobenzoxadiazole (NBD) fluorophore to be used in gel assisted formation method or electroformation method, to aid the

## 2. MATERIALS & METHODS

self assembly of the lipids into vesicles. Both the stock and diluted solution were kept refrigerated at  $-20^{\circ}\text{C}$ .

Lipid	Complete name	Mw (g/mol)	$T_m$ , Transition temperature ( $^{\circ}\text{C}$ )	Chemical formula
POPC(16:0-18:1)	1-palmitoyl-2-oleoyl-sn-glycero-3-phosphocholine	760	-3.5	
DOPC(18:1)	1,2-dioleoyl-sn-glycero-3-phosphocholine	785.6	-17	

**Table 2.3:** Properties of POPC and DOPC lipids.

According to Reeves and Dowben(1969) [90], GUVs can be obtained in high yield by spreading a dry film of the bilayer on a substrate and slowly hydrating it at room temperature. For successful GUV formation, the lipids must be in their fluid state which refers that the hydration/swelling of the GUVs must be carried out at  $T > T_m$  of the lipids, where the combination of osmotic pressure, electrostatic interactions, and the hydrophobic effect appears to be the driving mechanisms for vesicle formation [91]. Although many different methods have been developed we primarily use the two methods below to aid the self assembly and subsequent hydration of the vesicles (Figure 2.7).

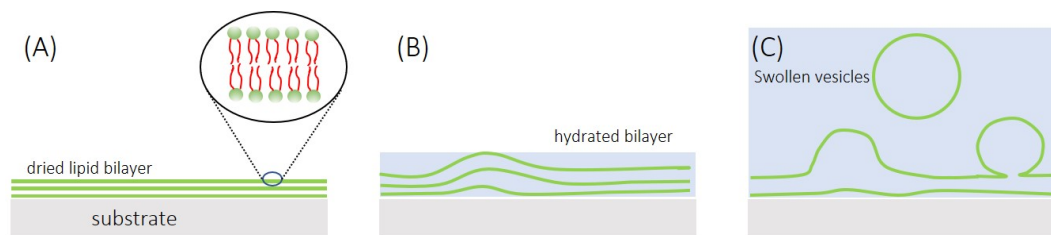


**Figure 2.7:** Schematic illustrating three steps during swelling of lipid bilayer: (A) dried lipid bilayers on a substrate, (B) beginning of hydration and self assembly of vesicles, (C) swollen vesicles detaching from the bilayer.

### 2.2.1 Gel Assisted Swelling

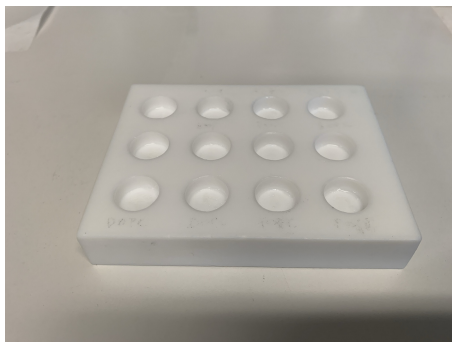


**Figure 2.8:** Image of a home made PTFE plate with  $4 \times 3$  grid of wells for vesicle growth. Each well is 12 mm wide and 10 mm deep.

The approach of gel-assisted swelling was developed by our team and remained our method of choice for growing vesicles for this study [92]. This method approaches the GUV growth in a similar manner originally proposed in Reeves and Dowben(1969), with a few modifications to the swelling process where instead of a pristine glass substrate a polymer-based gel is used. After the lipid solution was spread and dried on the gel, after hydration with sucrose solution, a continuous buffer influx flow from the porous gel significantly reduces the swelling time of the GUVs from days to minutes. Although this approach can be used for various lipids, for our system we mainly concentrated on POPC and DOPC phospholipids where giant vesicles obtained from this method can be observed even after 20-30 minutes of hydration and most of the obtained vesicles were unilamellar without much of any visible defects like attached debris or internal structures. For a polymer gel base, we use chemically cross-linked polyvinyl alcohol (PVA) and circumvent polymer encapsulation as the lipids do not penetrate the PVA film, but are stacked on the top of the matrix as bilayers. The detailed protocol for this method is as follows:

- We first start with a homemade polytetrafluoroethylene (PTFE/Teflon) plate as shown in Figure 2.8, having a  $4 \times 3$  grid of chambers with 12 mm of width and 10 mm of depth for vesicle growth. The plate is thoroughly cleaned with solvents (Chloroform/Acetone/Ethanol) and Milli-Q water before being dried in the oven for at least 10 minutes.

## 2. MATERIALS & METHODS

---

- Then we prepare the PVA solution in Phosphate-Buffered Saline (PBS) by first dissolving a PBS tablet ( $\sim 2$  g) in 200 mL of Milli-Q water, after which a 5% w/w PVA ( $M_w = 149000$  kg/Mol) solution is prepared by constant stirring at  $80^\circ\text{C}$  for 3 hours. Simultaneously, we also prepared 150 mM solutions of sucrose and glucose for lipid hydration and sedimentation respectively.
- After cleaning the PTFE plate,  $100\ \mu\text{L}$  of PVA gel is spread in the chambers and dried in the oven for 45 minutes at  $80^\circ\text{C}$ .
- $10\ \mu\text{L}$  of the lipid solution in chloroform (1 mg/mL concentration) is spread on the dried gel and then kept in a desiccator for 10 minutes for evaporation of any remaining chloroform.
- $300\ \mu\text{L}$  of sucrose solution is added to the lipid bilayer for hydration after which the PTFE plate is sealed with a cap and the vesicles are left to grow for 2-3 hours to have a higher yield.
- The vesicle solution is then removed from the chamber into a 2 mL centrifugation tube (Eppendorf, France) and 1 mL of glucose is added to the vesicles to sediment them to the bottom of the tube because of the density mismatch in the interior and exterior of the vesicles.

The average size of GUVs obtained from this method was  $R_{GUV} = 11 \pm 5\ \mu\text{m}$  in radius as seen from Figure [2.9](#), which was determined using vesicle tracking and characterization method detailed in the later section (section [2.4.2](#)).



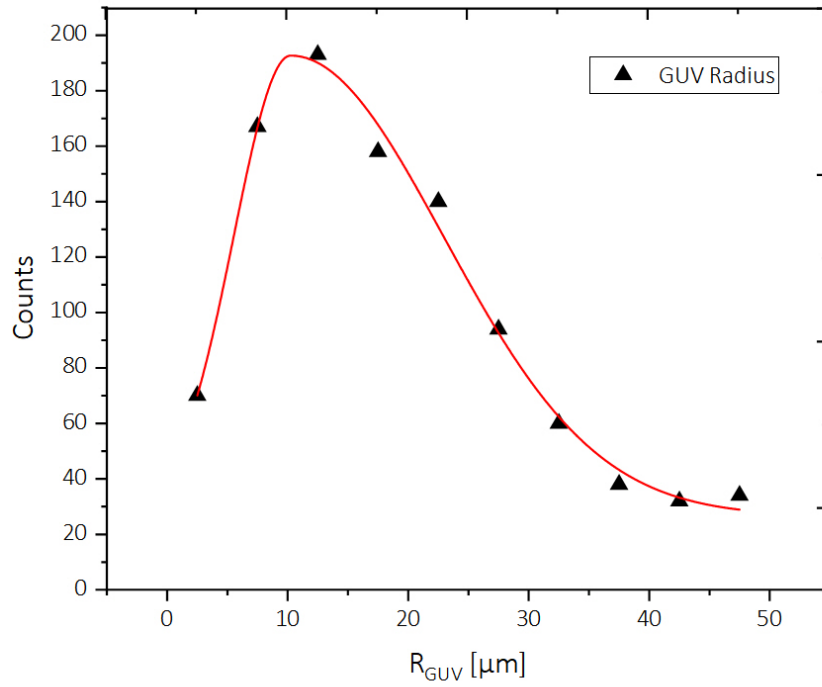


**Figure 2.9:** Radius size distribution histogram curve for GUVs where the solid line is a fit yielding average size of  $R_{GUV} = 11 \pm 5 \mu\text{m}$ .

## 2. MATERIALS & METHODS

---

### 2.2.2 The Electroformation/Electroswelling method



**Figure 2.10:** Image of a home made PTFE electroformation cap with platinum electrodes. The gap between the electrodes was about 2.5 mm.

Perhaps one of the most commonly used method in GUV formation is "Electroformation" or "Electroswelling", first developed by Angelova and Dimitrov in 1986 [93] by which the GUVs are generated by controlling the hydration of bilayer-forming lipids that have been deposited as a thin film on a solid surface. Unlike gel assisted swelling, in electroformation method, the lipid film hydration is aided by externally applied alternating current (AC) and hence requires an electrically conductive surface on which the lipids are spread. In our case, we use a homemade Teflon cap with platinum electrodes on which the lipids are spread (see Figure 2.10). The brief protocol for the electroformation process is described below:

- First, we start by thoroughly cleaning the platinum electrodes of the cap where the lipids are to be spread with Milli-Q water and solvents. The washed electrodes are then thoroughly dried with pressured air to remove any traces of solvent residue.
- 5  $\mu\text{L}$  of lipid stock solution (1 mg/mL) was then spread on the inside of each electrode using a glass micro syringe. The lipids are properly spread throughout the electrodes to achieve maximum lipid coverage.
- The Teflon cap is then placed in a desiccator and dried for 15-20 minutes to completely dry the lipids and rid of any remaining solvent from the stock solution

## 2.3 Interaction between Janus colloids and GUVs

---

as well as the cleaning process.

- In a 2 mL centrifugation tube, 300  $\mu\text{L}$  of swelling solution is filled which in our case was 150 mM sucrose solution, after which the Teflon cap is inserted so that the platinum electrodes are completely immersed in the swelling solution. The silicon ring around the Teflon cap provides a vacuum seal keeping the immersed electrodes secured from atmospheric disturbances.
- The electrodes are then connected to an AC field generator set at a frequency of 10 Hz and the voltage applied across the electrodes was kept at 0.1 V and the vesicles were allowed to grow for 3-4 hours.
- After the swelling, the connectors are first removed from the cap before removing the Teflon cap altogether from the centrifugation tube. After which, 1 mL of 150 mM glucose solution was added to sediment the vesicles to the bottom.

## 2.3 Interaction between Janus colloids and GUVs

In order to study emerging dynamics resulting from the interaction of giant vesicles and Janus particles, we consider two different routes to trigger the interaction. In the first case, we simply mix a solution containing GUVs and a dispersion of Janus colloids in the presence or not of Hydrogen Peroxide. In the second method, in order to trigger particle engulfment by GUV membranes, we applied external forces in the range of  $10^{-12}$  N up to  $10^{-9}$  N by optical trapping and centrifugation respectively.

## 2. MATERIALS & METHODS

---

### 2.3.1 Spontaneous interaction of Janus colloids and GUVs

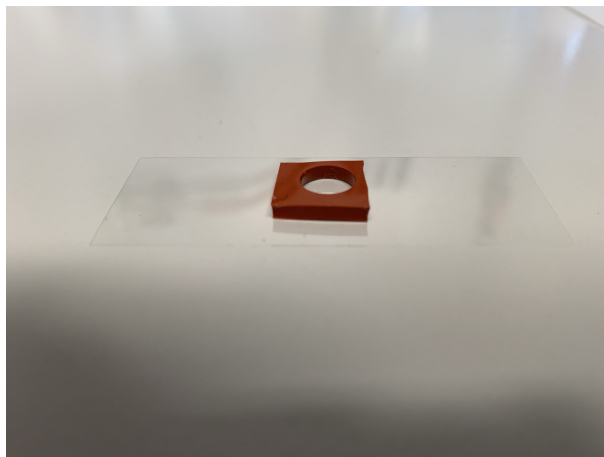


**Figure 2.11:** Image of a self adhesive Silicon isolator well (volume of  $150 \mu\text{L}$ ) on a glass slide for microscopy where particle-GUV contact is only by sedimentation due to gravity.

To observe the spontaneous interaction between a Janus colloid and a GUV, we simply mix a dispersion of colloids with a solution of GUV in a sample cell that constitutes of glass coverslip of  $0.17 \text{ mm}$  thickness on which a self-adhesive silicon isolator is placed as seen from Figure [2.11](#). This silicone isolator acts as a trough of roughly  $150 \mu\text{L}$  in volume. For a typical experiment, the spontaneous interaction between Janus colloids and GUVs occurs only under the force of gravity. First, the trough is filled with  $120 \mu\text{L}$  of glucose solution to maintain the same osmotic pressure in the solution as the vesicles are already sedimented in glucose. The Janus colloids are then detached from the silicon wafer using  $10 \mu\text{L}$  of glucose solution along with gentle agitation using pipette tip [94](#) and this dispersion of colloidal particles is then added to the sample cell before adding  $1\text{--}5 \mu\text{L}$  of vesicles collected from the bottom of the centrifugation tube. The silicon isolator is then closed from the top using a second coverslip to avoid cell contamination, reduce evaporation, and inhibit convective flows within the system. Note that all components from both the coverslip to the silicon isolator are cautiously cleaned with chloroform, acetone, ethanol, and Milli-Q water before being thoroughly dried to keep the sample as clean as possible.

### 2.3.2 Force driven interaction between Janus colloids and GUVs

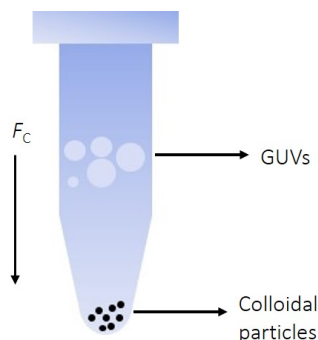


**Figure 2.12:** Schematic for force driven interaction between GUVs and Janus colloids. Particles are sedimented to the bottom of the centrifugation tube and the vesicles are added and brought in contact with different force of centrifugation ( $F_c$ ).

To impose forced contact between particles and the GUVs, we implemented a centrifugation routine [80]. We begin with filling 120  $\mu\text{L}$  of glucose solution into a 1 mL centrifugation tube which is followed by the addition of 10  $\mu\text{L}$  of glucose-colloidal suspension extracted from the silicon wafer as mentioned in the section above. The particles being heavier, they do not require longer centrifugation time to reach the bottom of the centrifugation tube. After the particles are sedimented to the bottom the 1  $\mu\text{L}$  of GUVs are added to the centrifugation tube (Figure 2.12) which are then centrifuged and brought in contact with the already sedimented Janus particles with different centrifugation forces. For our experiments we primarily focused on Relative Centrifugal Force (RCF) of  $RCF/g = 106 - 1700$ .  $RCF = 1.12r \left(\frac{RPM}{1000}\right)^2$ , where RPM (Revolutions Per Minute) is the speed of the centrifuge and  $r$  is the rotor radius (95 mm). The centrifugation time was kept constant at 4 minutes for all different RCF trials. Apart from centrifugation, the optical force from the optical tweezer (described in section 2.5) was also used to initiate force-driven contact between bare colloids and GUVs.

## 2.4 Image Analysis and tracking

### 2.4.1 Motion tracking for Janus colloids

Tracking of the centre of mass (COM) and orientation for Janus colloids in both active and passive conditions was realised using a Hamamatsu Orca Flash-4 CMOS camera

## 2. MATERIALS & METHODS

---

with x60 Nikon water immersion objective mounted on Nikon Elipse TE2000 inverted microscope. The videos were recorded in both fluorescent and bright-field microscopy at a resolution that ranges from  $[128 \times 128 - 2048 \times 2048 \text{ pixel}]$  in a 10 to 1000 frames per second (fps) range. Videos having a wide field of view can aid to improve data analysis statistics, while higher magnification videos, on the other hand, provide information on the orientation and rotation of the Janus colloids which will be discussed in the next section.

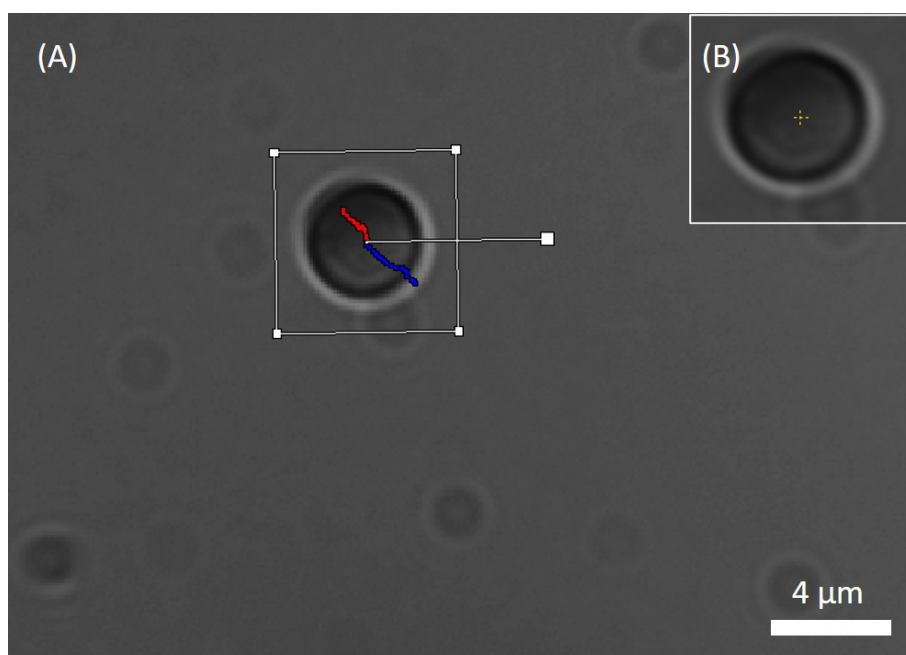


**Figure 2.13:** Tracking COM of a SiO<sub>2</sub>-Pt colloid using *Blender*. (A) Marker following the centre of the particle with the red and blue worms indicating the position of the particle in the previous and next 50 frames of the trajectory. (B) Precise position of the marker on the colloid.

Particle tracking was performed using the motion tracking feature of an open-source software called *Blender* which utilizes Kanade-Lucas-Tomasi feature tracking algorithm [95] using spatial intensity information to direct the search for a particle position yielding the best match. As we add the marker to the COM of particle to be tracked as seen from Figure 2.13, that area of pixels comprised in the marker known as reference pattern are analysed over the range of frames in the movie clip to lock onto the pattern as the particle moves on the 2D space. During the analysis, as the tracking proceeds to the

subsequent frame, many positions are sampled in the search region around the centre point of the tracker. While some of those sampled positions match with the reference pattern more closely than the other, the tracking algorithm finds the position in the search region which is closest in resemblance to the reference pattern with sub-pixel accuracy. The tracker then assigns a correlation value to each frame that is analysed by measuring how close the match is to the reference pattern. This tracking method was the one we found the fastest as most reliable for tracking the COM of the colloids in both active (Figure 2.14) and passive (Figure 3.1) conditions. The other tracking methods tested included "Stat tracker St. Andrews" developed by Graham Milne on LabView (National Instruments), Python based particle tracking module "Trackpy" and also Mosaic suit from ImageJ. However, for the our system in bright-field microscopy, *Blender* proved to be the most reliable and the fastest. *Blender* also includes Python console along with a standalone module "bpy" which allows us to easily extract the particle position over time [time t (s), x ( $\mu\text{m}$ ), y ( $\mu\text{m}$ )] in lab coordinate system. The raw Python script to extract the coordinates for the position can be read in Appendix A1.

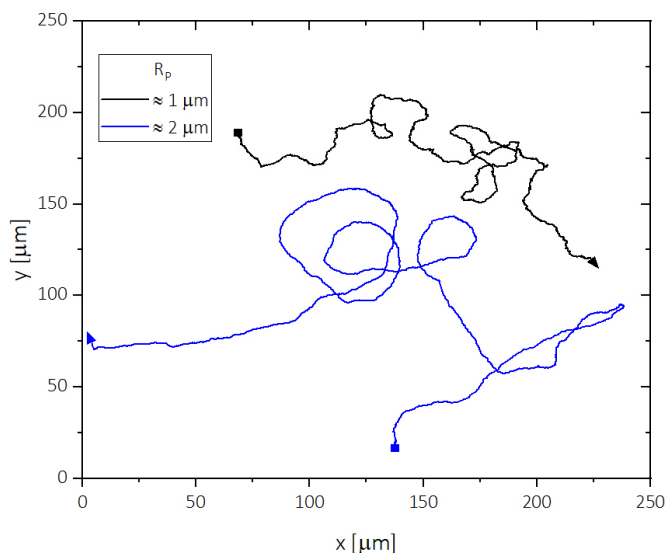


**Figure 2.14:** Center of mass trajectory for self propelled MF-Pt ( $R_P \approx 1 \mu\text{m}$ ) and SiO<sub>2</sub>-Pt ( $R_P \approx 2 \mu\text{m}$ ) colloids in 2% H<sub>2</sub>O<sub>2</sub>, sedimented close to the bottom of the sample cell, where the solid square and triangle indicate the beginning and the end of the trajectory respectively.

## 2. MATERIALS & METHODS

---

### 2.4.1.1 Tracking of Janus orientation

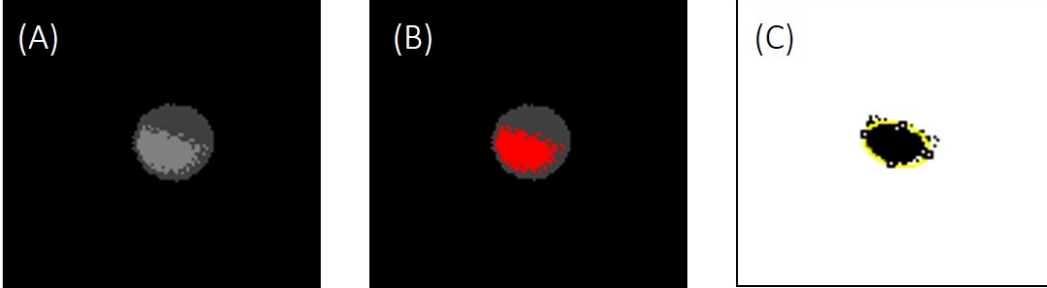


**Figure 2.15:** (A) Fluorescent image of an MF-Pt colloid in bulk where the darker side is platinum coating. (B) After adjusting threshold the bare MF side is selected (in red) for conversion into black pixels. (C) Binary image after fitting an ellipse (yellow line) on the bare side of the colloid to track the orientation.

As discussed in the previous section, we aim at extracting the orientation information of the Janus colloids. We use ImageJ thresholding technique, for that we first start our analysis with MF-Pt colloids ( $R_P \approx 1 \mu\text{m}$ ) in fluorescent microscopy. As the MF colloids themselves are fluorescent to begin with (Excitation/Emission range at 560 nm/584 nm) the platinum coating on these colloids results in the reduction in fluorescence from the platinum coated hemispheres which makes them a suitable candidate to extract information on the orientation of the colloids. As we are only interested in the rotational behaviour of the particles, the videos were recorded in fluorescent conditions with a high frame rate ( $\sim 1000$  fps). To analyse the video using ImageJ, first, the clips were treated by adjusting the brightness and contrast (Figure 2.15(A)) to have distinct regions of the colloids reducing the effect of anomalies due to fluorescence. After the contrast adjustment, we proceed to threshold treatment of the image where the lower limit of threshold is selected based on the contrast maximum (Figure 2.15(B)), the pixels which lie below this lower threshold will be converted to black (Pt surface) while the others are transformed to white pixels (MF surface) resulting in a binary image. On the resulting image using the "create selection" functionality of ImageJ that yields a selection of the entire area, which serves as a basis to fit an ellipse on the centroid of the visible MF face in the image (Figure 2.15(C)), we also use "fill" functionality to cover any gaps that might be present inside the ellipse. The ellipse fit then yields the area (used to calculate out-of-plane rotation) of the bare side along with information like in-plane angle, aspect



ratio, as well as the coordinates of the ellipse. As imageJ treats only the selected frame of a video, a simple macro can be written to run the routine over the whole video. This ImageJ routine macro can be found in Appendix A2. For the rotational analysis, we mainly focused on MF-Pt colloids as the SiO<sub>2</sub>-Pt colloids could only be observed in bright-field microscopy and in the transmission mode of such microscopy it was very difficult to observe the rotation of the colloids clearly. Larger particles  $R_P \approx 2 \mu\text{m}$  even fluorescent are difficult to analyse compared to smaller particles  $R_P \approx 1 \mu\text{m}$  because of a minimum in the fluorescent intensity around the COM of the particle.

### 2.4.2 Vesicle Size and position

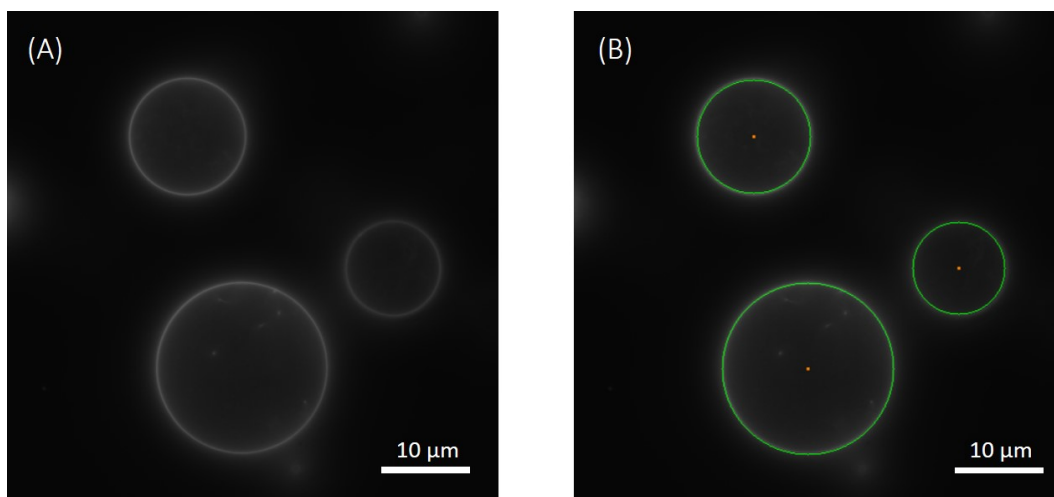


**Figure 2.16:** (A) Fluorescent image of GUVs prepared using gel formation method. (B) Tracking vesicle size and position after fitting a circle (green) on the vesicle periphery using HOUGH circle algorithm.

For vesicle analysis, fluorescent microscopy was preferred over bright-field as in later a clear contour of the vesicles is hard to detect as the difference in contrast between the vesicles and the background is negligible which makes it harder to get precise information on vesicle periphery. To begin the characterisation of a vesicle, firstly, the GUV prepared using gel-assisted formation method are taken in an observation chamber and enough time is allowed to pass for the vesicles to sediment to the bottom. Images were then taken by fluorescence microscopy spanning around the whole sample space staying near the substrate and numerous images were saved for analysis. To track the size and

## 2. MATERIALS & METHODS

position of the vesicle we implement Hough Circle Transform in the OpenCV module of Python. The Hough Circle gradient [96] method is made up of two main stages, the first stage involves edge detection and finding the centres of possible circles, while the second stage is based on finding the best radius for the possible centres. The algorithm detects the edges of the vesicles using "canny edge detection". The python script for vesicle size detection can be found in Appendix A3.

### 2.5 Optical tweezer

#### 2.5.1 Setup

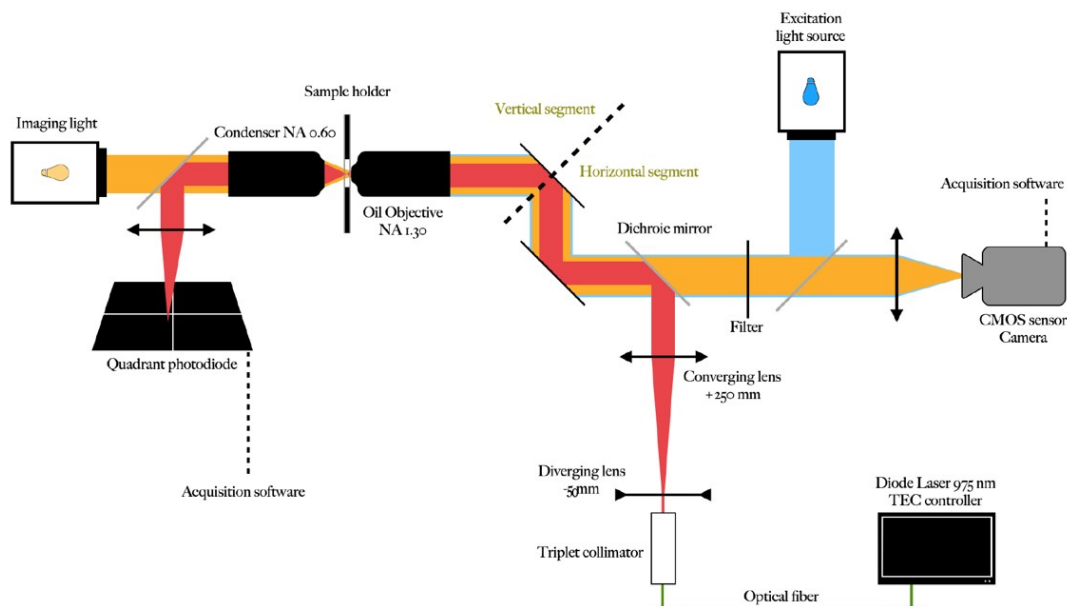


**Figure 2.17:** Scheme of modular optical tweezer setup (Thorlabs, United States)

During my PhD, I installed the OTKB Modular optical tweezers setup from Thorlabs. It was used for the experiments on bare colloids shown in Chapter 5. Schematic of the optical tweezer is shown in Figure 2.17. It consists of a laser source of 976 nm single-mode laser diode which is temperature controlled using a TEC controller and thermistor to ensure uninterrupted laser power output for consistent trapping force, where the laser power can be adjusted in the range of 0-700 mW. The laser beam is then delivered to

a triplet collimator of focal length 6.11 mm and  $NA = 0.28$  via a single mode optical fibre resulting in an output beam of 1.7 mm in diameter.

The beam then passes through a Galilean beam expander comprising of achromatic doublets with focal lengths of -50 mm and +250 mm . This expands the beam to fill the back of the objective resulting in an efficient trap. The beam is then directed towards the back aperture of the objective using a dichroic mirror along with a set of simple mirrors. We use a x100 Nikon Plan Fluorite Oil Immersion objective ( $NA = 1.3$ ,  $WD = 0.16$  mm), to focus the trapping laser beam and to image the sample.

Opposite to the laser propagation direction, is placed an illumination light generated by white light LED. This white light passes through a condenser (Nikon  $\times 10$  air condenser,  $NA = 0.25$ ) which illuminates the sample using the condensed light which then, in turn, is collected by the objective. This light received by the objective is passed through a dichroic mirror followed by a short pass filter (to avoid laser to reach camera sensor) before being focused by a tube lens (Focal length = 200 mm) onto the camera sensor plane.

In addition to the bright-field imaging of the system with white light, the tweezer setup is also capable of fluorescence microscopy which allows deeper analysis of vesicle deformation when the particles are brought in contact with the GUVs. To achieve this, an excitation light source (Nikon Intensilight C-HGFI mercury lamp) was added to the setup which is capable of exciting the NBD fluorescent marker attached to the phospholipids having an excitation peak at 470 nm and emission at 550 nm.

### 2.5.2 Calibration

Together with Florent Fessler (Intern, M2), calibration of the optical tweezer was done to achieve a precise and efficient force measurement setup since it allows access to the stiffness  $\kappa_x$  of the optical trap. While there are several methods to determine the trap stiffness the one described here is using Mean Squared Displacement of a trapped colloid. We first start by preparing a sample as mentioned in section [2.3.1](#) and trapping  $\text{SiO}_2$  bare colloids with different laser powers. The video of trapped particles was recorded with the highest frame rate possible with a CMOS camera. From the recorded video, we track the position of COM of the colloid using *Blender* as mentioned in section [2.4.1](#). When the frame rate of the recorded is sufficiently high, we can compute  $MSD$  and

## 2. MATERIALS & METHODS

---

recover the trap stiffness  $\kappa_x$  from the equation:

$$\langle [\Delta x(t)]^2 \rangle = MSD_x = \frac{2k_B T}{\kappa_x} \left[ 1 - \exp\left(-\frac{\kappa_x \Delta t}{\zeta_{Tr}}\right) \right] \quad (2.1)$$

Where  $k_B$  is the boltzman constant,  $T$  being the temperature,  $\kappa_x$  is the trap stiffness,  $\zeta_{Tr}$  the translational drag and  $\Delta t$  is the lag time. A typical  $MSD$  curve as a function of lag time is shown in Figure 2.18 for different laser powers 0-150 mW. As clear from Figure 2.18, the  $MSD$  curves feature a transition from a linear growth at short time scales which corresponds to the free diffusion behaviour which progresses to a plateau because of confinement due to the optical trap at long time scale. The higher the optical power and stronger the trap, the sooner the  $MSD$  curve reaches the plateau.

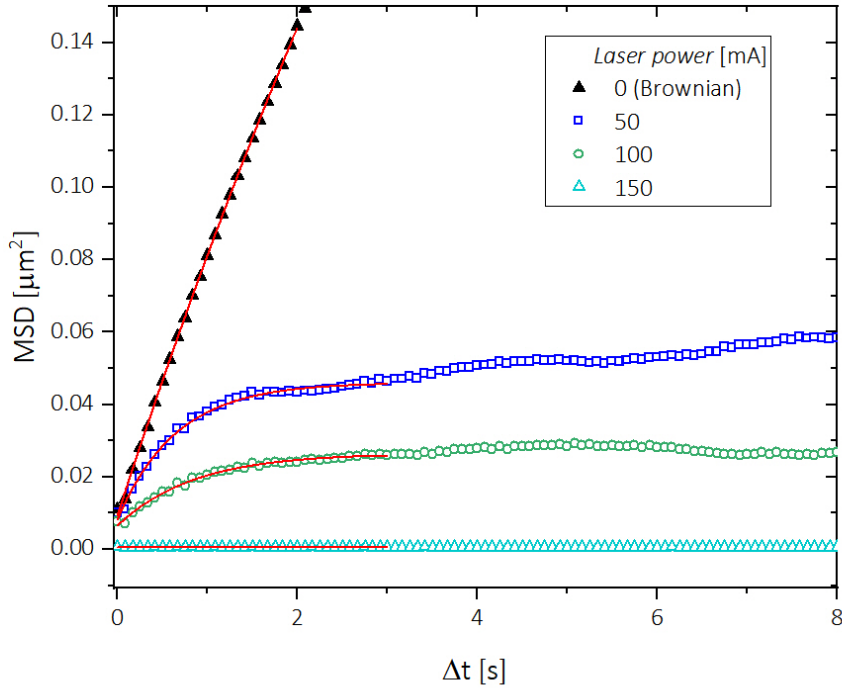


**Figure 2.18:**  $MSD$  curves corresponding to an MF colloid ( $R_P \approx 1 \mu\text{m}$ ) in Brownian and optically trapped conditions trapped with 50, 100, 150 mW laser power. The symbols are the experimental  $MSDs$  and the solid line is the theoretical fit corresponding to equation 2.1. At short time scales the  $MSD$  is diffusive while at long time scales it reaches a plateau due to trap confinement. The stronger the trap is the smaller is the value of the plateau.

### 2.5.3 Particle manipulation

We were able to trap and manipulate  $\text{SiO}_2$  and MF bare colloids to study the deformation of vesicles and uptake of colloidal particles by vesicles. Samples for analysis were prepared as per the protocol described in section [2.3.1](#). The particle is trapped at different trap strengths and manipulated along all 3 axis using manual differential micrometer drives mounted on the side of the flexure stage on which the sample is kept for observation. Apart from the manual drives, the setup is also equipped with piezo controllers which can be used to move the stage with nanometric precision. [Figure 2.19](#) shows displacement of  $\text{SiO}_2$  colloid moving in 3D space.

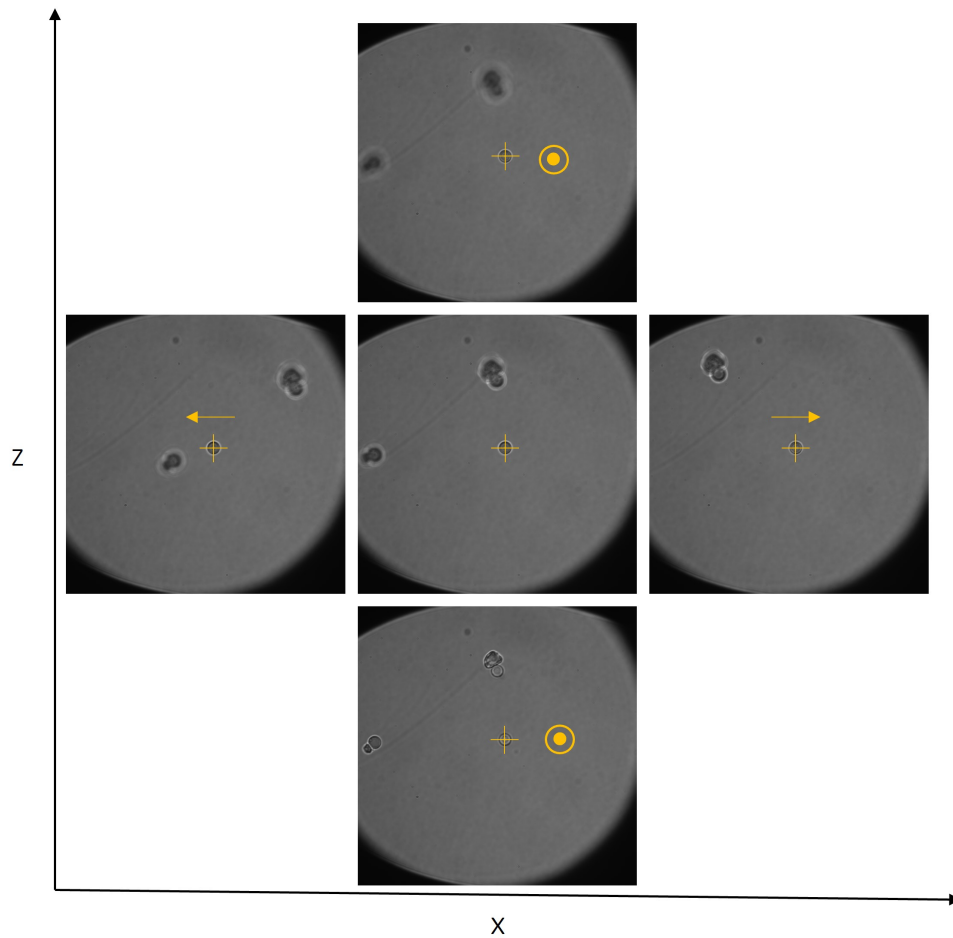


**Figure 2.19:** Manipulation of  $\text{SiO}_2$  bare colloid in X and Z direction using optical tweezer. The trapped particle is denoted by yellow plus sign and the movement can be clearly observed using the free reference colloids around the trapped particle.

## 2. MATERIALS & METHODS

---

## Chapter 3

Particle motion close to a solid wall  
in- and out- of thermal equilibrium

### 3. PARTICLE MOTION CLOSE TO A SOLID WALL IN- AND OUT- OF THERMAL EQUILIBRIUM

---

In this chapter, we investigated the 2D Brownian motion of passive SiO<sub>2</sub> and MF Janus colloids sedimented close to a solid wall, and characterized the slowing down of the rolling rotational diffusion ( $D_{R,\perp}$ ) and translational diffusion parallel to the interface ( $D_{Tr,\parallel}$ ). We also characterize the active motion of isolated Janus colloids in order to evaluate the linear self-propulsion velocity ( $V$ ) as well as the active angular velocity ( $\omega$ ). Moreover, the effect of active motion on the rotational and translational motion is also discussed in this chapter. In this way, we characterize the passive and active motion of Janus particles under our experimental conditions before studying the dynamics encountered when the particles interact with giant vesicles (Chapters 4-6).

#### 3.1 Thermal Brownian trajectories of Janus colloids

Even a microscopically homogeneous liquid undergoes continuous fluctuations on a molecular scale giving rise to Brownian motion. This seemingly endless and random movement of particles suspended in a liquid is a consequence of the thermal fluctuations of molecules surrounding the suspended particle as first explained by Einstein and Sutherland [59]. Brownian motion can be observed also for microparticles suspended in a liquid using optical microscopy as described in section 2.4.1. In Figure 3.1 the particle center of mass trajectories of SiO<sub>2</sub>-Pt ( $R_P \approx 2 \mu\text{m}$ ) and MF-Pt ( $R_P \approx 1 \mu\text{m}$ ) Janus particles are shown. The pattern of particle displacement is completely random due to thermal fluctuations. Taking a closer look at Figure 3.1, the MF-Pt colloids ( $R_P \approx 1 \mu\text{m}$ ) diffuses almost twice further (see Figure 3.1) as compared to the SiO<sub>2</sub>-Pt ( $R_P \approx 2 \mu\text{m}$ ) for the same observation time. This observation reflects the fact that as the size of the particle increases, the drag felt by the particle increases linearly with it.



### 3.1 Thermal Brownian trajectories of Janus colloids

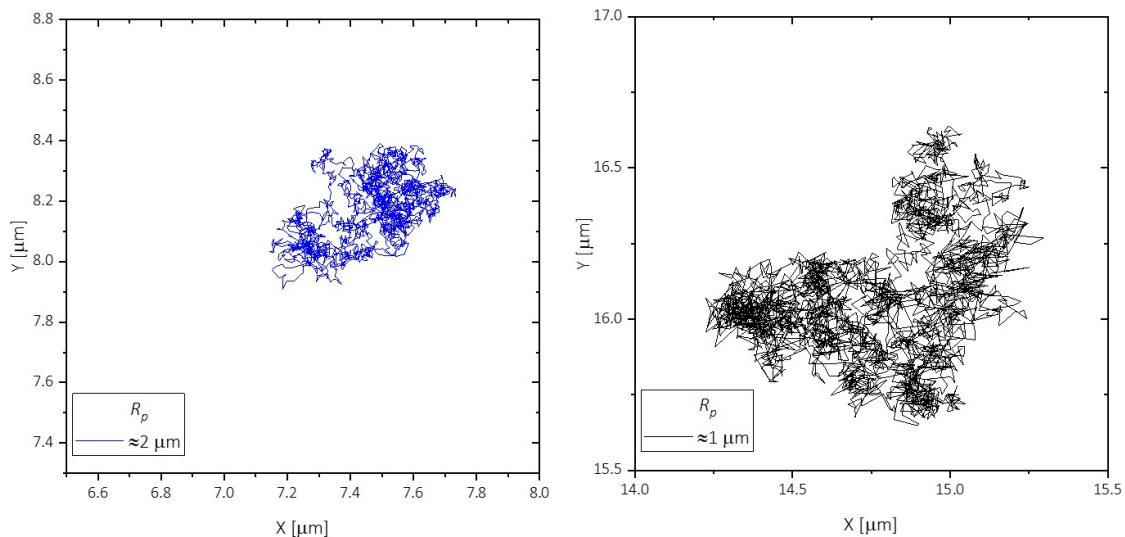


**Figure 3.1:** Brownian trajectories for SiO<sub>2</sub>-Pt (left) and MF-Pt (right) Janus colloids sedimented close to a solid-liquid interface (observation time = 5 s).

#### 3.1.1 Particle translational diffusion

In general, a submerged particle is free to move in all three dimensions. However, the colloids in this study, possessing a density of 1.85 g/cm<sup>3</sup> (SiO<sub>2</sub>) and 1.51 g/cm<sup>3</sup> (MF), sediment to the bottom and move near the substrate close to the solid-liquid interface. The translational diffusion of these heavy colloids is confined in the  $Z$  direction due to this gravity effect. Hence, for our experiments, we will focus our attention on the translational diffusion parallel to the solid-liquid interface ( $D_{Tr,\parallel}$ ). The expression for the mean squared displacement ( $MSD$ ) of a Brownian particle in two dimensions reads [69, 97]:

$$MSD = 4D_{Tr}\Delta t \quad (3.1)$$

The theoretical value for the translational diffusion coefficient ( $D_{Tr,b}$ ) in the bulk is  $D_{Tr,b} = k_B T / \zeta_{Tr,b}$ , where  $k_B$  is the Boltzmann constant,  $T$  is the temperature and  $\zeta_{Tr,b} = 6\pi\eta R_P$  is the Stokes friction coefficient for a spherical particle of a radius  $R_P$  in a fluid of viscosity  $\eta$  (for 100 mM glucose aqueous solution  $\eta$  is 1.02 mPa.s). In Figure 3.2, the mean squared displacement of SiO<sub>2</sub>-Pt and MF-Pt Janus beads as a function of lag time ( $\Delta t$ ) is plotted up to 10<sup>-1</sup> s.  $MSD$  calculations at short time scale are generally more robust since drift effects are negligible. In 3.2,  $MSD$  shows a linear behaviour in Brownian conditions and fitting experimental  $MSD$  values with equation 3.1 yields

### 3. PARTICLE MOTION CLOSE TO A SOLID WALL IN- AND OUT- OF THERMAL EQUILIBRIUM

---

$D_{Tr,\parallel} = 0.08 \mu\text{m}^2.\text{s}^{-1}$  and  $0.03 \mu\text{m}^2.\text{s}^{-1}$  for MF-Pt and SiO<sub>2</sub>-Pt colloids respectively, which lie within the theoretical predictions [63, 98, 99] framework for particles close to a rigid wall. Note that these values are significantly lower than the theoretical value in the bulk ( $\zeta_{Tr,b} = 6\pi\eta R_P$ ),  $D_{Tr,b} = 0.16 \mu\text{m}^2.\text{s}^{-1}$  (MF-Pt) and  $0.10 \mu\text{m}^2.\text{s}^{-1}$  (SiO<sub>2</sub>-Pt), which we will discuss further in section 3.1.3.

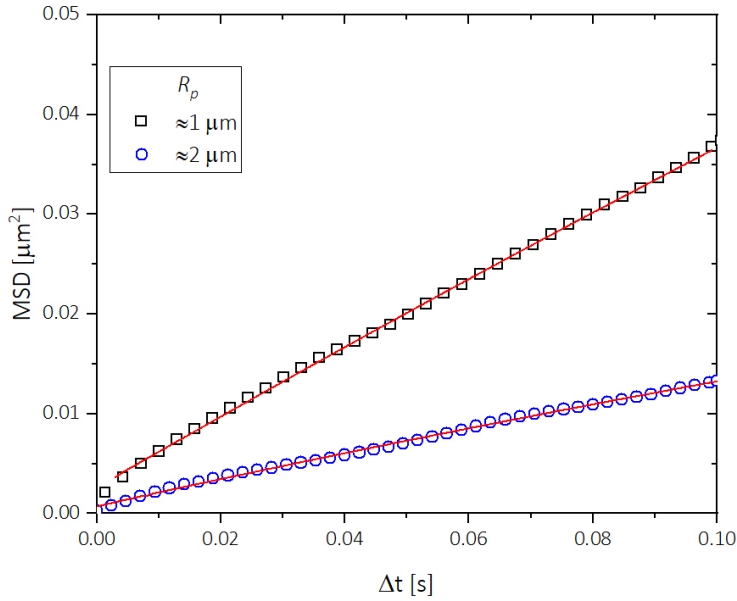


**Figure 3.2:** Mean squared displacement ( $MSD$ ) curve as a function of lag time  $\Delta t$  for SiO<sub>2</sub>-Pt ( $R_P \approx 2 \mu\text{m}$ ) and MF-Pt ( $R_P \approx 1 \mu\text{m}$ ) Janus particles in Brownian motion where the solid line indicates a linear fit over the curve.

Compared to the motion inside an unbounded fluid, the particle hydrodynamics significantly changes close to the solid-liquid interface resulting in the slowing down of translation diffusion, which can be related to the distance  $h$ , separating the colloid from the interface. Goldman *et al.* [62] derived an approximate analytical expression for the diffusion coefficient associated with the motion parallel to the wall:

$$D_{Tr,\parallel} = \frac{k_B T}{6\pi\eta R_P} \frac{1}{f_{Tr,\parallel}} \quad (3.2)$$

$$\frac{1}{f_{Tr,\parallel}} = 1 - \frac{9}{16} \left( \frac{R_P}{R_P + h} \right) + \frac{1}{8} \left( \frac{R_P}{R_P + h} \right)^3 - \frac{45}{256} \left( \frac{R_P}{R_P + h} \right)^4 - \frac{1}{16} \left( \frac{R_P}{R_P + h} \right)^5 \quad (3.3)$$

### 3.1 Thermal Brownian trajectories of Janus colloids

---

where  $f_{Tr,\parallel}$  is the correction factor for translational drag felt by the colloid due to the nearby solid wall. In Figure 3.3 we plot the parallel translation diffusion coefficient for MF-Pt ( $R_P \approx 1 \mu\text{m}$ ) as a function of normalized gap height  $h/R_P$ . The solid lines denote the theoretical prediction from reference [63, 100] for 3 different particle sizes considering the size polydispersity of the colloids (see Chapter 2). The gap distance from the surface  $h$  was found in the range from ca. 0.1 to 1.6 times the particle radius: 260 nm to 2  $\mu\text{m}$ . For similar Janus polymeric colloids close to a solid wall, recent experimental studies reported  $h = 0.6 \mu\text{m}$  [63] or even lower gaps [101]. These values were obtained assuming a unique particle radius  $\bar{R}_P$  in the experiments:  $D_{Tr,\parallel}/D_{Tr,b} = 1/f_{Tr,\parallel}$  and they can be rationalised as the equilibrium distance due to gravity attraction and electrostatic repulsion between the particle and the solid substrate. Indeed, typical Debye screening lengths for very dilute aqueous solutions lay in the range between 100 nm to 1  $\mu\text{m}$  [102]. In order to show that a tiny difference in the assumption on the particle size may impact the evaluation of the gap distance, we consider two arbitrary points in the Figure 3.3:  $D_{Tr,\parallel} = 0.08 \mu\text{m}\cdot\text{s}^{-1}$  and  $D_{Tr,\parallel} = 0.13 \mu\text{m}\cdot\text{s}^{-1}$ . For the latter point  $h = 2 \mu\text{m}$  if  $R_P = 1.29 \mu\text{m}$  but it becomes  $h = 1.5 \mu\text{m}$  if  $R_P = 1.23 \mu\text{m}$ . This difference of 500 nm due to a different assumption on the particle size becomes smaller for the points on the left showing a strong slowing down of the translational diffusion, but it is still significant (ca. 50 nm). Hence, in general, one can not extract the gap distance from the particle translational diffusion data alone. In order to correctly evaluate the value of  $h$ , we measured both the translational and rotational diffusion for the same particle. In the following sections, we will show these measurements and discuss the evaluation of  $h$  and  $R_P$ . We anticipate that indeed the two arbitrary points represented by the empty symbols correspond to  $R_P = 1.29 \mu\text{m}$  and a shorter gap distance. Still, in Figure 3.3, a wide range of separation gaps could be discussed as the result of heterogeneous surface properties of the Janus colloids, as the colloids not only possess two faces: MF and Platinum, but also roughness due to the fabrication (metal sputtering) as described in Chapter 2. For the liquid-gas interface, the gap distance was also found to depend on the particle orientation and the presence of surface defects, which considerably affect the rotational motion of the colloidal particles [103].

### 3. PARTICLE MOTION CLOSE TO A SOLID WALL IN- AND OUT- OF THERMAL EQUILIBRIUM

---

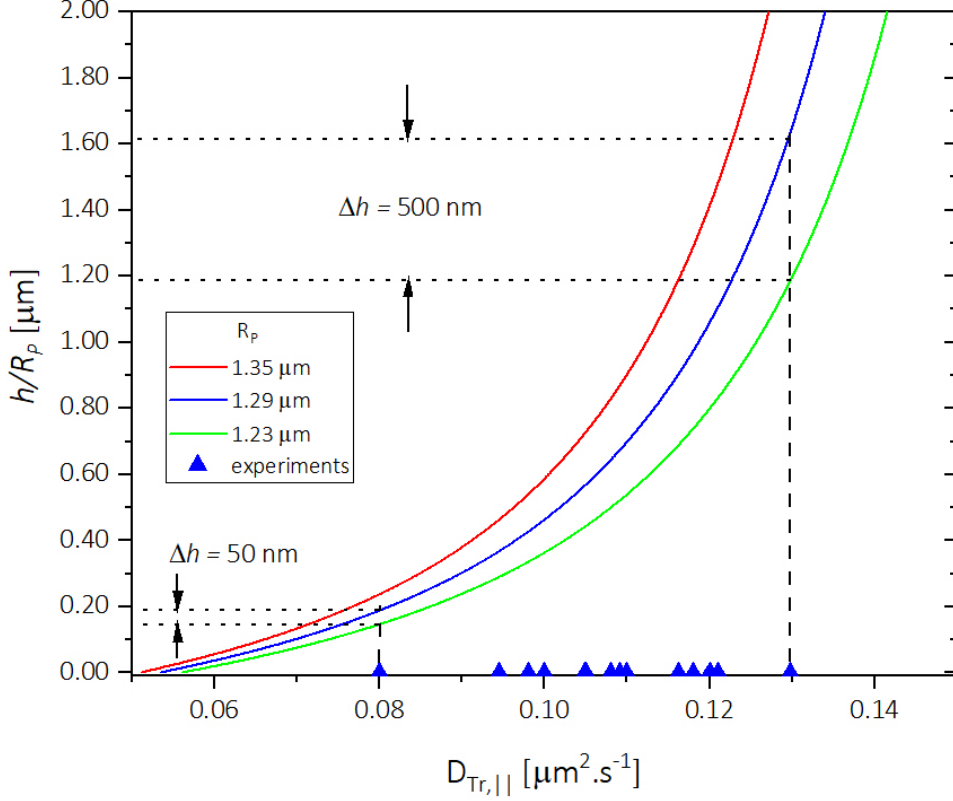


**Figure 3.3:** Normalized gap height  $h/R_P$  as a function of Translational diffusion ( $D_{Tr,||}$ ), comparison of experimental data with theoretical prediction [60, 104] close to an interface.

#### 3.1.2 In-plane and out-of-plane particle rotational diffusion

Colloidal particles immersed in a fluid not only undergo translational diffusion but are also subjected to rotational diffusion due to thermal fluctuations [98, 99, 105]. In this section, we investigate the rotational dynamics of Janus colloids near a solid-liquid interface using fluorescent microscopy and by exploiting the Janus geometry of the colloid to determine its in-plane and out-of-plane rotation (see Chapter 2). As shown schematically in Figure 3.4(A), out-of-plane rotation of the colloid refers to rolling. This change in orientation is defined by the angle  $\beta$  between the axis normal to the Janus boundary and normal to the solid-liquid interface. Aside from out-of-plane rotation, an in-plane rotation can be defined by the angle  $\varphi$ . Figure 3.4(B) shows the in-plane

### 3.1 Thermal Brownian trajectories of Janus colloids

rotation of a Janus colloid separated by a distance  $h$  from the substrate.

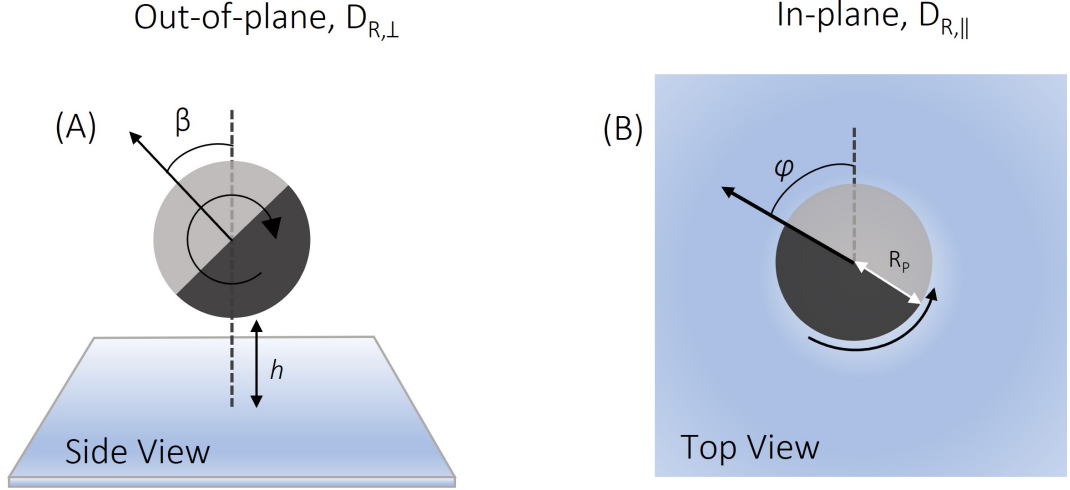


**Figure 3.4:** Schematic representation of the rotation of a Janus sphere about its axis: (A) out-of-plane (perpendicular) rotation defined by  $\beta$ , (B) In-plane (parallel) rotation with respect to the solid-liquid interface,  $\varphi$  is the angle between the Janus boundary and the Y-axis of the laboratory frame (XY plane).

For spherical colloids away from any interface, a unique rotational diffusion can be defined as  $D_{R,b} = k_B T / \zeta_{R,b}$  where  $\zeta_{R,b}$  is the rotational bulk friction:  $\zeta_{R,b} = 8\pi\eta R_P^3$  in no slip boundary conditions ( $\zeta_{R,b} = 0$  for perfect slip conditions) [100].

As mentioned in section (2.4.1.1) because of the limits of transmission mode bright-field microscopy, rotational tracking investigations were restricted to the fluorescent MF-Pt colloids, as the larger SiO<sub>2</sub>-Pt colloid did not emit any fluorescence in their pristine conditions. Furthermore, for relatively large size colloids ( $R_P \approx 2 \mu\text{m}$ ), fluorescently labelled, complex fluorescence profiles were observed, which render the thresholding analysis difficult. For colloids near a solid-liquid interface, the particle's in-plane and out-of-plane rotation can be measured and mean squared angular displacement (*MSAD*) can be calculated. Hence we were able to compute the out-of-plane/perpendicular ( $D_{R,\perp}$ ) and in-plane/parallel ( $D_{R,\parallel}$ ) rotational diffusion coefficients close to the interface, which will be discussed in the following sections.

### 3. PARTICLE MOTION CLOSE TO A SOLID WALL IN- AND OUT- OF THERMAL EQUILIBRIUM

---

#### 3.1.2.1 In-plane rotational diffusion close to the solid-liquid interface

As described in section (2.4.1.1), we were able to evaluate changes in the particle in-plane/parallel rotational motion. The fluorescent region of the Janus colloid not covered by Platinum was monitored and its contour was fitted by an ellipse which yields the angle  $\varphi$  of the projected Janus boundary in the laboratory frame. In Figure 3.5, we plot the  $\varphi$  as a function of time  $t$ (s), which fluctuates in a range of  $\Delta\varphi \approx 50^\circ$  for duration up to 4 s.

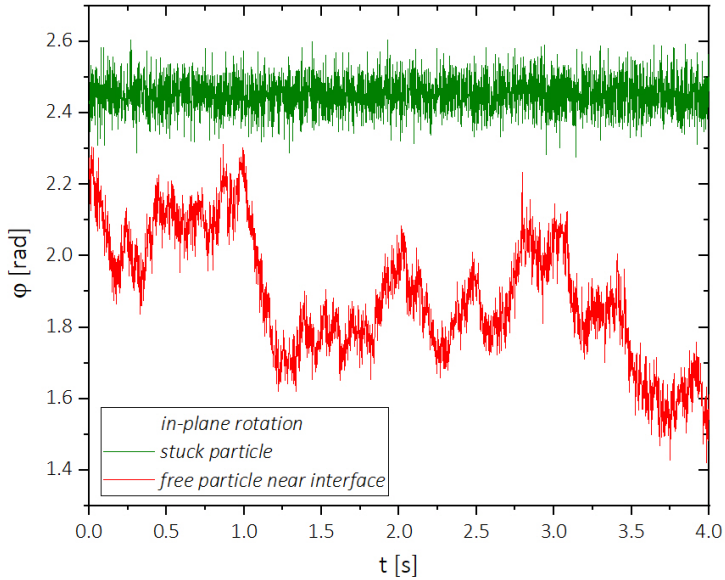


**Figure 3.5:** Comparison between the orientation angle  $\varphi$  for a ( $R_P \approx 1 \mu\text{m}$ ) MF-Pt Janus particle freely diffusing close to the solid-liquid interface and for a Janus particle stuck on the substrate.

As a reference for our analysis, a Janus colloid stuck on the substrate was considered (see the green curve in Figure 3.5). The noise of the in-plane rotation angle ( $\varphi$ ) of a stuck colloid is restricted to  $\approx 2\text{-}3^\circ$ . From the *MSAD* analysis,  $MSAD(\varphi) = 2D_{R,\parallel}\Delta t$ , we evaluate the in-plane rotational diffusion, which is comparable to the  $D_{R,b}$  [106] and observed that the  $MSAD(\varphi)$  of the stuck particle remains flat. Indeed  $D_{R,\parallel}$  does not significantly vary close to an interface when compared to  $D_{R,\perp}$ . For this reason, we will focus our attention on the out-of-plane rotation of the Janus colloid. Moreover,

### 3.1 Thermal Brownian trajectories of Janus colloids

---

as explained in the following sections, the theoretical models considered in many cases only the out-of-plane rotation of a particle close to a solid wall.

#### 3.1.2.2 Out-of-plane rotational diffusion close to the solid-liquid interface

Turning our attention towards the out-of-plane motion, measuring the area of the fluorescent MF region of the Janus colloid  $A_{MF}$ , we calculate the particle orientation angle  $\beta$  (Figure 3.4(A)) by,  $A_{MF} = 1/2\pi(1 - \cos \beta)R_P^2$  [105]. Figure 3.6 shows the evolution of perpendicular rotation angle as a function of time ( $t$ ), where the blue curve corresponds to a free colloid near the interface whose  $\Delta\beta$  varies over  $\approx 51^\circ$  (1 rad) during 4 s. The green curve in Figure 3.6, corresponds to a reference Janus particle stuck on the substrate exploring less than  $\approx 2^\circ$  which corresponds to the noise of our experimental analysis. From the evaluated  $\beta$ , we calculated  $MSAD(\beta)$ . In Figure 3.7, we plot  $MSAD(\beta)$  as a function of the lag time ( $\Delta t$ ) for different MF-Pt particles in the short time limit ( $\Delta t = 0.05$  s). We fitted the  $MSAD$  data using equation:

$$MSAD(\beta) = MSAD_0 + 2D_{R,\perp}\Delta t \quad (3.4)$$

where the term  $MSAD_0$  takes into account the noise which could be introduced by the image treatment.

### 3. PARTICLE MOTION CLOSE TO A SOLID WALL IN- AND OUT- OF THERMAL EQUILIBRIUM

---

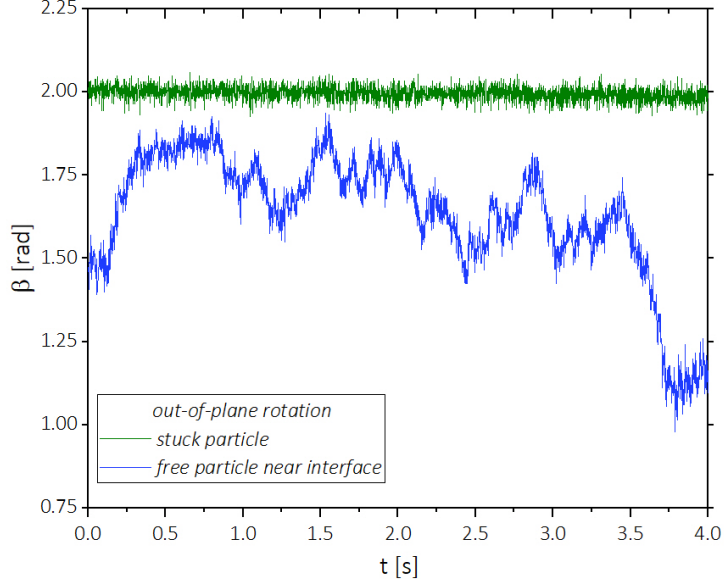


**Figure 3.6:** Comparison between the orientation angle  $\beta$  for a ( $R_P \approx 1 \mu\text{m}$ ) MF-Pt Janus freely diffusing close to the solid-liquid interface and for a Janus particle stuck on the substrate.

In Figure 3.7 the  $MSAD$  fits yield  $D_{R,\perp}$ . In our experiments,  $D_{R,\perp}$  is in the range between  $0.13 - 0.045 \text{ s}^{-1}$  giving a rotational diffusion time ( $\tau_{R,\perp} = 1/D_{R,\perp}$ ) between 8 to 22 s, which is similar or in most cases larger than the theoretical rotational diffusion time in the bulk  $\tau_{R,b}(=\zeta_{R,b}/k_B T) = 13 \pm 2 \text{ s}$ . The slowing down of  $D_{R,\perp}$  close to a solid wall [107, 108, 109] can be traced back to hydrodynamic interaction between the spherical particle and the solid wall. The rotational drag is infinite for  $h = 0$  and it approaches to the bulk value with increasing gap distance between the particles and the solid-liquid interface.  $MSAD(\beta)$  in Figure 3.7 exhibit non-monotonic behavior with the particles translational diffusion, which will be discussed in terms of particle distance from the interface as well as the variation in the colloidal size itself.



### 3.1 Thermal Brownian trajectories of Janus colloids

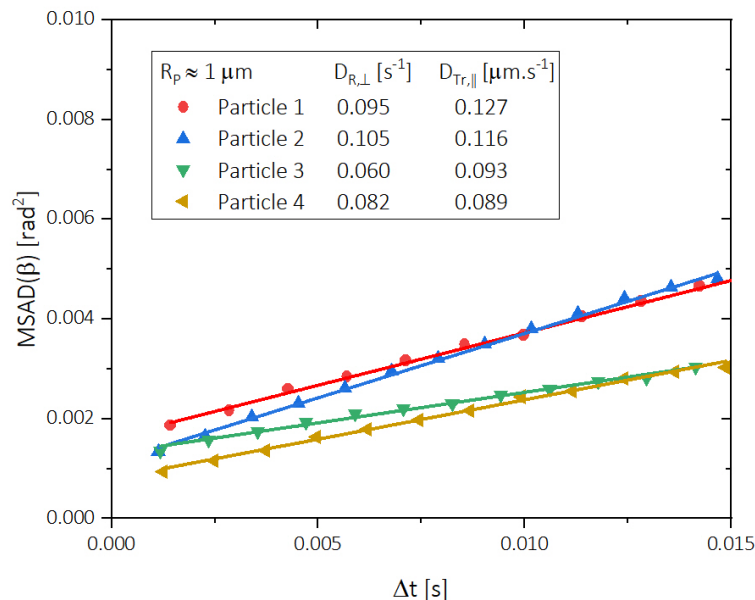


**Figure 3.7:** Mean Squared Angular displacement for the out-of-plane rotation of various MF-Pt colloids close to the interface where the solid lines are the linear fits of the experimental data (equation 3.4).

#### 3.1.3 Comparison between experiments and hydrodynamic models

Rolling rotation and parallel translational diffusion coefficients close to a solid-liquid interface can be written as [62, 99, 110]  $D_{R,\perp} = \frac{k_B T}{k_{(R,\perp)} \eta R_P^3}$ ;  $D_{Tr,\parallel} = \frac{k_B T}{k_{(Tr,\parallel)} \eta R_P}$ , where  $k_{(R,\perp)}$  and  $k_{(Tr,\parallel)}$  are functions of  $h/R_P$  (see eqs 3.2 and 3.3,  $k_{(Tr,\parallel)} = 6\pi f_{Tr,\parallel}$ ). According to Faxen,  $k_{(R,\perp)}$  ranges from  $12\pi$  at  $\frac{h}{R_P} = 0.1$  close to the interface to  $8\pi$  in the bulk. Similarly,  $k_{(Tr,\parallel)}$  varies from  $14\pi$  at  $\frac{h}{R_P} = 0.1$  and approaches  $6\pi$  for large gap distances. Hence,  $D_{R,\perp}$ ,  $D_{Tr,\parallel}$  are the slowest for the largest colloids nearest to the interface and fastest for the smallest colloids farthest from the interface. Figure 3.8 shows experimental values of  $D_{R,\perp}$  as a function of  $D_{Tr,\parallel}$  for MF-Pt colloids, where the solid lines are the theoretical predictions according to Faxen's model for particle sizes  $1.1 \mu m < R_P < 1.45 \mu m$ . Almost all of the experimental data can be described by the theoretical predictions using  $1.1 \mu m < R_P < 1.45 \mu m$ , which consider both the effects of gap distance and particle size on diffusion coefficients. As anticipated in the previous section when discussing translational diffusion  $D_{Tr,\parallel}$  results, now by measuring  $D_{R,\perp}$  we

### 3. PARTICLE MOTION CLOSE TO A SOLID WALL IN- AND OUT- OF THERMAL EQUILIBRIUM

are able to evaluate the gap distance and the particle size for each experimental point described by the Faxen's hydrodynamic model. Note that for gap distance  $\frac{h}{R_P} \geq 1$ , the particle is assumed to be far away from solid boundary without any hydrodynamic effect of the solid wall.

Hence, by measuring simultaneously both the rotational and translational diffusion coefficient, we are able to determine both the gap distance and the particle size. In most of the cases the experimental data was found to lie within the frame  $0.4 < h/R_P < 1$  and  $1.1 < R_P < 1.45 \mu\text{m}$ .

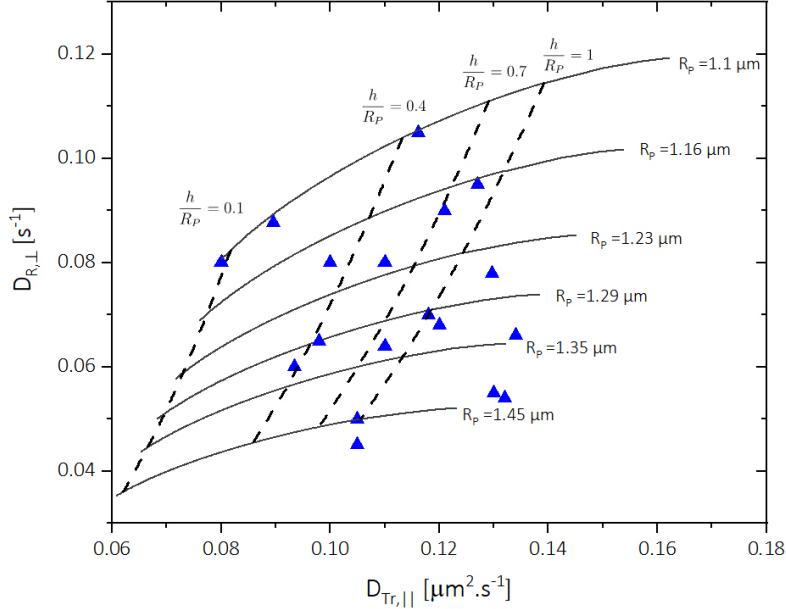


**Figure 3.8:** Rotational diffusion coefficient ( $D_{R,\perp}$ ) vs Translational diffusion coefficient ( $D_{Tr,\parallel}$ ). Comparison between experimental results and theoretical prediction for MF-Pt colloids close to a single wall. The solid line shows the theoretical predictions for the diffusion coefficients at different  $R_P$ , while the dashed lines depict the predictions for normalized gap distance ( $\frac{h}{R_P}$ ).

### 3.2 Active motion of isolated Janus colloids

Aside from Brownian diffusion in thermal equilibrium, Janus colloids are capable of producing autonomous motion in out-of-equilibrium conditions in the presence of a

## 3.2 Active motion of isolated Janus colloids

---

chemical propellant, which in this study was Hydrogen Peroxide ( $\text{H}_2\text{O}_2$ ). To observe particle self-propulsion, the sample was prepared as mentioned in section 2.3.1 but before closing the sample cell with a glass slide, a volume ( $\approx 7.8 \mu\text{L}$ ) of  $\text{H}_2\text{O}_2$  solution was added in the cell to obtain a final concentration of 2%. Before measuring, enough time was allowed for  $\text{H}_2\text{O}_2$  to diffuse uniformly throughout the cell (5 - 10 minutes) [11]. The recorded videos were then analysed to track translational and orientational displacement in time using Blender and ImageJ routines as discussed in section 2.4.1 - 2.4.1.1.

### 3.2.1 Particle self-propulsion velocities

For the characterization of active motion of Janus colloids moving close to the solid-liquid interface, the velocity auto-correlation function (*VACF*) was determined  $\langle \nu_i(t + \Delta t) \cdot \nu_i(t) \rangle$  by following the translational displacement of the center of mass of the Janus colloid. *VACF* reflects on the likelihood of a colloid to consistently maintain its velocity after a lag time  $\Delta t$ . This probability is lost when there is a considerable change in the velocity vector (direction or modulus) of the moving colloid. *VACF* were calculated from the discrete velocity vector  $\bar{\nu} = (\nu_x, \nu_y)$ , where  $\nu_x(t) = \frac{x(t + \Delta t_1) - x(t)}{\Delta t_1}$ ,  $\nu_y(t) = \frac{y(t + \Delta t_1) - y(t)}{\Delta t_1}$  and  $\Delta t_1$  is the lowest time interval ( $=1/\text{fps}$ , for 10 - 1000 fps) dictated by our camera detector. From  $\bar{\nu}$ , discrete velocity vector auto-correlation function was calculated:  $\langle \bar{\nu}(t + \Delta t) \bar{\nu}(t) \rangle = \langle \nu_x(t + \Delta t) \nu_x(t) \rangle + \langle \nu_y(t + \Delta t) \nu_y(t) \rangle$ . For active colloids possessing both active linear  $V$  and angular  $\omega$  velocities, *VACF* of the instantaneous velocity  $\bar{\nu}_i$  in two dimensions can be written as [12]:

$$\langle \nu_i(t + \Delta t) \cdot \nu_i(t) \rangle = 4D_{Tr} \delta(\Delta t) + V^2 \cos(\omega \Delta t) f_r \quad (3.5)$$

where the term  $4D_{Tr} \delta(\Delta t)$  is related to the translational diffusion in 2D space, while the second term  $V^2 \cos(\omega \Delta t) f_r$ , relates to the active propulsion. When a particle undergoes active propulsion in an unbound fluid,  $f_r = \exp(-D_R \Delta t)$  and the rotational diffusion  $D_R$ , completely randomizes the active motion at long time scales. Equation 3.5 can be used to describe experiments for active Janus colloids. For  $\Delta t > \Delta t_1$ , the *VACF* data were fitted by the following equation, which takes into account also the presence of a drift velocity  $V_d$ :

$$\langle \bar{\nu}(t + \Delta t) \cdot \bar{\nu}(t) \rangle = V^2 \cos(\omega \Delta t) f_r + V_d^2 \quad (3.6)$$

### 3. PARTICLE MOTION CLOSE TO A SOLID WALL IN- AND OUT- OF THERMAL EQUILIBRIUM

---

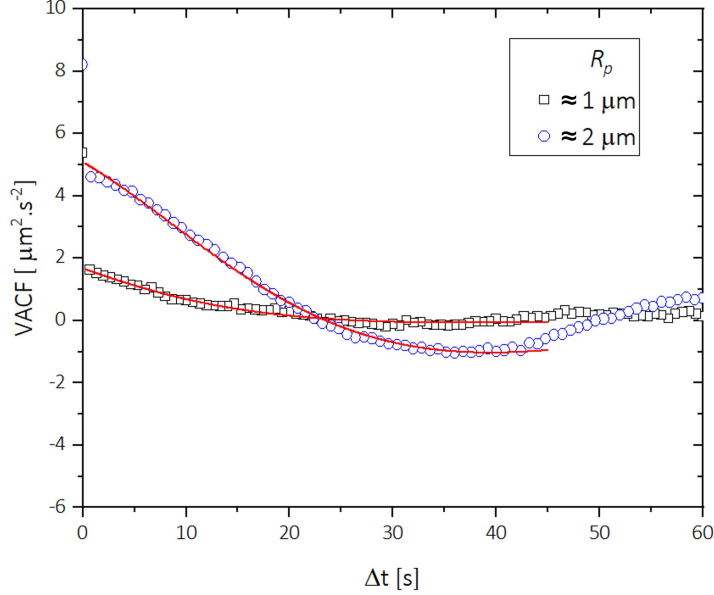


**Figure 3.9:** Velocity autocorrelation function as a function of lag time  $\Delta t$  for active SiO<sub>2</sub>-Pt ( $R_P \approx 2 \mu\text{m}$ ) and MF-Pt ( $R_P \approx 1 \mu\text{m}$ ) Janus particles. Corresponding trajectories are shown in Figure [2.14](#).

Hence, the linear  $V$  and angular  $\omega$  velocities can be evaluated by fitting the experimental data to the previous equation. To measure the particle translational diffusion coefficient in active conditions, we calculate the mean squared displacement  $MSD$  and consider that in the short lag time limit, for  $\Delta t < 1/D_R$  and  $1/\omega$  [\[112\]](#):

$$MSD = 4D_{Tr}\Delta t + V^2\Delta t^2 \quad (3.7)$$

Note that for  $\Delta t \ll 4D_{Tr}/V^2$  (= ca. 0.4 s in our experiments), only the linear term is relevant. In Figure [3.9](#),  $VACF$  is plotted for SiO<sub>2</sub>-Pt ( $R_P \approx 2 \mu\text{m}$ ) and MF-Pt ( $R_P \approx 1 \mu\text{m}$ ) as a function of the lag time ( $\Delta t$ ), which corresponds to the active trajectory shown in Figure [2.14](#). Active velocities were found to be  $V = 2.2 \mu\text{m.s}^{-1}$  and  $1.4 \mu\text{m.s}^{-1}$  for SiO<sub>2</sub>-Pt and MF-Pt particles respectively, by obtaining the best fit for the  $VACF$  curves over equation [3.6](#). For the same trajectories, angular velocity  $\omega$  was evaluated to be  $0.06 \text{ s}^{-1}$  for SiO<sub>2</sub>-Pt and  $0.098 \text{ s}^{-1}$  for MF-Pt colloids. Rotational diffusion coefficients evaluated from  $VACF$  were found to be  $D_{R,\parallel} = 0.10 \pm 0.03 \text{ s}^{-1}$

### 3.2 Active motion of isolated Janus colloids

---

for  $R_P \approx 1 \mu\text{m}$  and  $D_{R,\parallel} = 0.03 \pm 0.01 \text{ s}^{-1}$  for  $R_P \approx 2 \mu\text{m}$ , as obtained by the fits of equation 3.6, which are comparable to the calculated bulk values  $D_{R,b} = k_B T / (8\pi\eta R_P^3) = 0.11 \text{ s}^{-1}$  ( $R_P \approx 1 \mu\text{m}$ ) and  $D_{R,b} = 0.02 \text{ s}^{-1}$  ( $R_P \approx 2 \mu\text{m}$ ).

In Figure 3.10 we plot *MSD* curves for the MF-Pt colloids in both active and passive Brownian conditions. A fit of equation 3.7 over the *MSD* curve yield  $D_{T_r,\parallel} = 0.13 \mu\text{m}^2.\text{s}^{-1}$  for active Janus colloid. However, the average translational diffusion obtained for active Janus colloids was  $\bar{D}_{T_r,\parallel} \approx 0.12 \mu\text{m}^2.\text{s}^{-1}$  which is comparable to the  $\bar{D}_{T_r,\parallel} \approx 0.08 \mu\text{m}^2.\text{s}^{-1}$  in Brownian motion. This similarity in the  $D_{T_r,\parallel}$  could indicate that the gap distance between the colloid and the wall remains unaffected by the addition of propellant in the system, which is somewhat in contrast to some recent experimental results [63]. The inset in Figure 3.10 shows the parabolic behaviour of the *MSD* (up to 2 s) where the change in slope introduced by the active velocity is clearly noticeable. Note that in our experiments we can clearly decouple the information about the Brownian translation and the active velocity given the high frame rate (up to 1000 fps) used in our detection. The presence of an active velocity could indeed affects the evaluation of the translational diffusion for the experiments performed at a normal frame rate of 10-30 fps [63].

### 3. PARTICLE MOTION CLOSE TO A SOLID WALL IN- AND OUT- OF THERMAL EQUILIBRIUM

---

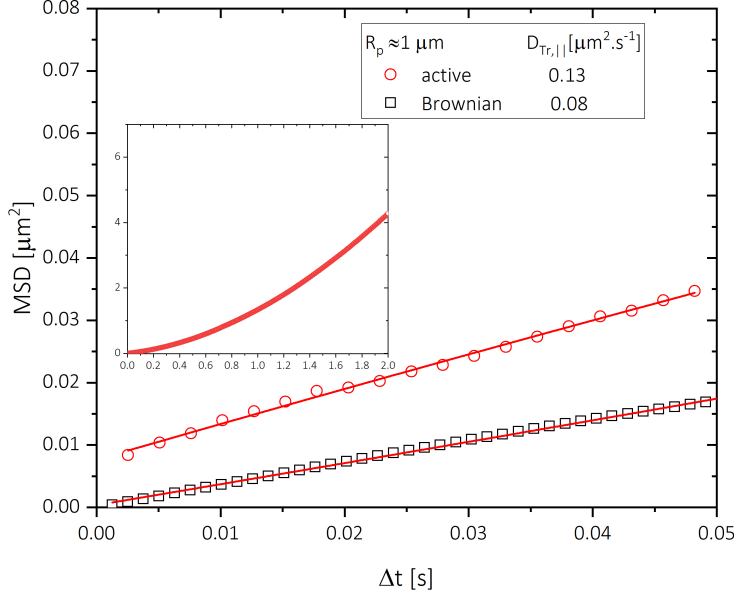


**Figure 3.10:** *MSD* as a function of lag time  $\Delta t$  for Janus colloids in active vs passive condition. The solid line fits the data with equation 3.7. The inset shows the parabolic behaviour of the *MSD* curve for active Janus colloid.

Janus colloid	Active Velocity (V) $\mu\text{m}\cdot\text{s}^{-1}$	Angular velocity ( $\omega$ ) $\text{rad}\cdot\text{s}^{-1}$
SiO <sub>2</sub> -Pt	0.95 - 4.5	0.05 - 0.09
MF-Pt	1.2 - 5	0.1 - 0.3

**Table 3.1:** Range of active and angular velocities for SiO<sub>2</sub>-Pt and MF-Pt Janus colloids in a free trajectory.

Table 3.1 shows the the range of active velocities as well as angular velocities observed for SiO<sub>2</sub>-Pt ( $R_P \approx 2 \mu\text{m}$ ) and MF-Pt ( $R_P \approx 1 \mu\text{m}$ ) colloids. All the experiments were carried out at 2% H<sub>2</sub>O<sub>2</sub>. For both particle sizes, the highest active velocity observed was found to be around 4.5 - 5  $\mu\text{m}\cdot\text{s}^{-1}$ . The highest active velocity was obtained soon after the addition and subsequent diffusion of H<sub>2</sub>O<sub>2</sub> which also agrees with previously reported velocity for active particle moving in bulk by Gibbs and Zhao [47] at 2% fuel concentration. However, for long time measurements, the measured active velocity

varies from  $1 - 5 \mu\text{m}\cdot\text{s}^{-1}$ . This range of active velocity arises from the observation of a Janus colloid in active conditions at various times after the addition of  $\text{H}_2\text{O}_2$ , and as time passes, the  $\text{H}_2\text{O}_2$  propellant is consumed by the system to maintain activity, resulting in a depletion of its concentration in the system, which in turns slows down the particle's active velocity. In an ideal case, if the Janus colloid would exhibit a perfect symmetry (Figure 3.11(A)), one would expect the active free trajectory to be a straight line. However, as seen from Figure 2.14 the active trajectory for Janus colloid in bulk comprises of straight paths along with circular and rectilinear motion. This circular motion can be attributed to the break in symmetry by non-uniform surface properties, seen in Figure 3.11(B). This broken non-ideal symmetry, as a consequence, gives rise to a finite angular velocity ( $\omega$ ) component on a free trajectory. Despite the fact that surface defects were found in a large number of colloidal particles, it was difficult to determine a critical size for the shape of the surface defect.

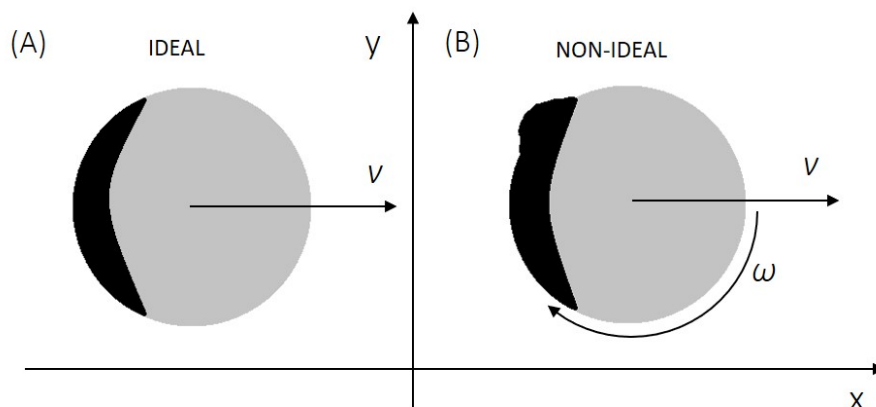


**Figure 3.11:** Top view sketches of: (A) an ideal Janus colloid with a linear propulsion velocity  $V$ . (B) A non-ideal Janus colloid with a linear active velocity  $V$ , and angular velocity  $\omega$ .

#### 3.2.2 Janus colloid orientation in active motion

As discussed in section 2.4.1.1, information on the orientation of the Janus colloids in active conditions can be extracted using the same protocol. Figure 3.12 shows the in-plane ( $\varphi$ ) and out-of-plane ( $\beta$ ) rotation angles for a Janus colloid as a function of time. Compared to the passive Brownian rotational dynamics, the introduction of particle self-propulsion leads to a confinement of the out-of-plane colloid rotation.  $\beta$  varies over

### 3. PARTICLE MOTION CLOSE TO A SOLID WALL IN- AND OUT- OF THERMAL EQUILIBRIUM

---

less than  $30^\circ$  ( $\approx 0.5$  rad) for  $t = 25$  s, whereas  $\varphi$  varies by more than  $60^\circ$  ( $\approx 1$  rad). The explanation for the confinement effect of the out-of-plane rotational dynamics is related to the polarization force generated by an active particle close to a wall [66]. A preferential particle orientation with the Janus boundary perpendicular to the interface was in fact described both in experiments and in theory [72, 113].

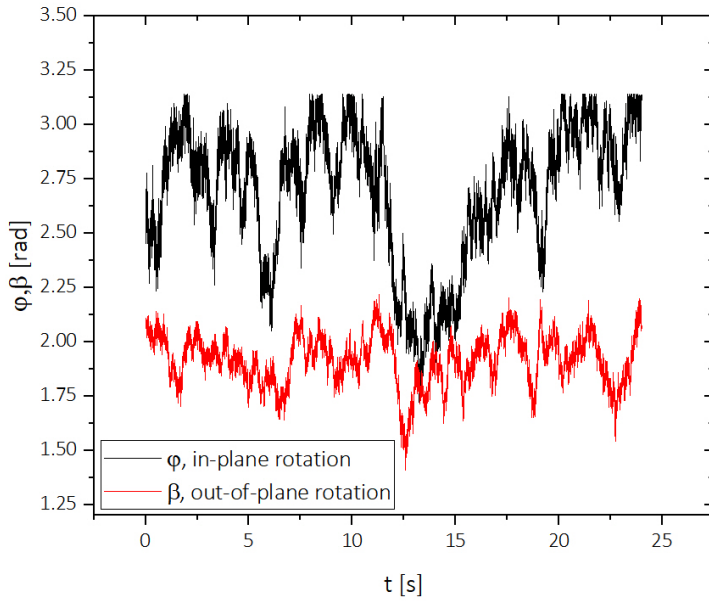


**Figure 3.12:** In-plane and out-of-plane rotation angle of an MF-Pt colloid in active condition close on the interface.

In figure 3.13, we plot  $MSAD(\varphi, \beta)$  as a function of the lag time ( $\Delta t$ ) for an MF-Pt active colloid. In the short lag time limit, evaluating the coefficient of rotational diffusion in active conditions yields  $D_{R,\parallel} = 0.065 \text{ s}^{-1}$  and  $D_{R,\perp} = 0.01 \text{ s}^{-1}$ . A corresponding rotational diffusion time  $\tau_{R,\parallel} = 1/D_{R,\parallel} = 15 \text{ s}$  is comparable to the theoretical rotational diffusion time in the bulk  $\tau_{R,b}(=\zeta_{R,b}/k_B T) = 13 \pm 2 \text{ s}$ . A slowing down of the out-of-plane rotation of the Janus colloid in active condition can be observed by the rotational diffusion time  $\tau_{R,\perp} = 1/D_{R,\perp} = 100 \text{ s}$ , which is about 7 times the bulk value. This factor of 7 is surprisingly high, as the gap distance in active conditions was found to be similar to free motion from the translational diffusion data. According to Goldman *et al.* [62] even with a gap distance of  $h/R_P = 10^{-3}$ ,  $D_{R,\perp}$  is expected



### 3.2 Active motion of isolated Janus colloids

to be 3 times slower than the bulk rotational diffusion. No quantitative explanation of this strong slowing down can be provided at the moment. It is important to note that our experiments are performed with a very good resolution on  $D_{R,\perp}$  given the large number of experimental points in the short lag time limit in comparison to other recently reported experiments [66].

The inset in Figure 3.13 depicts the behavior of the *MSAD* for the in- and out-of-plane rotations up to  $\Delta t = 2$  s. As shown, a diffusive behavior is observed at short time scales ( $< 0.5$  s), but at longer time scales a plateau is observed due to the confinement effect generated by the particle activity, which restricts the rolling motion of the colloid and keeps the Janus boundary perpendicular to the interface.

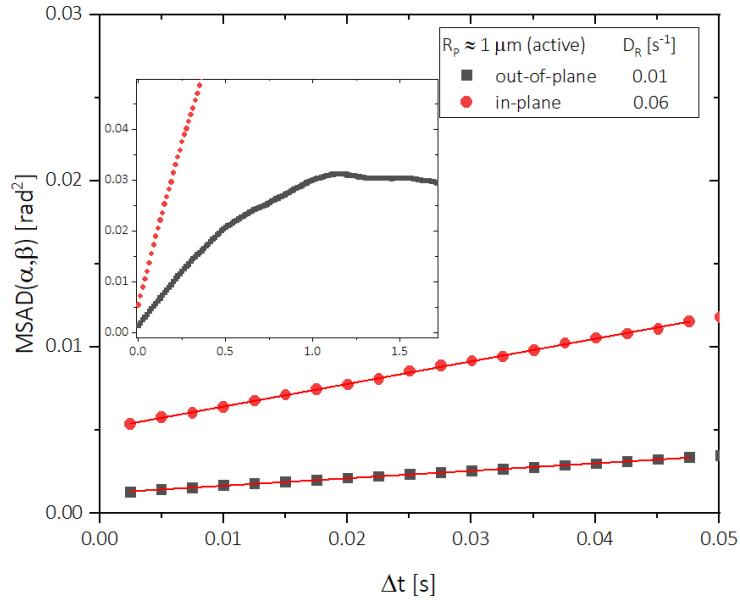


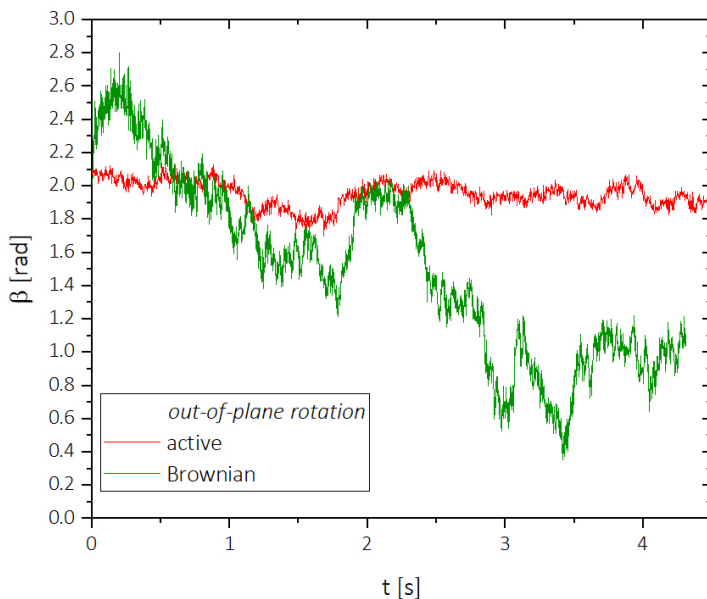
**Figure 3.13:** *MSAD* as a function of lagtime ( $\Delta t$ ) for in- and out-of-plane rotation of an active MF-Pt Janus colloid. The solid line fits the data linearly for  $\Delta t \ll 4D_{Tr}/V^2 =$  ca. 0.4 s.

### 3. PARTICLE MOTION CLOSE TO A SOLID WALL IN- AND OUT- OF THERMAL EQUILIBRIUM

---

#### 3.3 Comparing rotational diffusion in active and passive motion

As we have already addressed in the previous section, the out-of-plane rotation is severely confined and slowed down for an active Janus particle moving close to a solid wall. In this section, we compare the out of plane rotational dynamics in passive and active conditions. In Figure 3.14, we plot the out-of-plane angle ( $\beta$ ) as a function of the time for an MF-Pt colloid for lag times of up to 5 seconds.  $\Delta\beta$  in passive Brownian motion varies more than 20 times than in active conditions. For passive Brownian motion,  $\beta$  changes by more than  $130^\circ$  ( $\approx 2.4$  rad) while the same colloid explores less than  $5^\circ$  when in active motion ( $\approx 0.1$  rad).



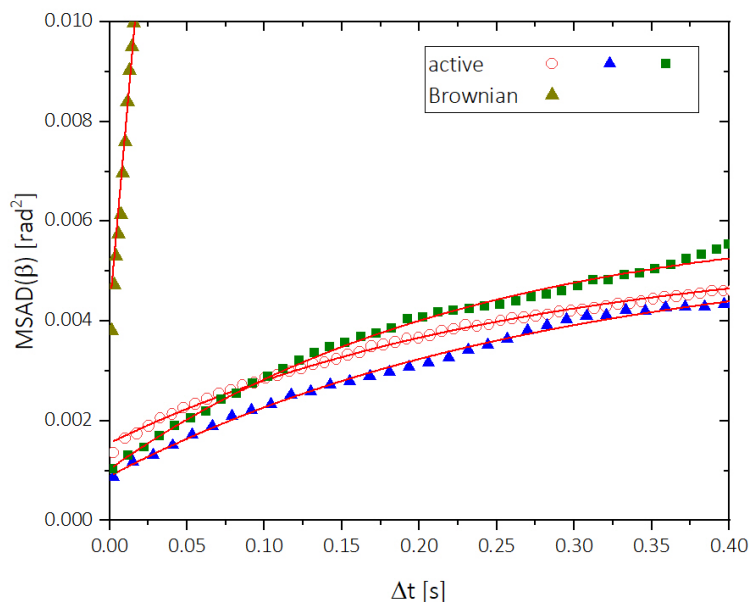
**Figure 3.14:** Comparison between the out-of-plane angle  $\beta$  of MF-Pt colloid in active and passive conditions.

Figure 3.15, depicts the  $MSAD(\beta)$  as a function of the lag time for MF-Pt Janus particle.  $MSAD$  for a passive colloid shows a linear behaviour, whereas  $MSAD$  for an active colloid is diffusive for very short lag times and reaches a plateau at long  $\Delta t$ . For

this confined angular dynamics, data can be described by [113]:

$$MSAD(\beta) = \langle \Delta(\beta)^2 \rangle = \frac{D_{R,\perp}}{\Gamma} [1 - \exp(-2\Gamma\Delta t)], \quad (3.8)$$

where  $\Gamma$  is the effective elastic coefficient, which was found to be  $\Gamma = 1.8 - 2.1 \text{ s}^{-1}$  (from fit in Figure 3.15), which is comparable to what was reported by Das *et al.* ( $\Gamma = 2.2 \text{ s}^{-1}$ ) for active PS-Pt particles interacting with a solid wall.



**Figure 3.15:** Mean squared angular displacement curve for out-of-plane rotation of MF-Pt colloid in active and passive conditions.

### 3.4 Conclusion

In this chapter, we experimentally investigated at a single particle level, the translational and rotational behaviour of a Janus colloid close to the solid-liquid interface in both active and passive conditions. Translational diffusion is confined to a 2-dimensional motion due to gravity. In thermal equilibrium, by simultaneously measuring the translational diffusion parallel to the interface  $D_{Tr,\parallel}$  and rolling rotational diffusion  $D_{R,\perp}$  we were able to evaluate the gap distance  $h$  between the Janus colloid and the bottom wall. We found  $h$  in between 300 nm and 1.5  $\mu\text{m}$ , which is an equilibrium distance due

### 3. PARTICLE MOTION CLOSE TO A SOLID WALL IN- AND OUT- OF THERMAL EQUILIBRIUM

---

to the gravity attraction and electrostatic repulsion [63]. This large range of values of  $h$  may depend on the Janus colloid orientation and surface properties. The in-plane rotational diffusion  $D_{R,\parallel}$  was also measured both in passive and active conditions and it is very similar to the theoretical bulk value  $D_{R,b}$  as predicted by hydrodynamic models [106]. We characterize the active propulsion of Janus colloids in the presence of a given concentration of Hydrogen Peroxide. Active velocity observed for both the colloidal sizes peaks at 4.5 - 5  $\mu\text{m}\cdot\text{s}^{-1}$  and usually decreases as a function of the observation time. Active Janus colloids also show an angular active velocity, which is associated with a broken symmetry in the Janus geometry due to fabrication. In active conditions, the out-of-plane rotational dynamics is significantly confined and slowed down when compared to the same dynamics in passive conditions.

## Chapter 4

# Janus colloids in GUV neighbourhood

## 4. JANUS COLLOIDS IN GUV NEIGHBOURHOOD

---

In the previous chapter, we discussed in detail about the Brownian and active motion of Janus colloids close to a single wall, while this chapter focuses on the experimental investigation at the single particle level of the interaction between isolated active colloids and GUVs. The sample preparation for such experiments was mentioned in section [2.3.1](#) where the colloids as well as the vesicles are sedimented close to the substrate. GUVs sedimented on the substrate exist without any strong adhesion between the solid wall and the membrane boundary. As mentioned in previous chapter, 2% H<sub>2</sub>O<sub>2</sub> aqueous solution was always used to trigger the self-propulsion of Janus colloids [\[47, 114\]](#). For these experiments mainly POPC lipids were utilized to study their interaction with both SiO<sub>2</sub>-Pt and MF-Pt colloids and the observations are discussed in this chapter as following.

### 4.1 Brownian motion of a Janus colloid near a vesicle

For Janus colloids when observed in a close vicinity with the vesicles, the particles exhibit Brownian translational diffusion very similar to the free motion close to the interface. As seen from Figure [4.1](#), the Brownian motion trajectories for Janus colloid of both sizes which show a similar displacement in two dimensional space for colloids near a vesicle when compared to trajectories when the colloids are far from a vesicle for short time scales of  $\approx 2-3$  s (Figure [3.1](#)). For long time measurements, it was observed that when a Janus colloid which is only subjected to Brownian motion would approach a vesicle but then subsequently move away without any abrupt disturbances in the particle displacement, neither there was a any change in the COM of the GUV. This point towards absence of any particular adhesion between the particle and vesicle in passive conditions. Also, no spontaneous engulfment [\[83\]](#) or wrapping of the Janus colloids by GUVs was observed without any external force (Discussed in chapter 5).

## 4.1 Brownian motion of a Janus colloid near a vesicle

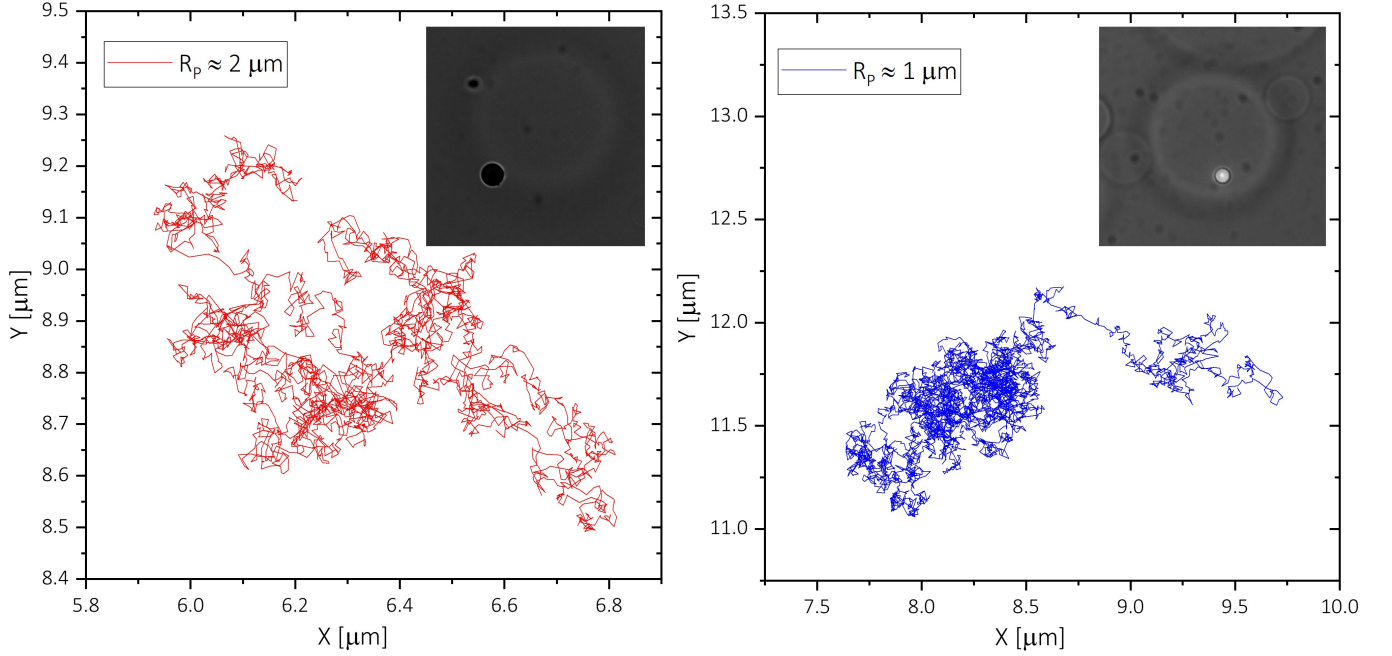


**Figure 4.1:** Brownian trajectories for SiO<sub>2</sub>-Pt (left) and MF-Pt (right) Janus colloids close to a GUV near the solid-liquid interface.

In Figure 4.2, the experimental  $MSD$  curves were fitted using equation:  $MSD = 4D_{Tr,\parallel}\Delta t$ , to obtain the translational diffusion coefficient ( $D_{Tr,\parallel}$ ) for SiO<sub>2</sub>-Pt ( $R_P \approx 2 \mu\text{m}$ ) and MF-Pt ( $R_P \approx 1 \mu\text{m}$ ) particles for short times when the particles are closest to the vesicle periphery.  $D_{Tr,\parallel}$  measured from the  $MSD$  curves was  $\sim 0.06 \mu\text{m}^2 \cdot \text{s}^{-1}$  for SiO<sub>2</sub>-Pt ( $R_P \approx 2 \mu\text{m}$ ) and  $\sim 0.15$  for MF-Pt ( $R_P \approx 1 \mu\text{m}$ ) colloids. These values are similar to the values previously obtained close to a single solid wall discussed in the previous chapter [15]. As the  $D_{Tr,\parallel}$  found for particle close to a vesicle is almost similar to its diffusion far away, it can be assumed that the fluid vesicles contribute to a very negligible drag on the nearby colloids in Brownian conditions.

## 4. JANUS COLLOIDS IN GUV NEIGHBOURHOOD

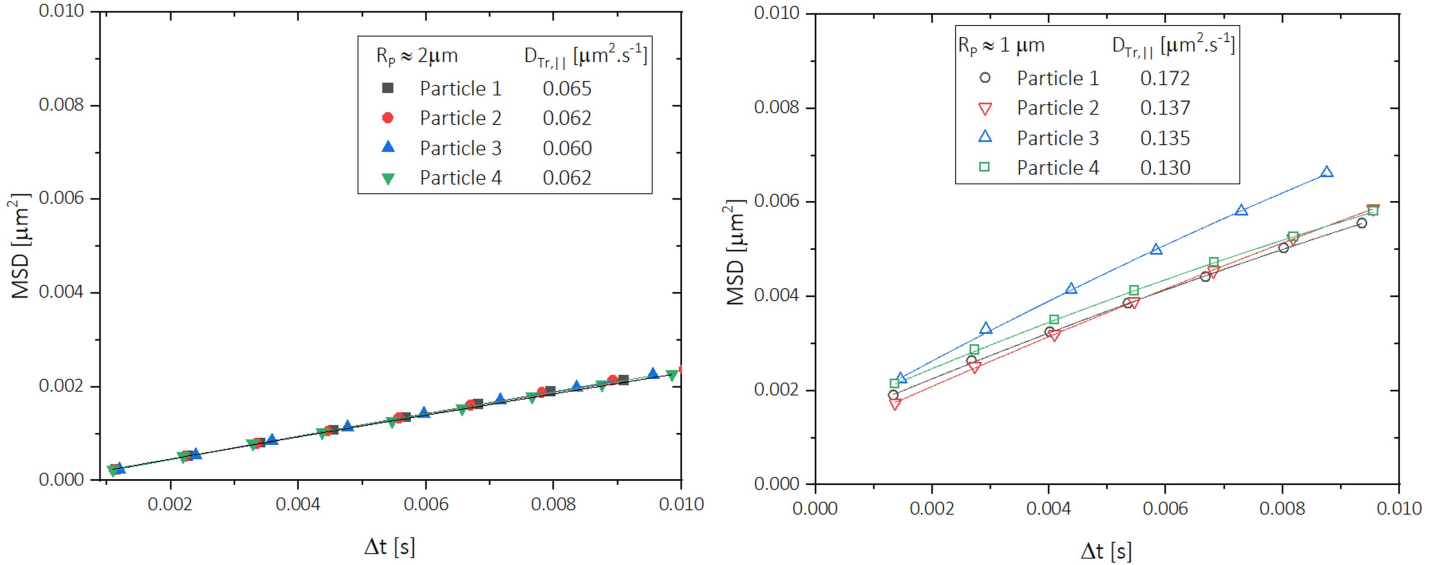


**Figure 4.2:** Mean Squared Displacement curve as a function of lag time  $\Delta t$  for Janus colloids (*left*) SiO<sub>2</sub>-Pt and (*right*) MF-Pt, in Brownian translation motion near a GUV, where the solid line indicates a quadratic fit over the curve.

### 4.2 Active motion in a diluted regime close to a GUV

In this section we experimentally investigate the interaction between self propelled Janus colloids and GUVs driven by active motion.

We observe that when an actively moving Janus colloids encounters a vesicle in its path, it is captured in a striking orbital motion around the GUV periphery along the Janus boundary. Orbital motion has previously been observed for Janus colloids rotating around passive solid objects [70] [71]. However, activity driven interaction with GUVs has never been explored. The interactions dynamics of such orbital motion are discussed in the following sections. As a constant propellant concentration of 2% H<sub>2</sub>O<sub>2</sub> was used to trigger particle activity, no adverse effect on the GUV was observed and the average size and properties of the GUVs appear to remain unchanged (see Figure 4.3).

In our experimental system, force and torque transfer (see section 4.4.1) was also observed due to active Janus colloids.



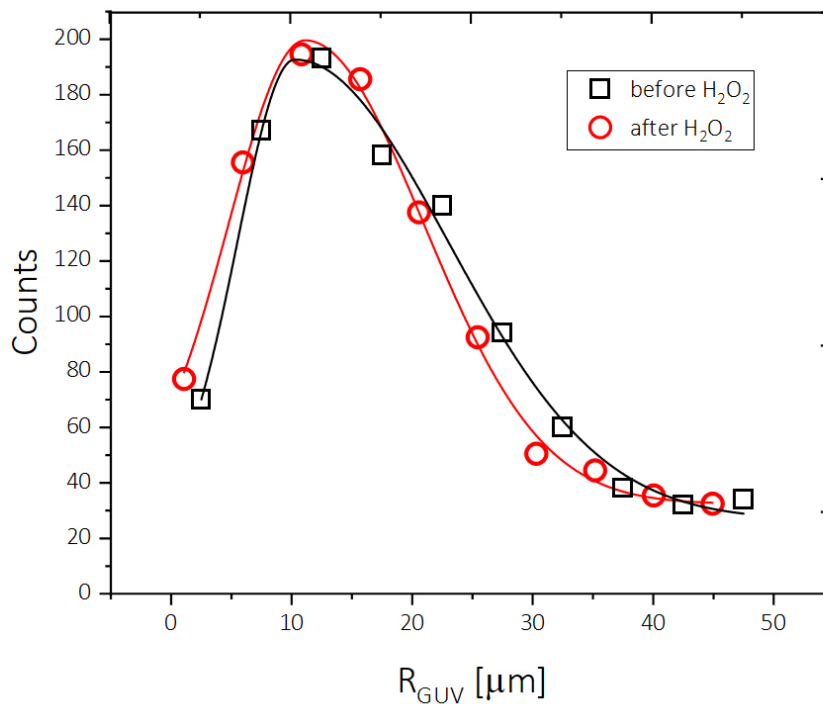


**Figure 4.3:** Size distribution curve for GUV before and after addition of 2%  $\text{H}_2\text{O}_2$ . The average size of the GUV close to interface was observed to be almost the same  $R_{GUV} \approx 11 \pm 6 \mu\text{m}$  before and after adding  $\text{H}_2\text{O}_2$ .

#### 4.2.1 Capture in persistent orbital motion

For diluted enough particle and vesicle concentrations, we were able to observe the interaction between single active Janus colloids and single GUV. In most of our experiments, whenever the trajectory of the active particle reached the vesicle boundary, the active particle initiated a striking orbital motion around the GUV. Figure 4.4 shows a typical trajectory of an active colloid orbiting around a GUV observed. For this particular example the GUV has a larger but comparable size to the active particle of radius  $R_P \approx 2 \mu\text{m}$ . For times  $t < 1$  s, the GUV is still not perturbed by the active particle. For  $1 < t < 2$  s, the silica face of the Janus particle pushes on the GUV membrane, which starts to translate a distance  $\Delta L$  with approximately constant speed  $V_{GUV} = 0.7 \mu\text{m.s}^{-1}$ . For  $t > 2$  s, the active particle performs a persistent orbital motion around the

#### 4. JANUS COLLOIDS IN GUV NEIGHBOURHOOD

GUV.

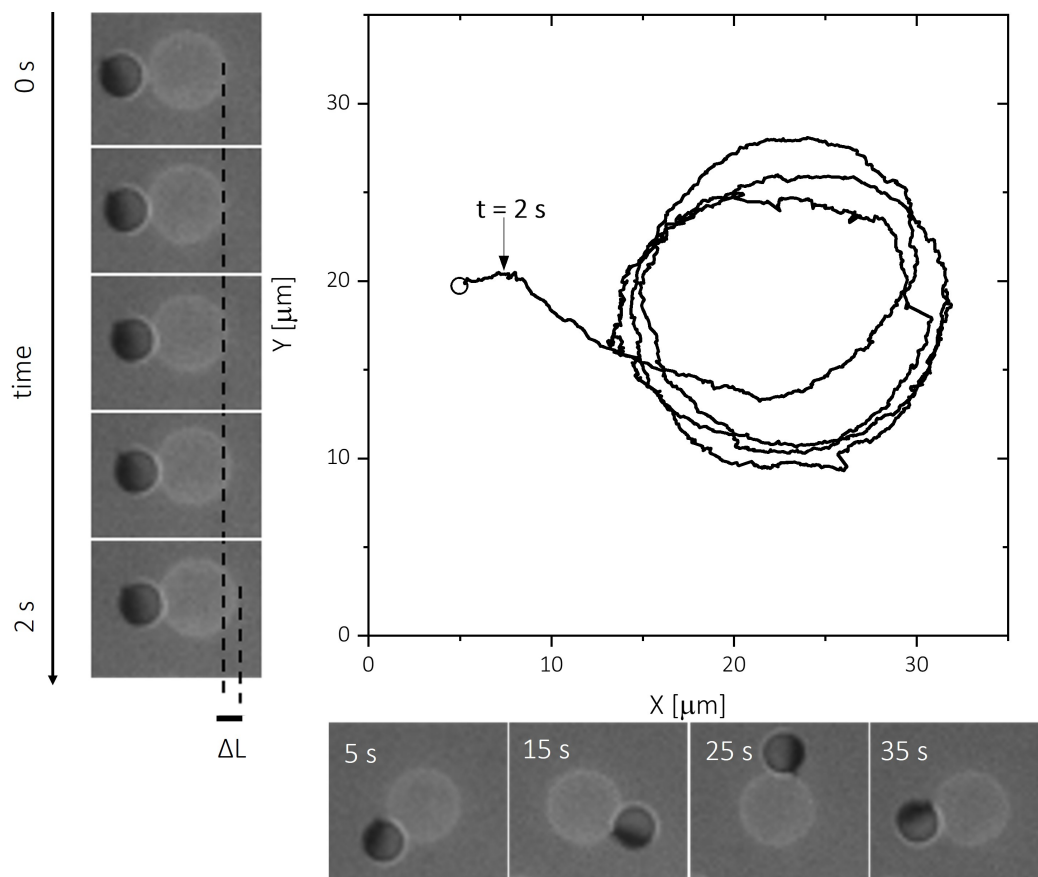


**Figure 4.4:** (A) Centre of mass trajectory of an active colloid of radius  $R_P \approx 2 \mu\text{m}$  interacting with a GUV. Time lapse images of the interaction between an active particle and a GUV are shown in the insets.

The time spent by the particles in the GUV orbits vary from few seconds up to a thousand seconds. If enough time is allowed to pass, the active colloid eventually leaves the GUV orbit and initiates again an active "free" motion before encountering another GUV. Even if the Janus colloid seems to adhere to the GUV, with the Janus boundary oriented radially with respect to the GUV centre (Figure 4.4), no membrane deformation (partial membrane wrapping)<sup>[9]</sup> or adhesion was observed by fluorescence microscopy. However, nanoscale membrane deformations below the resolution of our methods may occur. By measuring the vertical positions of the GUV and particle equators (by detecting their respective focal planes using the z-stage of the microscope), we confirmed that both colloid and vesicle sediment to the bottom of the container,

## 4.2 Active motion in a diluted regime close to a GUV

and the active motion of the Janus colloids occurs in the wedge defined by the planar substrate and the GUV (see Figure 4.5).

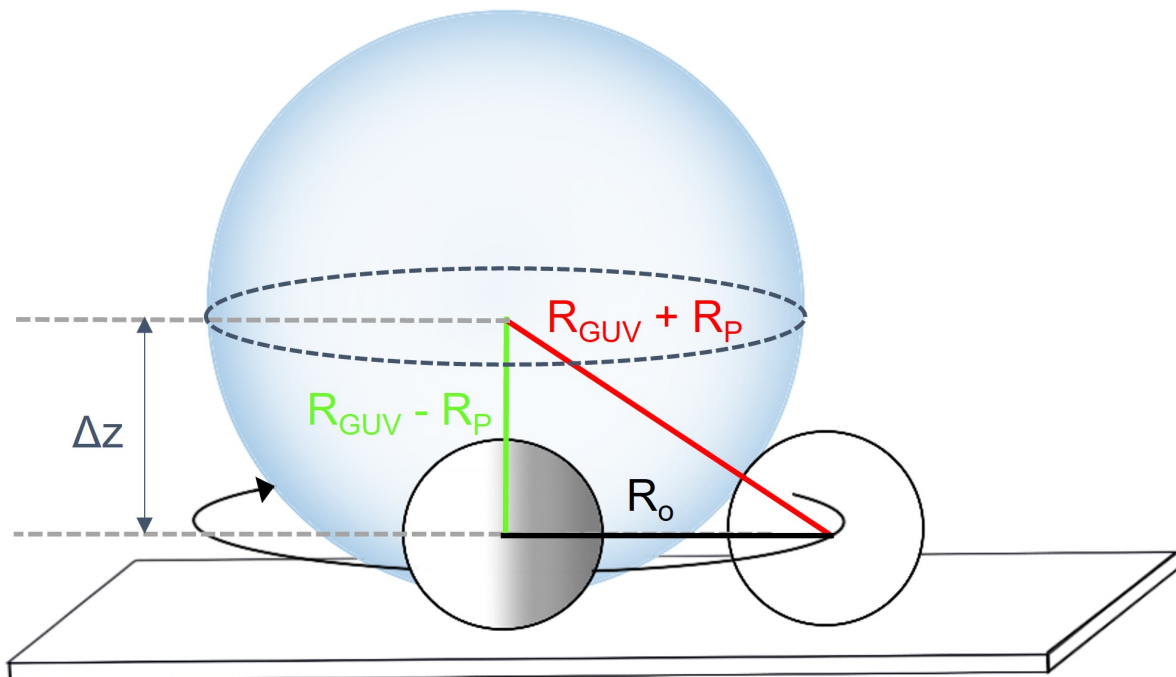


**Figure 4.5:** Sketch of the experimental geometry: a Janus colloid orbiting a GUV along the substrate.  $\Delta z$  is the difference between the focal plane of the GUV and the particle equator.  $R_O$  is the radius of the orbital trajectory (see also Figure 4.6).

Orbital trajectories were observed for both of the particle sizes that we used (MF-Pt,  $R_P \approx 1 \mu\text{m}$  and SiO<sub>2</sub>-Pt,  $R_P \approx 2 \mu\text{m}$ ) and in the whole range of GUV sizes investigated here. We observed both rotation directions with a comparable statistics between clockwise (CW) and counter clockwise (CCW) orbital motion directions.

For  $R_P \approx 1 \mu\text{m}$  active colloids, in some cases, we also observed switching events between the two rotation directions during an ongoing orbital motion: an active colloid rotating CW (CCW) is able to remain close to a GUV and change to CCW (CW) direction, without escaping the GUV, see Figure 4.6 (two CCW–CW and one CW–CCW switching events). This switching may result from both in plane and out of plane Brownian rotational motion of the colloid. For  $R_P \approx 2 \mu\text{m}$  active colloids, instead, we did not detect switching events between the two possible orbital directions, see Figure 4.6.

#### 4. JANUS COLLOIDS IN GUV NEIGHBOURHOOD

From the circular path of particle trajectories, one could evaluate an orbital radius  $R_O$  (see Figure 4.5 and 4.6) and estimate the size of the GUV. Assuming spherical objects in close contact are both resting on the planar substrate,  $R_{GUV} \approx R_O^2/(4R_P)$ . For some trajectories we also measured directly the GUV size (in fluorescence or bright field microscopy) by changing the focal plane from the particle equator to the GUV. These GUV size measurements agree with the estimated value from the orbital radius. Preliminary Reflection Interference Contrast Microscopy (RICM) experiments (see Appendix A5) show in some cases the signature of a vesicle flattening close to the substrate due to the gravity, which is however very small compared to the vesicle size.

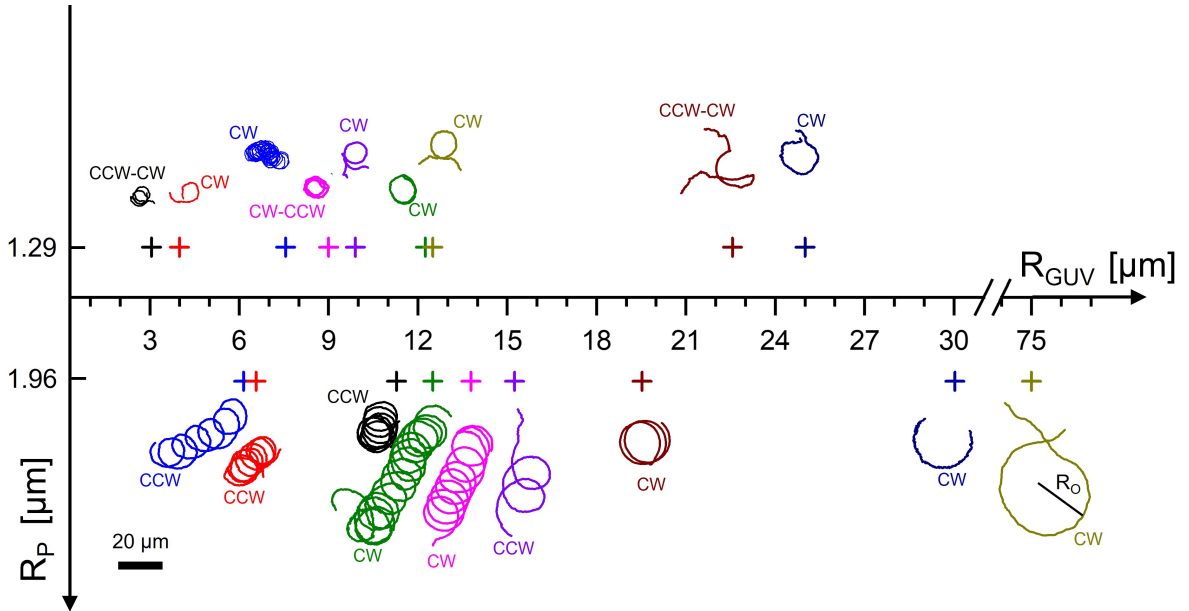


**Figure 4.6:** Centre of mass trajectories of active Janus colloids ( $R_P \approx 1$  and  $2 \mu\text{m}$ ) around GUVs of different sizes. The range of observation time is 30–788 seconds. Clockwise (CW) and counterclockwise (CCW) directions are also reported close to the trajectories.

Trajectories shown in Figure 4.6 demonstrate that orbital motion appears in a wide range of GUV and active particles sizes, covering vesicle to particle radii ratios  $R_{GUV}/R_P \approx 1.5$  to 20. Note that some trajectories in Figure 4.6 are clearly affected by some drift velocity due to convective flows. However, this drift velocity is significantly lower than the particle speed and it can be easily decoupled from the particle motion in our analysis.

We observe that active colloids display persistent orbital motion around GUVs, that can be viewed as soft spheres with fluctuating surfaces, a feature also seen for active rod particles orbiting around isolated solid obstacles; and for spherical active Janus colloids orbiting in a crystal made of large solid particles [70, 71]. In the bulk, far-field hydrodynamics is able to explain such persistent orbital motion for active particles behaving as a "pusher" squirmer. This squirmer category pushes the liquid in the front and in the rear, and entrains the liquid on the sides (here the Janus boundary), which leads to an effective hydrodynamic attraction with an obstacle (here the GUV) located in close proximity [70, 75].

However, our experimental results for sedimented active colloids and GUVs show also a clear difference with respect to the bulk far-field hydrodynamic predictions for orbital motion around either spherical solid or liquid obstacles [70, 75]. In fact, in our experimental system we did not observe any critical radius of the GUVs for the onset of the orbital motion (see Appendix A4). Hydrodynamic models predict that in the bulk, for obstacle size lower than a critical value  $R_C$  ( $\approx 10\text{--}15R_P$ ), the active particle shows a scattering behaviour; whilst for obstacle radii larger than  $R_C$ , a persistent orbital motion of the active particle around the obstacle occurs.

### 4.2.2 Orbital time statistics

Analysing about two hundred trajectories showing the interaction between an active colloid and a GUV, we evaluate the time spent by the particle around the GUV, which we call the orbital time ( $t_{orb}$ ). In Figure 4.7, we plot the normalized counts of orbital time  $t_{orb}$  (or trapping time [75]) for both particle sizes. It varies from few seconds to several minutes. An exponential function  $\sim \exp(t_{orb}/t^*)$  can be used to approximately describe the  $t_{orb}$  distribution [70]. From the fits, we find characteristic times  $t^* = 23 \pm 1$  s for  $R_P \approx 1 \mu\text{m}$  and  $t^* = 46 \pm 5$  s for  $R_P \approx 2 \mu\text{m}$  (see inset in Figure 4.7). It is important to remark that  $t^*$  for  $R_P \approx 2 \mu\text{m}$  particles is approximately twice that of  $R_P \approx 1 \mu\text{m}$  particles. Interestingly, this proportionality correlates thus with the bulk translational friction coefficient of spheres  $6\pi\eta R_P$ . It is thus tempting at this stage to speculate on the possible reasons for a particle to escape the orbit where it has been captured. The strength of the attraction of a pusher to a wall is known to depend on the velocity of the particle [66]. A significant slowdown of the orbital velocity could then allow for escaping the orbit. However, all the escaping events that we have observed

#### 4. JANUS COLLOIDS IN GUV NEIGHBOURHOOD

were not found to be associated with a stalling or a significant change in the particle velocity. Another possible explanation for orbital escape could reside on the spontaneous stochastic rotation of the particle into an angular position where its propulsion would drive it away from the membrane [75].

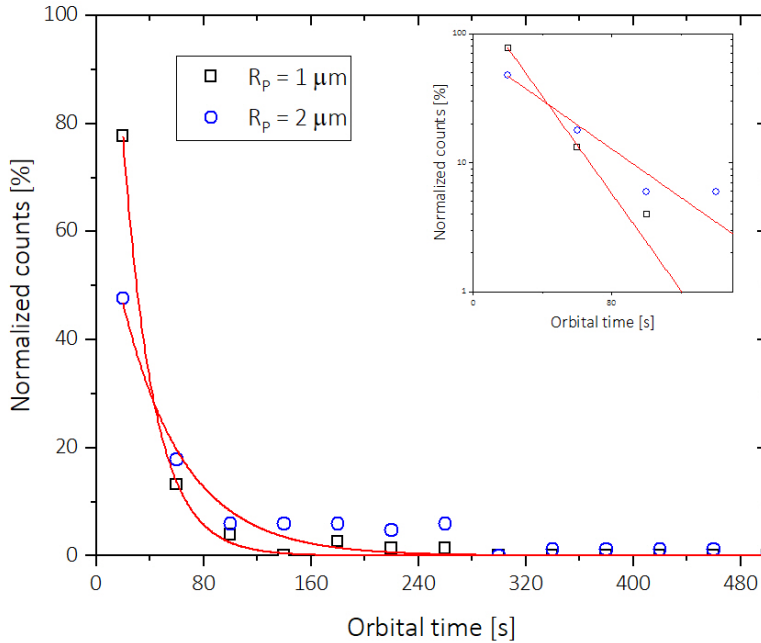


**Figure 4.7:** Normalized counts of orbital times of  $R_p \approx 1$  &  $2 \mu\text{m}$  particles rotating around GUVs. The red curves are exponential functions  $\sim \exp(-t_{orb}/t^*)$ . A log-linear representation of the data is shown in the inset.

Indeed, as we will further study below, the orbital motion of the Janus pusher proceeds with a propulsion direction close to the tangent of the circular orbit, a strong deviation from this orientation could potentially drive the particle away. However, we have in a few instances observed clockwise movement spontaneously changing into counterclockwise, and conversely. During such changes of orbital direction, the particles are favorably oriented to move away from the wall but stay trapped instead. Hence, the escape dynamics may be governed by the Brownian translational diffusion of the particle as predicted by Spagnolie *et al.* [75]; or by the membrane–particle repulsive interaction observed in the absence of  $\text{H}_2\text{O}_2$ . Indeed, our passive colloids do not tend

to adhere to GUVs in thermal Brownian motion, even when colloids were very close to the GUV membranes.

### 4.2.3 Characterization of orbital motion

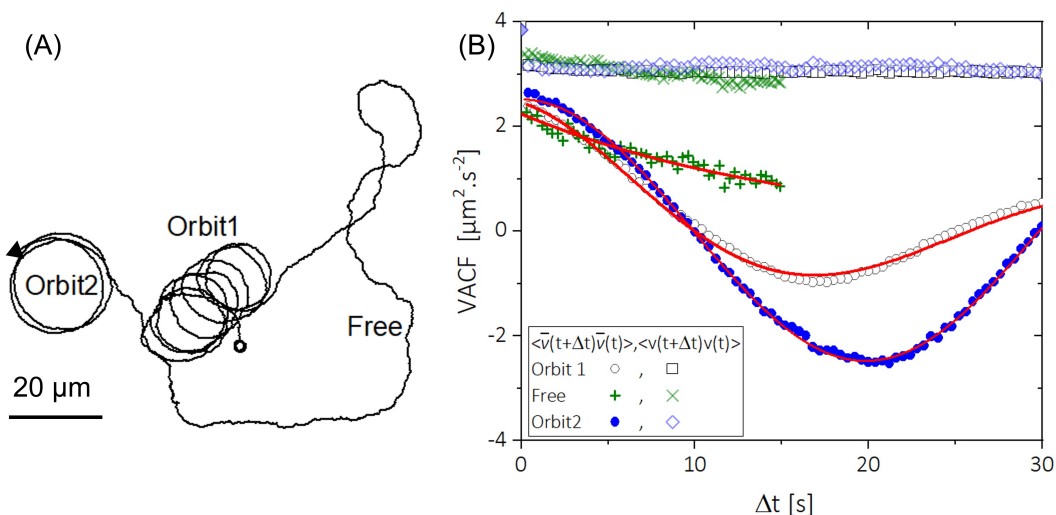


**Figure 4.8:** (A) Trajectory of a  $R_P \approx 2 \mu\text{m}$  active colloid orbiting around two GUVs and performing a "free" motion in between. (B) Velocity autocorrelation functions as a function of lag time  $\Delta t$  for the trajectory shown in (A).

In order to elucidate the strength and the nature of the interaction between an active colloid and a giant unilamellar vesicle, we performed a detailed analysis of the trajectories and of images taken during the orbital motion and compared them to data describing active colloids far away from the GUVs. From the active particle tracking, we calculated the discrete velocity vector  $\bar{\nu}$  (described in section 3.2.1) along with its associated modulus  $\nu = \sqrt{\nu_x^2 + \nu_y^2}$ . From  $\bar{\nu}$  and  $\nu$ , discrete velocity vector  $\langle \bar{\nu}(t + \Delta t) \bar{\nu}(t) \rangle = \langle \nu_x(t + \Delta t) \nu_x(t) \rangle + \langle \nu_y(t + \Delta t) \nu_y(t) \rangle$  and velocity modulus  $\langle \nu(t + \Delta t) \nu(t) \rangle$  correlation function can be measured.

In Figure 4.8(A), we show a typical trajectory of an active colloid orbiting around a GUV for about seven times (Orbit1). Then, the particle escapes from the first orbit and perform "free" active motion before encountering a second GUV (Orbit2). VACF corresponding to this trajectory divided in three ranges (Orbit1, Free and Orbit2) are shown in Figure 4.8(B).

#### 4. JANUS COLLOIDS IN GUV NEIGHBOURHOOD

---

In the orbital and "free" motion,  $\langle \nu(t + \Delta t) \cdot \nu(t) \rangle$  as a function of the lag time is approximately constant, which shows the absence of three-dimensional motion and negligible out of plane rotational dynamics of the active Janus colloid. A decay of the autocorrelation function of the active velocity modulus  $\nu = \sqrt{\nu_x^2 + \nu_y^2}$  could in fact indicate a non-zero z-component of the velocity,  $\nu_z$  [69]. During the "free" motion, a decay of  $\langle \bar{\nu}(t + \Delta t) \cdot \bar{\nu}(t) \rangle$  due to the in-plane rotational diffusion ( $D_{R,\parallel}$ ) could be also fitted by equation,

$$\langle \bar{\nu}(t + \Delta t) \cdot \bar{\nu}(t) \rangle = V^2 \cos(\omega \Delta t) f_r + V_d^2 \quad (4.1)$$

with a zero angular velocity (no orbital motion), which also provides  $f_r = \exp(-D_R \Delta t)$  and leads to the rotational diffusion in the "free" motion. The orbital motion of the particle around a GUV is not in general described by equation 4.1. The interactions of the particle with the vesicle introduces a number of other force sources. Beyond the particle propulsion (translation and rotation) and Brownian noise leading to the form in equation 4.1, dynamical confinement forces and the resulting confined Brownian rotation and translation motions, vesicle shape fluctuations, all conjugate into a complex evolution of the particle orbital trajectory. It is however simple to show that for a perfectly circular orbital motion at constant orbital frequency  $\omega$ , the autocorrelation function would have the form of equation 4.1 with  $f_r = 1$ , thus providing a convenient manner to directly extract orbital velocities from the particle trajectory data alone.  $\langle \bar{\nu}(t + \Delta t) \cdot \bar{\nu}(t) \rangle$  in Orbit1 shows a clear oscillation due to the angular velocity  $\omega$ . In Orbit1, damping of  $\langle \bar{\nu}(t + \Delta t) \cdot \bar{\nu}(t) \rangle$  does not prevent the evaluation of the angular velocity. Fitting the data by equation 4.1, we were able to evaluate,  $V$  and  $\omega$ ; and measure a negligible drift velocity ( $< 0.15 \mu\text{m} \cdot \text{s}^{-1}$ ). We evaluate  $\omega$  in the range 0.25–0.76  $\text{rad} \cdot \text{s}^{-1}$  for  $R_P \approx 1 \mu\text{m}$  and in between 0.15 and 0.5  $\text{rad} \cdot \text{s}^{-1}$  for  $R_P \approx 2 \mu\text{m}$  and verified that consistently  $V = \omega R_O$  for all orbital motions, while active velocity  $V$  was found to be between 0.9 to 4.4  $\mu\text{m} \cdot \text{s}^{-1}$  for the MF-Pt ( $R_P \approx 1 \mu\text{m}$ ) and 1.1 to 3.4  $\mu\text{m} \cdot \text{s}^{-1}$  for SiO<sub>2</sub>-Pt ( $R_P \approx 2 \mu\text{m}$ ) colloids, where the variation in speeds for similar colloids could be due to the different time of observation after addition of H<sub>2</sub>O<sub>2</sub>.



## 4.2.4 Velocity comparison between orbital and free motion

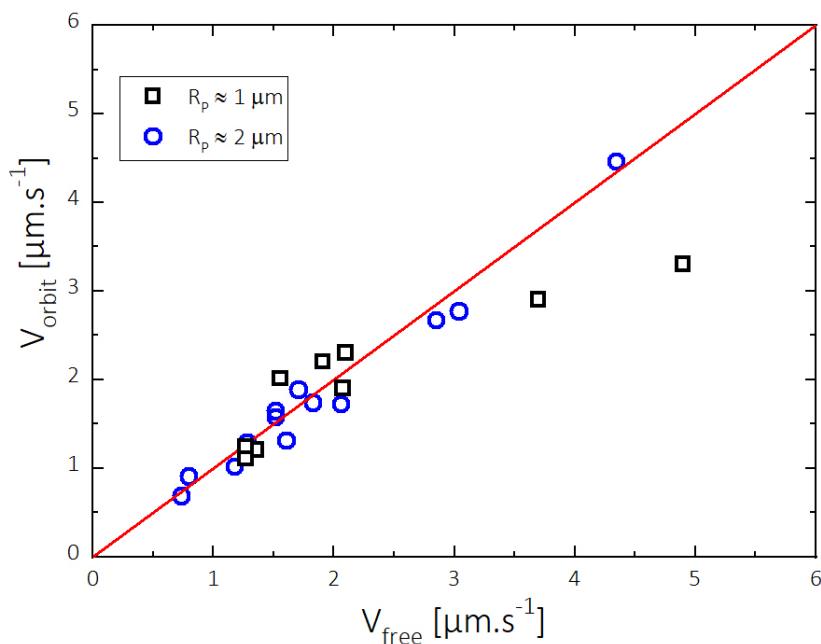


**Figure 4.9:** Orbital speed of  $R_p \approx 1$  and  $2 \mu\text{m}$  active colloids as a function of the speed far from the orbit.

In Figure 4.9, we plot the particle speed in the orbit as a function of the speed when the active particle is far from the GUV (for each particle whose trajectory allows a robust measurement of  $\langle \nu(t + \Delta t) \cdot \nu(t) \rangle = V^2$  in the "free" and orbital motion, see Figure 4.8(B)). Even if the  $\text{H}_2\text{O}_2$  fuel concentration is fixed at 2%, a range of velocities is observed due to different observation times (from few minutes to some hours after the addition of  $\text{H}_2\text{O}_2$ , which is consumed in time) and an intrinsic variability in the catalytic coating due to the Janus colloid fabrication [116].

Most of the data lies on the line  $V_{orb} = V_{free}$ , in agreement with results obtained for active rods orbiting around solid spherical obstacles, and pointing to a speed independent from the active particle-obstacle distance [70]. However, for the velocities above  $3 \mu\text{m}\cdot\text{s}^{-1}$ , several points show  $V_{orb} < V_{free}$ . The equality of velocities in the free and orbital motions can be rationalized within two opposite scenarios. Obviously,

velocity equality would hold if no additional dissipation was involved as the particle is captured into the orbital motion. However, this is unlikely due to the proximity to the membrane wall and to the strong distortion of the flow environment in the confinement wedge.  $V_{orb} = V_{free}$  could also result from an increase of the propulsion mechanism due to a wall effect [66], which would be compensated by an increase of the translational drag [117]. Whether this perfect compensation is a coincidence or a consequence of the self-propelled motion confined wedges remains to be elucidated.

### 4.3 Particle rotation dynamics in orbital motion

In order to gain a deeper insight into the rotational dynamics of an active colloid bound to an orbital trajectory, we performed image analysis of both the particle and the GUV around which it orbits. For some cases of  $R_P \approx 2 \mu\text{m}$  particles, we were able to detect both the orientation of the particle Janus boundary and the centre of mass of the GUV (see Section 2.4.2). In this way, we could find the particle location angle  $\theta$  and orientation angle  $\varphi$  in the GUV frame, see Figure 4.10. Hence, to evaluate the Brownian rotational diffusion of the Janus particle in the orbit we calculated the mean squared angular displacement  $\langle \Delta(\varphi - \theta)^2 \rangle$ , which is plotted as a function of the lag time in Figure 4.10(B).

For very short lag times,  $\langle \Delta(\varphi - \theta)^2 \rangle$  shows a linear behaviour; whilst a saturation could be observed already before  $\Delta t = 1 \text{ s}$ , which is related to a confinement effect as also seen in Figure 4.10(A). Such saturation is the signature of confined rotational diffusion due to the fluid flow generated by the active particle, which tends to align the particle Janus boundary towards the GUV centre [74]. For confined Brownian dynamics,  $\langle \Delta(\varphi - \theta)^2 \rangle$  can be written as [66]:

$$\langle \Delta(\varphi - \theta)^2 \rangle = \frac{D_{R,orb}}{\Gamma} [1 - \exp(-2\Gamma\Delta t)], \quad (4.2)$$

where  $\Gamma$  is an effective elastic constant for the angular velocity:  $\omega = -\Gamma(\varphi - \theta)$  which tends to restore the particle angular position  $\varphi = \theta$  (see inset in Figure 4.10(B)), with the particle Janus boundary orientated radially to the centre of the GUV.

The fit of equation 4.2 to the data shown in Figure 4.10(B) leads to  $D_{R,orb} = 0.013 \pm 0.001 \text{ rad.s}^{-1}$ , which indicates a clear slowing down of the orbital rotational diffusion when compared to the theoretical  $D_{R,b} = 0.02 \text{ rad.s}^{-1}$  or the experimental  $D_{R,free} =$

## 4.4 Force transfer between vesicle and particle

$0.03 \pm 0.01 \text{ rad}\cdot\text{s}^{-1}$ . Moreover, for active particles interacting with a single wall,  $\Gamma \cong V/R_P \cong 2.2 \text{ s}^{-1}$  was predicted by Das *et al.*, which is comparable to  $\Gamma = 1.15 \pm 0.09 \text{ s}^{-1}$  from the fit shown in Figure 4.11. Hence,  $\langle \Delta(\varphi - \theta)^2 \rangle$  data confirm a slowing down of the rotational diffusion with respect to the bulk rotational diffusion, which can be associated to a friction due to the active colloid–GUV interaction.

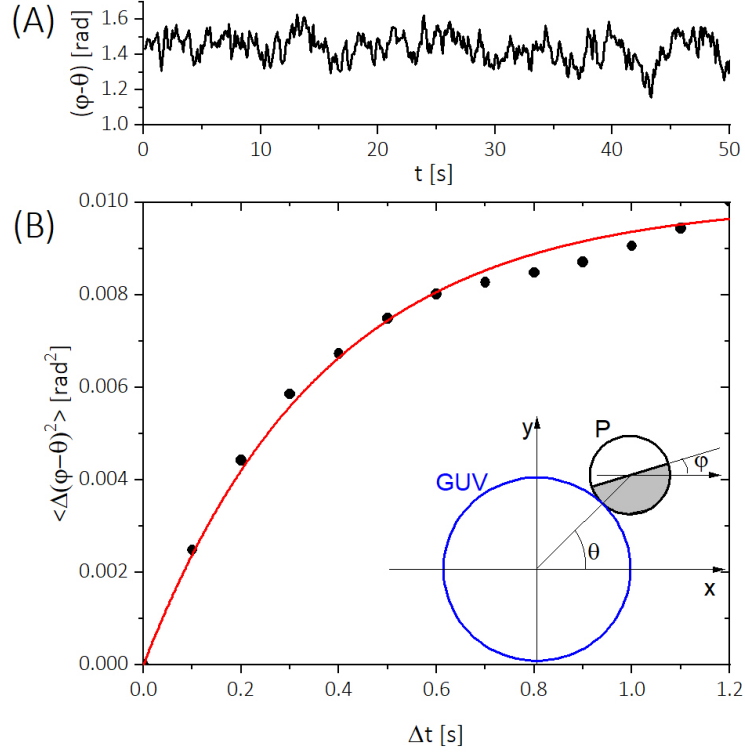


**Figure 4.10:** (A)  $\varphi - \theta$  as a function of the experimental time for a  $R_P \approx 2 \mu\text{m}$  active colloid orbiting a GUV. (B) Mean squared angular displacement  $\langle \Delta(\varphi - \theta)^2 \rangle$  as a function of the lag time. Solid line is a fit of equation 4.2 to the data. In the inset, a sketch of a Janus particle (P) orbiting around a GUV together with the polar location angle  $\theta$  and the orientation angle  $\varphi$  in the GUV frame are displayed.

## 4.4 Force transfer between vesicle and particle

Force and torque transfers can indeed occur when an active particle interacts with a GUV. Already in Figure 4.4, we showed that a GUV can translate a distance  $\Delta L$  with a speed  $V_{GUV} = 0.7 \mu\text{m}\cdot\text{s}^{-1}$  when an active colloid comes in close contact. An effective force  $F_{GUV}$  on the GUV can be calculated as  $F_{GUV} = \zeta_{tr} V_{GUV} \approx 6\pi\eta R_{GUV} V_{GUV} \approx 46$

## 4. JANUS COLLOIDS IN GUV NEIGHBOURHOOD

fN, where  $\zeta_{tr}$  is a simple estimate for the GUV translational friction coefficient. These few tens of femto- newtons were measured several times in our experiments during the impact of active colloids on GUVs.

### 4.4.1 Torque transfer in the system

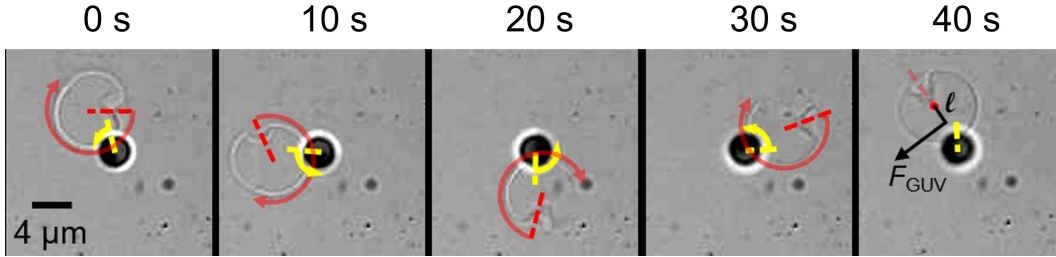


**Figure 4.11:** Time lapse images of an  $R_P \approx 2 \mu\text{m}$  active colloid rotating in a CCW direction (yellow arrow) but not translating and interacting with a GUV, which is both revolving around the Janus colloid and rotating in a CW direction (red arrow). Arrow arc length shows the rotation around its own axis between two frames (time is given on the top of the image).

An additional experimental result is now presented to describe how an active colloid is able to impart also a torque on a GUV. Figure 4.11 shows a complementary observation for an active colloid ( $R_P \approx 2 \mu\text{m}$ ), which is not translating but only rotating in a CCW direction around an axis parallel to the normal to the substrate and passing through its centre of mass. Presumably, the colloid is partially stuck onto the solid substrate, but keeps its rotational activity. A GUV (whose size is approximately twice the particle size) revolves around the active Janus colloid also in a CCW direction. The GUV position appears to follow the orientation of the Janus boundary, with the centre of mass of the GUV slightly off with respect to the radial direction defined by the Janus boundary. Angular velocities of the GUV in the orbital motion and Janus colloid rotation are approximately the same,  $\omega = 0.155 \pm 0.005 \text{ rad.s}^{-1}$ : a passive GUV is orbiting around an active colloid with a tangential velocity  $V_{GUV} = \omega(R_{GUV} + R_P) \approx 0.9 \mu\text{m.s}^{-1}$ . An effective tangential force acting on the centre of mass of the GUV can be calculated as  $F_{GUV} = \zeta_{Tr,GUV}V_{GUV} \approx 72 \text{ fN}$ . Some defects present on the GUV (see Figure 4.11) also allow monitoring the rotation of the GUV around its own axis. The GUV rotates in a CW direction (opposite to the orbital motion) with  $\omega_{GUV} = 0.415 \text{ rad.s}^{-1}$ , and a

corresponding torque,

$$M = \zeta_{R,GUV} \omega_{GUV} \approx 8\pi\eta R_{GUV}^3 \omega_{GUV} \quad (4.3)$$

41 fN  $\mu\text{m}$ , where  $\zeta_r$  is the GUV rotational friction coefficient. The simultaneous force and torque acting on the GUV, generated by the local fluid flow of the active colloid, could be explained considering that the centre of mass of the GUV is slightly off with respect to the Janus boundary direction. An effective lever arm  $l = M/F_{GUV} = 0.57 \mu\text{m}$  could thus describe the offset between the GUVs centre of mass and the location of the effective force acting on the GUV (see Figure 4.11 at 40 s).

To summarize, our experiments (Figure 4.4, 4.10 and 4.11) clearly show the possible translation and rotation of GUVs under the effects of the fluid flow generated by the active particle. Note that our findings are in contrast with previous observations reporting no torque transfer and no rotation of solid spherical particle during the orbital motion of active rods [70].

## 4.5 Conclusion

We have experimentally investigated at the single particle level, the interaction between an isolated active colloidal particle and a giant unilamellar vesicle. Persistent orbital motion was observed in the whole range of GUV-particle size ratios investigated. Hence, no critical size for the onset of orbital motion was detected, which is in net contrast to far field hydrodynamic models for solid or fluid spherical obstacles in the bulk. In our experimental system, the tensionless and fluctuating nature of lipid bilayers leads to hydrodynamic boundary conditions that may be different to the ones considered so far [72, 73]. We also clearly show that a transfer of forces and torque occurs during the active colloid-GUV interaction, which results in a persistent translation of the GUV during the particle impact, a slowing down of the particle rotational diffusion with respect to the bulk, and a persistent GUV orbital motion around a rotating but not translating active particle. Still, far-field hydrodynamics can be used to explain not only the orbital motion due to a fluid flow generated by the active particle and pointing towards the particle Janus boundary, but also the role of the translational Brownian diffusion in the escape dynamics [73, 75].

#### 4. JANUS COLLOIDS IN GUV NEIGHBOURHOOD

---

Finally, our results provide new perspectives on the interaction between active particles and soft compartments, which go beyond the effect of guiding [118] and scattering [119] as observed for the interaction of a bacterium with a passive colloid. Active particles are indeed able to impart forces and torques on giant lipid vesicles, as it was very recently reported for active particles encapsulated inside a vesicle [120]. These results motivate future investigations in partial and complete particle engulfment regimes to study directional transport of GUV by active colloids and activity triggered particle endocytosis.

## Chapter 5

# Janus colloid engulfment by GUV membranes

### 5.1 Overview

In the previous chapter, we described the interaction of Janus colloids in either active or passive conditions (in the presence or absence of Hydrogen Peroxide respectively) with GUVs where the interaction between the particle and the vesicle is determined by the nature of the two surfaces and by the propelling forces, while in this chapter we aim at further adding an external force to promote particle engulfment by GUV membranes.

As the interaction of micro-sized particles with lipid membranes is critical for a variety of biological and industrial processes, the uptake of Janus colloids by GUVs deserves further investigation under controlled experimental conditions. Motivated by the recent investigation conducted by Spanke *et al.* [83] reporting the wrapping of PS colloids by floppy GUVs driven by depletion interactions, in this chapter we tune the force of interaction (using centrifugation and optical tweezers setups), as well as the type of Janus colloids (SiO<sub>2</sub>-Pt and MF-Pt) and GUVs (POPC and DOPC) to investigate what parameters drive the activation of either partial or complete engulfment of Janus colloids by GUVs. Up to this point of our manuscript, we have worked in the "free regime" depicted in Figure 5.1, as the spontaneous colloid-GUV interaction did not imply adsorption or membrane wrapping.

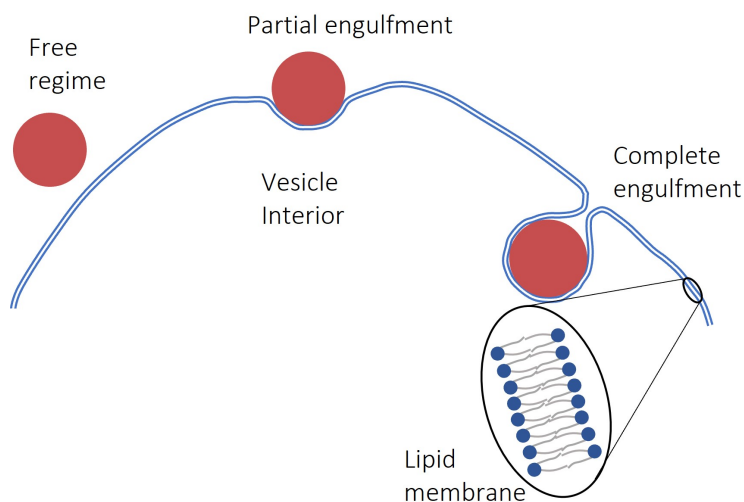


**Figure 5.1:** States of engulfment in a colloid-GUV system.

We aim at exploring the effect of various parameters on "partial engulfment," which occurs when the colloidal particle is partially wrapped by the membrane, or "complete



engulfment," which occurs when the colloidal particle is totally wrapped and exists in the membrane interior (i.e uptake by the GUV).

## 5.2 Particle engulfment by a membrane: theoretical background

For the wrapping of a colloidal particle by a GUV membrane, a balance of three energies plays a vital role. These three energies are: i) *adhesion*:  $E_{adhesion}$ , which is driven by a contact energy per unit area  $w$ ,  $E_{adhesion} = w \times A_{contact}$ , where  $A_{contact}$  ( $=2\pi R_P^2 z_p$ , for specified degree of wrapping  $z_p$ , see Figure 5.2) is the area of the particle that is in contact with the vesicles [121]; and opposed by the requirement for the membrane to ii) *bend*:  $E_{bend}$  is the bending energy, and iii) the work required against the membrane *tension*  $\sigma$  to pull the excess membrane towards the site of adhesion, whose energy is  $E_{tension}$ . The bending energy associated with the wrapping of a colloid is given by  $E_{bend} = \frac{1}{2}\kappa_b (c_1 + c_2 - m)^2 \times A_{contact}$  [122], with  $\kappa_b$  being the bending stiffness,  $c_1$  and  $c_2$  the principal curvatures of the membrane over the contact area and  $m$  the spontaneous membrane curvature. Considering a spherical particle and  $m=0$ ,  $E_{bend}$  can be written as  $E_{bend}=4\pi\kappa_b z_p$ , where the degree of wrapping  $z_p = 1 - \cos\theta$  (with  $\theta$  being the particle contact angle, see Figure 5.2). The energy cost to pull the excess membrane area  $A_{excess} = \pi R_P^2 z_p^2$ , to the site of adhesion is  $E_{tension} = \pi R_P^2 z_p^2 \sigma$ .

A *bendocapillary* length can be defined to describe the competition between membrane bending and tension. Membrane deformations that occurs for length scales smaller than the *bendocapillary* length  $\lambda_b = \sqrt{2\kappa_b/\sigma}$  [83] are mostly governed by bending energy while at larger length scale the membrane tension governs the deformation resistance.

Hence, for the micron-sized ( $R_P \approx 10^{-6}$  m) Janus colloids and GUVs used in this study showing  $\kappa_b \approx 20$  k<sub>B</sub>T, the bending resistance plays a major role for  $\sigma < 10^{-8}$  N.m<sup>-1</sup>. For  $\sigma > 10^{-8}$  N.m<sup>-1</sup>, the energy  $E_{tension}$  to stretch the membrane area should also be considered.

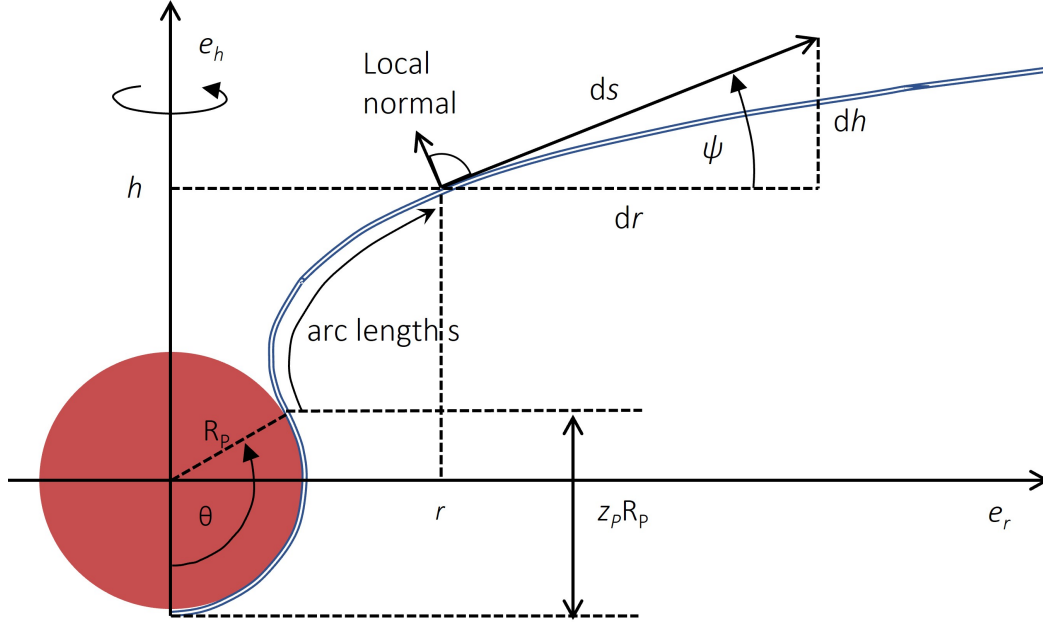


**Figure 5.2:** Illustration for wrapping geometry of a spherical colloid by a membrane. Image reproduced from [121]

### 5.3 Force driven interaction for Janus colloid engulfment by GUV

The competition between the above mentioned energies ( $E_{adhesion}$ ,  $E_{bend}$  and  $E_{tension}$ ) [123] leads to either the free or partial/complete engulfment regimes. Energy barriers that exist between free, partial or complete engulfment states can be overcome by means of an external force. Here, we have applied external forces by either centrifugation or optical tweezers (discussed in detail in the following sections).

#### 5.3.1 Centrifugation

Taking inspiration from Shingyou *et al.* [80], in order to drive the interaction between Janus colloids and GUV, we used centrifugation as an external force. The samples for centrifugation were prepared according to the protocol as mentioned in section 2.3.1. Using centrifugation, we were able to achieve forces in the range of  $10^{-11}$  to  $10^{-9}$  N, while the time of centrifugation was kept constant at 4 minutes, to ensure enough contact time between the colloids and GUVs. As described in the section 2.3.1 the

### 5.3 Force driven interaction for Janus colloid engulfment by GUV

colloids are already settled at the bottom of the centrifugation tube before the GUVs are added, meaning that the forces only operate on the vesicles and the centrifugation effect on the colloids can be neglected, thereby giving better control over the tuning of force effect on partial or complete engulfment of the colloids. The force curves as a function of vesicle radius ( $R_{GUV}$ ) for the three different levels of centrifugation force utilized in this experiment are shown in Figure 5.3, low force  $\leq 1000$  RPM (RCF/ $g \approx 100$ ), moderate force 2000 - 3000 RPM ( $400 \leq \text{RCF}/g \leq 1000$ ) and high force  $\geq 4000$  RPM (RCF/ $g \approx 1700$ ). As the GUVs prepared by gel formation method were obtained within the size range of  $R_{GUV} = 11 \pm 5 \mu\text{m}$  (see Figure 2.9), the effective force applied on the GUVs lies within the range of  $F_c = \Delta\rho\frac{4}{3}\pi R_{GUV}^3 (\text{RCF}) \approx 10^{-11} - 10^{-9}$  N.

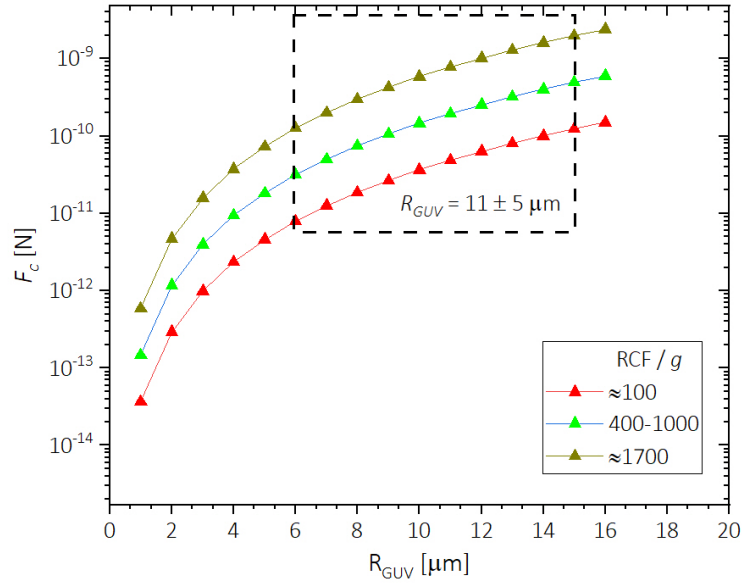


**Figure 5.3:** Force of centrifugation as a function of vesicle radius ( $R_{GUV}$ ) for different relative centrifugal force, RCF.

As seen in Figure 5.4, engulfment of Janus colloids was observed with centrifugation at moderate forces ( $10^{-9} < F_c < 10^{-11}$  N). For forces less than  $10^{-11}$  N the particles appear to remain in the free regime while at higher forces  $10^{-9}$  N the particles appear to either split or totally rupture the membranes (discussed in section 5.4). The partial engulfment for Janus colloids was mainly observed for MF-Pt colloids ( $R_P \approx 1 \mu\text{m}$ ) while

## 5. JANUS COLLOID ENGULFMENT BY GUV MEMBRANES

for SiO<sub>2</sub>-Pt colloids partial engulfment remained a fairly rare observation. After the centrifugation experiments using SiO<sub>2</sub>-Pt colloids and GUVs, we observed a dramatic decrease in the number of GUVs, which points to vesicle rupture due to the interaction between the lipid membrane and SiO<sub>2</sub>-Pt colloids.

Note that because of the optical asymmetry (due to the surface asymmetry and dielectric characteristics of the platinum coating) of Janus colloids, we were unable to trap them by optical tweezers (discussed in the next section) to study forces as low as 10<sup>-12</sup> N. Hence, optical tweezers experiments were performed on bare Silica and MF colloids.

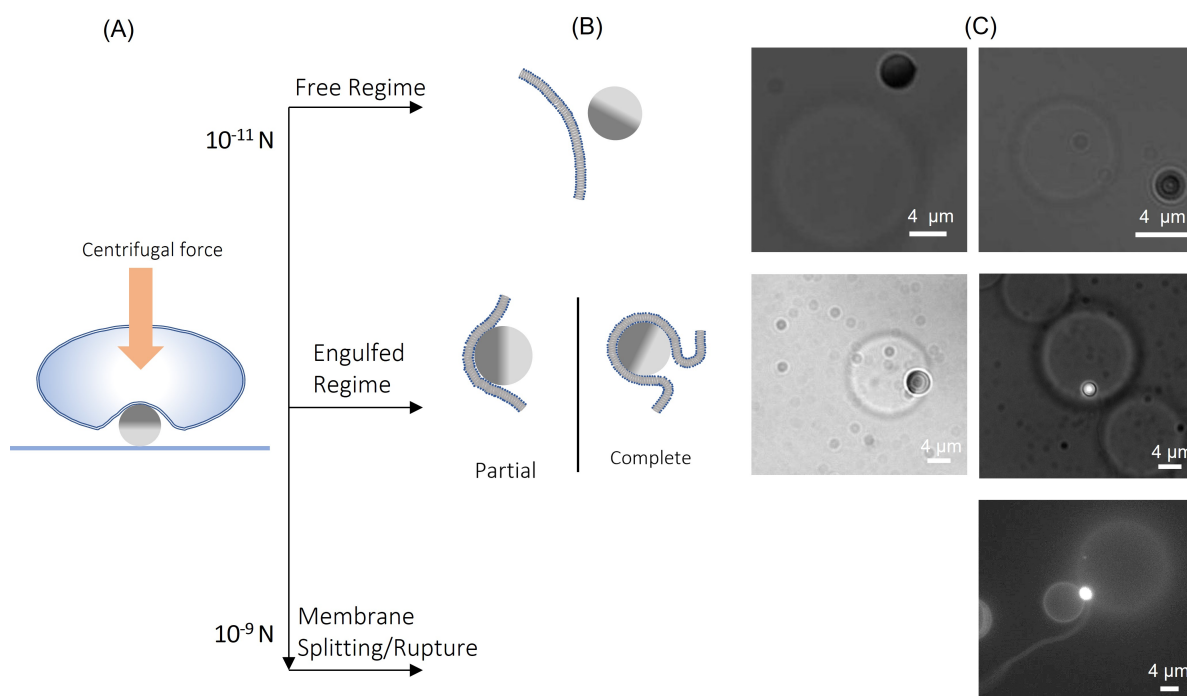


**Figure 5.4:** States of engulfment in a colloid-GUV system. (A) Schematic of GUV interacting with a Janus colloid under the force of centrifugation (10<sup>-11</sup> - 10<sup>-9</sup> N), (B) schematic for free, engulfed and membrane rupture regimes. (C) Brightfield (+ Fluorescence) microscopy image of SiO<sub>2</sub>-Pt (*Left Column*) and MF-Pt (*Right Column*) Janus colloid in various regimes after centrifugation.

### 5.3.2 Optical Tweezers study on the interaction between a bare colloid and a GUV

In order to understand the difference in engulfment between Janus MF colloids and Janus Silica colloids, optical tweezers experiments were performed on MF and Silica colloids. Optical tweezers experiments shown in this section were performed in collaboration with Florent Fessler (Intern, M2). These experiments allow monitoring of the engulfment dynamics at the single-particle level, monitoring both the membrane deformation and the force of interaction.

In a typical experiment to observe the engulfment of a bare microparticle by a GUV, the colloid is trapped by a laser beam (see section 2.5) and the sample stage is moved to manipulate the position of the particle in X, Y or Z direction to bring it in contact with a vesicle. The relative speed of the vesicle to the particles during contact is controlled by monitoring (see section 2.4.2) the center of mass of the particle and the vesicle. Taking advantage of the fluorescence microscope module built into the optical tweezer, we were able to observe the deformation of a GUV during its contact with a colloidal particle under the action of the optical force.

SiO<sub>2</sub> ( $R_P \approx 2 \mu\text{m}$ ) bare colloids and POPC GUVs were investigated first. We observed that when the approach speed of the SiO<sub>2</sub> colloids was high enough ( $\nu = 15 \mu\text{m.s}^{-1}$ ) a colloid becomes completely engulfed (see Figure 5.5) by the GUV.

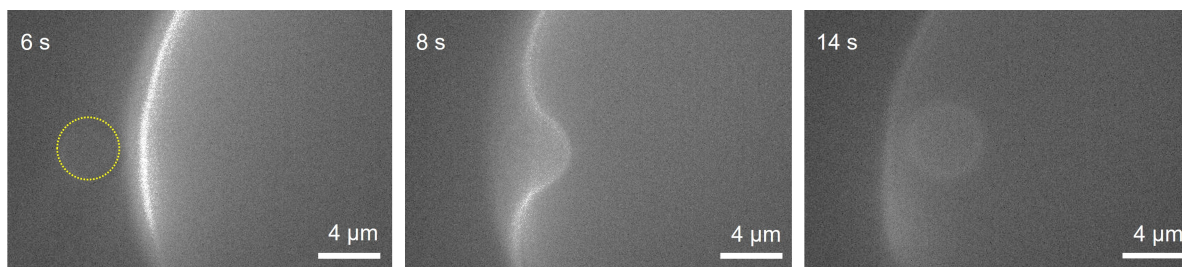


**Figure 5.5:** (Left to Right) Contact regimes of SiO<sub>2</sub> ( $R_P \approx 2 \mu\text{m}$ ) shown in dashed yellow approaching a floppy GUV, deforms the vesicle with the force provided by optical tweezer, and then is fully engulfed by the vesicle.

Engulfment was solely observed for floppy membranes. These membranes are floppy [124, 125] that constantly change their contour shape. Since all the GUVs were prepared with the same protocol using the same lipids and thus having equal bending rigidity, the floppiness of the GUVs is related to the low membrane tension:  $\sigma < 10^{-8} \text{ N.m}^{-1}$ .

## 5. JANUS COLLOID ENGULFMENT BY GUV MEMBRANES

---

At equal bending rigidity, a low membrane tension leads to a large excess area, which can be observed as the deviation around the equilibrium circular contour.

For tense membranes ( $\sigma > 10^{-8}$  N.m<sup>-1</sup>) we did not observe particle engulfment by the GUV membrane but the particle simply displaces the entire vesicle upon approaching the GUV rather than deforming or penetrating the GUV. Vesicle contour fluctuation analysis [124, 125] carried out in collaboration with Florent Fessler (Intern, M2) [126], was used to evaluate the membrane tension. Floppy vesicles show  $\sigma \approx 10^{-9}$  N.m<sup>-1</sup>, whereas the membrane tension for tense membranes was  $\sigma \approx 10^{-7}$  N.m<sup>-1</sup>.

Silica colloids were observed to be engulfed by GUVs when  $\sigma < 10^{-8}$  N.m<sup>-1</sup>. In this regime, the *bendocapillary* is  $\lambda_\sigma = \sqrt{2\kappa_b/\sigma} \approx 10^{-5}$  m (if  $\sigma = 10^{-9}$  N.m<sup>-1</sup>), which is higher than the deformation length due to the engulfed particle of size  $R_P = 10^{-6}$  m:  $R_P < \lambda_\sigma$ . In this regime, bending contributions are more important than tension contributions (membrane stretching). Hence, experimental findings shown in 5.5 can be described as a competition between bending and adhesion. Experiments showing tense GUV membranes correspond to *bendocapillary* lengths lower than the particle radius ( $R_P > \lambda_\sigma$ ), which are also governed by  $E_{tension}$  contributions.

As seen from Figure 5.5, with our optical tweezers setup we could achieve complete engulfment of SiO<sub>2</sub> ( $R_P \approx 2$  μm) colloids. However, in the same experimental conditions, bare MF colloids did not show any engulfment or persistent adhesion. In the experiments, MF colloids were found to be constantly displaced out from the trap upon encountering a vesicle, even when the approach speed was sufficiently high. As seen in Figure 5.6, we check the particle size effect by using SiO<sub>2</sub> colloids of a similar size ( $R_P \approx 1.1$  μm) compared to MF colloids. Silica colloids showed complete engulfment by a GUV membrane even at a lower approach speed of  $\nu = 5$  μm.s<sup>-1</sup>. The lack of engulfment or any persistent adhesion of MF colloids points to the fact that the surface properties of MF colloids are responsible for an unfavorable adhesion energy:  $E_{adhesion} > 0$  representing a cost and not an energetic gain.

### 5.3 Force driven interaction for Janus colloid engulfment by GUV

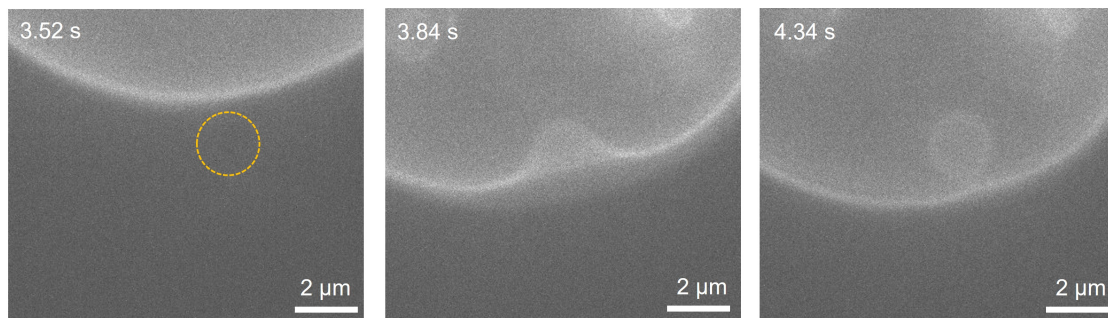


**Figure 5.6:** (Left to Right) Contact regimes of  $\text{SiO}_2$  ( $R_P \approx 1 \mu\text{m}$ ) shown in yellow approaching a floppy GUV, deforms the vesicle with the force provided by optical tweezer, and then is fully engulfed by the vesicle.

Now we have identified the first limiting parameters to trigger engulfment, which are the membrane tension and the adhesion energy dictated by the particle surface properties (silica *vs* MF).

Note that for Silica colloids, membrane wrapping can occur under the effect of an optical force but without the need of introducing depletion attraction as reported by Spanke *et al.* [83].

In Figure 5.7, we plot the force measured by optical tweezers as a function of time for a  $\text{SiO}_2$  colloid ( $R_P \approx 1 \mu\text{m}$ ) undergoing various transitions during engulfment. Insets correspond to the bright-field microscopy images of the observed regimes. In the first free regime, the force experienced by a colloid during the approach is negligible because the approach speed for the colloid is kept low enough ( $\nu = 5 \mu\text{m.s}^{-1}$ ) and the Stokes drag is negligible. Because of the bending stiffness of the membrane, the force increases when the colloid comes into contact with the vesicle and begins to deform it. This regime is referred to as the elastic deformation regime because, if the trap is removed while the membrane is in this deformation regime, the membrane returns to its original shape and the colloid is expelled away from the membrane. A critical force  $F_{max}$  is observed at the beginning of the particle engulfment, when the membrane wraps the colloid. Finally, the force drops in the last step of the process, which corresponds to the particle being entirely engulfed by the GUV.

The force  $F_{max}$  is related to the amount of energy required to overcome the energy barrier in order to trigger force-activated particle engulfment [83].



## 5. JANUS COLLOID ENGULFMENT BY GUV MEMBRANES

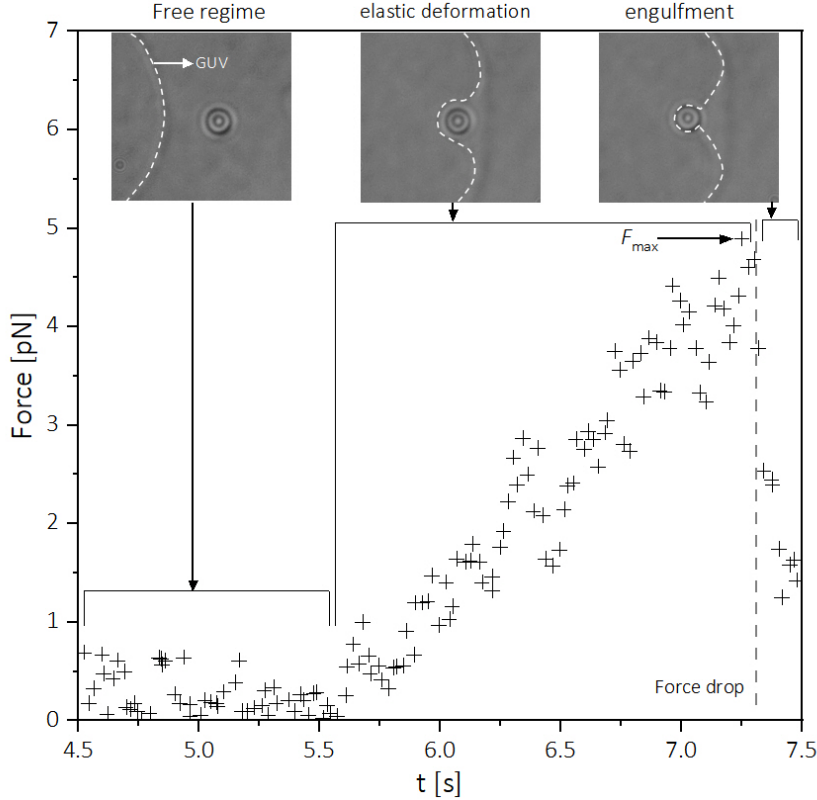


**Figure 5.7:** Force curve as a function of time ( $t$ ) during the engulfment for a  $\text{SiO}_2$  colloid  $R_P \approx 1 \mu\text{m}$  by a POPC GUV  $R_{GUV} \approx 25 \mu\text{m}$ .

We can now discuss  $F_{max}$  with respect to the involved energies ( $E_{bend}$ ,  $E_{tension}$  and  $E_{adhesion}$ ) [83]. As we know from the previous discussion (see section 5.3), the contribution of  $E_{tension}$  towards particle engulfment is negligible, hence the force  $F_{max}$  has to mainly work against the bending cost of the membrane. For our system, as POPC vesicles were used, the bending stiffness was  $\kappa_b \approx 20\text{-}25 k_B T$  [41, 127]. In our experiments, the typical force  $F_{max}$  lies in the range of few  $10^{-12}$  N. If we calculate the work performed to engulf the colloid by the membrane, we can consider the  $F$  vs. time curve by optical tweezers and knowing the particle velocity  $\nu = 5 \mu\text{m}\cdot\text{s}^{-1}$ , the power dissipated is  $F\nu = dE/dt$ . Hence the difference in free energy  $\Delta E = \int_{t_0}^{t_f} F\nu dt \approx 1/2 F_{max}\nu\Delta t \approx 10^3 k_B T$ . Bending energy can be calculated as  $E_{bend} = 4\pi\kappa_b z_P \approx 480 k_B T$ . The difference between  $\Delta E$  and  $E_{bend}$  can be attributed to the fact that during the process of engulfment not only the area that is in contact with the membrane deforms locally, but also the region around the contact site deforms as well which is



## 5.4 Tuning membrane and particle properties to trigger engulfment

significantly larger than the contact area  $A_{contact}$  (see figure 5.6, 5.5), considering also the fluctuations in the vesicle's contour in the floppy regime, the steric repulsion due to shape fluctuations significantly increases the energy required for engulfment.

It should be noted that only complete or no engulfment of the particle by the GUV was achieved by optical tweezers experiments. There was never a case of partial engulfment of bare silica particles by POPC GUVs of any size.

After the colloids were completely engulfed by the membranes, it was observed that the engulfment was irreversible, and manipulating the engulfed colloids with optical tweezers would drag and displace the whole GUV instead of releasing the particle from the engulfment (see Figure 5.8).

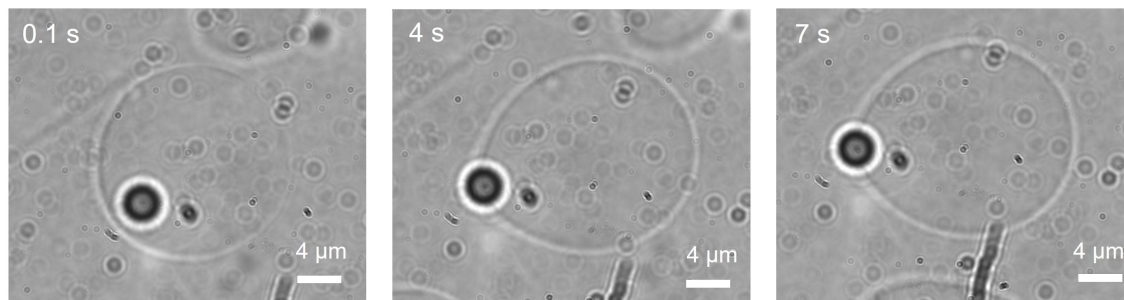


**Figure 5.8:** (Left to Right)  $\text{SiO}_2$  ( $R_P \approx 2 \mu\text{m}$ ) colloid fully engulfed by a POPC GUV. Trapped colloid drags the GUV along with its path after manipulation with optical tweezer. The pear shaped geometry of the GUV is due to the drag it encounters while it is being pulled by the colloid.

## 5.4 Tuning membrane and particle properties to trigger engulfment

As established in the previous sections, the membrane tension of the GUVs, the surface properties of the colloid, and the force of contact all play a significant role in the activated engulfment dynamics of a colloid by a GUV membrane. In this section, we utilized centrifugation forces to drive Janus colloid-GUV contact forces up to  $10^{-9}$  N. GUVs were prepared using DOPC and POPC lipids, which resulted in a variation in bending rigidity, while the use of  $\text{SiO}_2\text{-Pt}$  ( $R_P \approx 2 \mu\text{m}$ ) and  $\text{MF-Pt}$  ( $R_P \approx 1 \mu\text{m}$ ) yields in colloidal surface properties that were distinct from one another (Silica, MF and Pt surfaces). The centrifugation time was kept constant at 4 minutes for all the iterations.

## 5. JANUS COLLOID ENGULFMENT BY GUV MEMBRANES

---

Let's first discuss the results obtained by centrifugation of SiO<sub>2</sub>-Pt ( $R_P \approx 2 \mu\text{m}$ ) Janus colloids with POPC and DOPC GUVs which are reported in Table 5.1.

Vesicles	$F_c$ (N)	Type of event	
		adhesion/engulfment	membrane rupture
POPC	$10^{-11}$	-	-
	$10^{-10}$	• (< 10%)	-
	$10^{-9}$	• (< 5%)	•
DOPC	$10^{-11}$	• (< 2%)	•
	$10^{-10}$	-	•
	$10^{-9}$	-	•

**Table 5.1:** Effect of centrifugal force on POPC and DOPC GUVs interacting with SiO<sub>2</sub>-Pt Janus colloids, where (•) signifies observed events.

At low forces ( $10^{-11}$  N) neither engulfment nor any membrane rupture was observed for SiO<sub>2</sub>-Pt interacting with POPC vesicles and all the particles were found in the free regime. However, increasing the applied force up to  $10^{-10}$  -  $10^{-9}$  N, we observed a few cases < 10% where a particle appeared to be persistently adhered to a GUV and in such cases, the adhesion/engulfment was found to occur on the Pt face of the Janus colloid suggesting an affinity of the GUV towards the Platinum coating. One example of such an event is shown in Figure 5.9 where the colloid stays attached to the GUV via the platinum coating (for  $t= 140$  s). As discussed in chapter 4, when the colloids are brought in contact with the GUV by simple mixing the particle did not exhibit any persistent adhesion towards the vesicle and the colloids would approach and subsequently move away by its Brownian motion. The fact that the colloid stays persistently adhered to the GUV for a long time could point towards a partial engulfment of the Platinum face of the colloid by the GUV.

## 5.4 Tuning membrane and particle properties to trigger engulfment

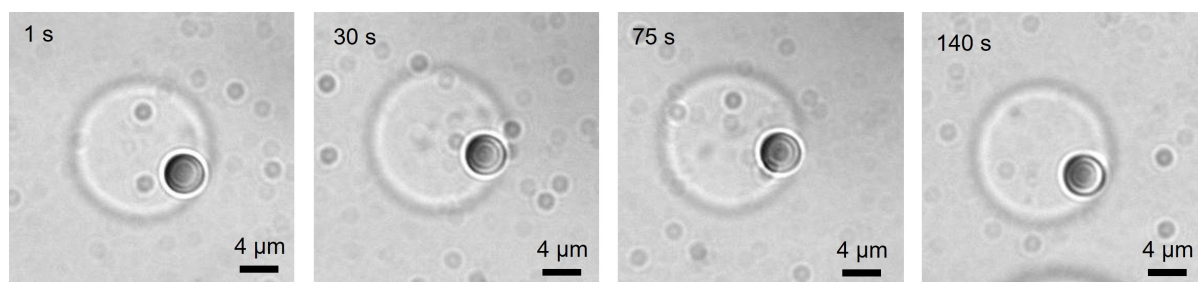


**Figure 5.9:** Bright field images of SiO<sub>2</sub>-Pt Janus colloid persistently adhered to a GUV.

For POPC vesicles and high centrifugation forces ( $10^{-9}$  N), it was observed that the yield of vesicles after centrifugation with the colloids was significantly lower than the one obtained after sedimentation under gravity or even after centrifugation at lower forces. This lower number of GUVs observed could be due to the fact that at high forces the colloids were able to rupture the membranes instead of being engulfed. Note that the rupturing of GUVs was not prominently seen when the GUVs were centrifuged without colloidal particles. When a SiO<sub>2</sub>-Pt Janus colloid ruptures a membrane, it was observed that lipids from the ruptured GUVs remain attached to the colloidal surface. As the SiO<sub>2</sub> colloids were inherently non-fluorescent, the attached lipids on its surface imparted fluorescence, which can be clearly seen under fluorescence microscopy (see Figure 5.10(A)). In Figure 5.10(B) is the intensity profile for fluorescence emitted by the colloid at different times. There can be seen a decay in the fluorescent intensity due to quenching, however, the rate of quenching was significantly slower (up to 100 seconds) than a GUV ( $< 60$  s), which could indicate the presence of multiple bilayers on the surface of the colloid (Discussed later in the section). By following the propulsion direction of SiO<sub>2</sub>-Pt Janus colloids in active conditions, the Si and Pt faces could be distinguished easily and the Silica face shows a larger fluorescent intensity (see Figure 5.10(A)). Note that no encapsulation (or complete engulfment) of SiO<sub>2</sub>-Pt Janus colloids inside a GUV was observed using the centrifugation approach. The particles were either found in the free regime or partially engulfed regime.

## 5. JANUS COLLOID ENGULFMENT BY GUV MEMBRANES

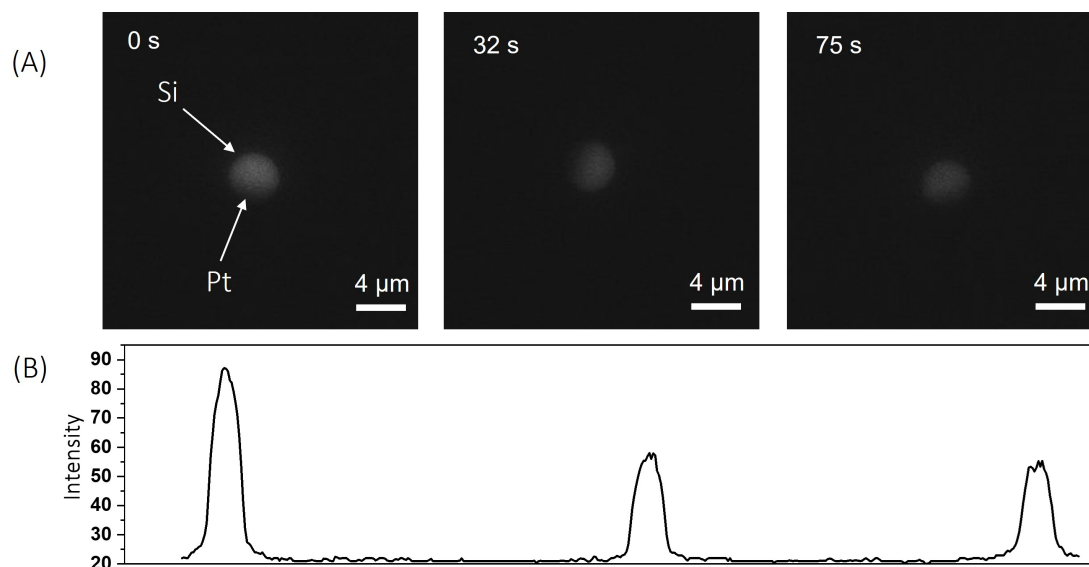


**Figure 5.10:** (A) SiO<sub>2</sub>-Pt Janus colloid under fluorescence microscopy after rupturing POPC GUVs and becoming fluorescent. (B) Intensity profile for the images in (A).

When centrifugation experiments for SiO<sub>2</sub>-Pt were carried out with DOPC vesicle, a decrease of the vesicle number due to rupture and SiO<sub>2</sub>-Pt colloids becoming fluorescent were observed even at low forces ( $F_c = 10^{-11}$  N) with rare cases of partial engulfment (see figure 5.11). Due to the lower bending stiffness of DOPC GUVs  $\kappa_b \approx 15 k_B T$  [127] along with the high force due to centrifugation, membrane ruptures may become significantly higher.

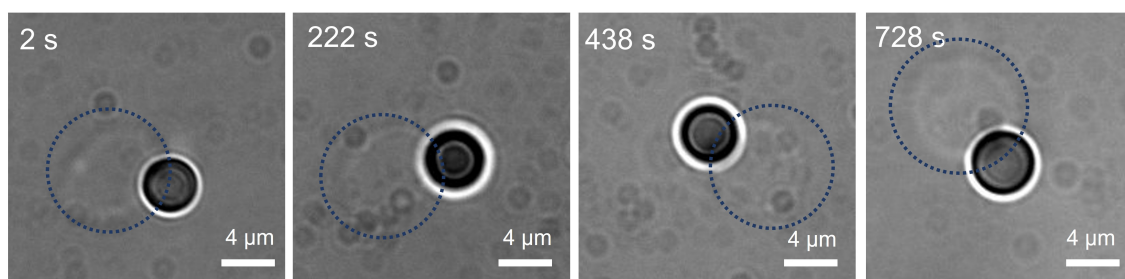


**Figure 5.11:** A montage SiO<sub>2</sub>-Pt Janus colloid persistently adhered/partially engulfed by DOPC GUV.

To better understand the role of particle's surface properties as well as their size SiO<sub>2</sub>-Pt ( $R_P \approx 2 \mu\text{m}$ ) Janus colloids were replaced with the smaller MF-Pt ( $R_P \approx 1 \mu\text{m}$ ) colloids, and the centrifugation experiments were repeated with the same forces.

## 5.4 Tuning membrane and particle properties to trigger engulfment

The rate of engulfment for MF-Pt colloids was observed to be significantly higher as compared to SiO<sub>2</sub>-Pt colloids, as seen from Table 5.2.

Vesicles	$F_c$ (N)	Type of event	
		adhesion/engulfment	membrane rupture
POPC	$10^{-11}$	• (< 10%)	-
	$10^{-10}$	• (30 - 40%)	-
	$10^{-9}$	• (< 10%)	•
DOPC	$10^{-11}$	• (20 - 30%)	-
	$10^{-10}$	• (> 40%)	-
	$10^{-9}$	• (< 10%)	•

**Table 5.2:** Effect of centrifugal force on POPC and DOPC GUVs interacting with MF-Pt Janus colloids, where (•) signifies observed events.

For both POPC and DOPC vesicles, the highest observed instances of engulfment were recorded for moderate forces ( $10^{-10}$  N). While at lower forces ( $10^{-11}$  N), far fewer occurrences of engulfment were observed when the colloid was found to be continuously adhered to a GUV, but in most of the cases the particle existed in free regime and did not show any special affinity towards a vesicle (discussed in section 5.3.2).

Note that for all the cases of engulfment of MF-Pt Janus colloid, the MF face of the colloid was oriented downwards and the particle appeared to be fully bright in fluorescent microscopy, see Figure 5.4(C). Hence, the Pt face of the colloid adheres to the GUV, which is usually on top of the Janus particle.

Note that we did not observe engulfment of bare MF colloids using optical tweezers, which would suggest that the MF face of the MF-Pt Janus colloid has no affinity towards the membrane. On the contrary, optical tweezers experiments show that Silica colloids can be engulfed by GUVs under the action of a relatively low force (few  $10^{-12}$  N). Thus, we can speculate that the rupture of vesicles observed for SiO<sub>2</sub>-Pt Janus colloid is the result of the engulfment of several bilayers on both sides of the SiO<sub>2</sub>-Pt Janus colloids, which results in the vesicle rupture and on a fluorescent lipid coating on the SiO<sub>2</sub>-Pt Janus colloids.

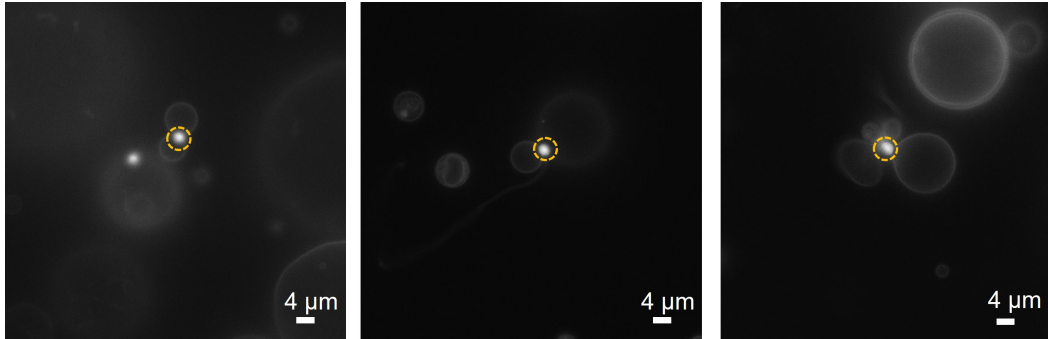


**Figure 5.12:** Fluorescence microscopy of MF-Pt Janus colloid splitting GUVs. The brighter spot stuck between membrane cleavage (highlighted in yellow) are the Janus colloids.

## 5.5 Particle rotational dynamics in the engulfment regime

In fluorescence microscopy, for the engulfed MF-Pt colloids, the rotational dynamics was observed to be considerably slowed down that even by visual inspection it was possible to discern between a colloid in the engulfed regime and in the free regime.

Particle rotational diffusion ( $D_{R,\perp}$ ) provides a strong and robust tool to investigate the interaction of a Janus particle with a surface as it has already been addressed in chapter 3 when describing the slowing down of the rotational diffusion near a single solid wall.

### 5.5.1 Rotational dynamics of engulfed MF-Pt colloids by GUVs

As described in the previous sections for MF-Pt Janus colloids, the Pt face of the particle can become adhesive to the membrane, whereas a lack of affinity between the MF and the membrane was observed. Hence, we may expect that measuring the orientational dynamics of partially engulfed Janus MF-Pt colloids will provide information on the different interactions between the two particle faces and the GUV membrane.

The evolution of the orientation of MF-Pt Janus colloids at different times in different regimes is shown by Fluorescence microscopy in Figure 5.13. When isolated Janus particles undergo free rotational diffusion, the area of the fluorescent MF face varies with time. For engulfed Janus particles, tiny variations of the MF area are instead observed. As a reference for our analysis, the area of a Janus colloid stuck on the substrate is also shown. Out-of-plane particle orientation angle  $\beta$  was evaluated using the same

## 5.5 Particle rotational dynamics in the engulfment regime

protocol mentioned in section 2.4.1.1 on the region marked by dashed yellow ellipse (see Figure 5.13). Note that in cases when the MF area detected is rather small and the Janus boundary does not appear clearly,  $\beta$  values are subject to uncertainty.

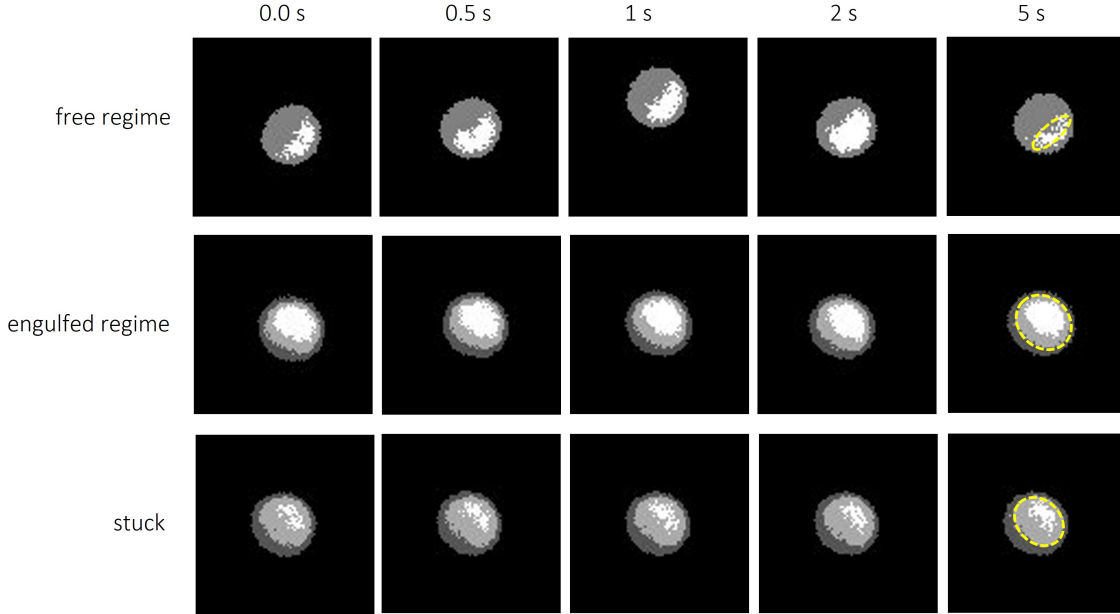


**Figure 5.13:** A montage of the MF-Pt Janus colloid in various regimes, where the difference in the particle rotation between the free and engulfed regimes can be inspected visually in Fluorescence microscopy.

Figure 5.14 shows the out-of-plane particle orientation angle  $\beta$  as a function of time obtained by analysing the images in fluorescence microscopy. Engulfed Janus colloid explores a rotational space significantly smaller than the one of a free Janus colloid. The change of the orientation was found to be  $\Delta\beta \approx 0.1$  rad ( $5^\circ$ ) for engulfed colloids which is comparable to the one of a stuck colloid ( $\Delta\beta \approx 0.02$  rad), while in free regime Janus colloids can explore more than  $\Delta\beta \approx 1$  rad ( $60^\circ$ ).

## 5. JANUS COLLOID ENGULFMENT BY GUV MEMBRANES

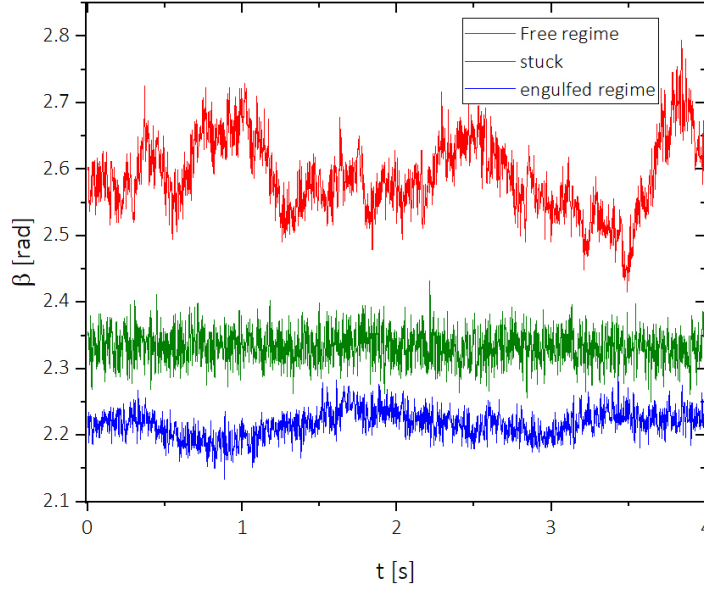


**Figure 5.14:** Out-of-plane rotational angle as a function of time for MF-Pt Janus colloids in free, stuck as well as engulfed regime .

Calculating the  $MSAD(\beta)$  in these three regimes (engulfed, free and stuck), we were able to distinguish between the rotational dynamics of engulfed and stuck Janus colloids given that  $MSAD(\beta)$  of stuck Janus particles does not significantly vary with the lag time, see Figure 5.15.

Considering that engulfed Janus colloids are trapped in a potential for their orientation angle  $\beta$ ,  $MSAD(\beta)$  data can be described (as equation 2.1 for the  $MSD$  in an optical trap) by:

$$\langle [\Delta\beta(t)]^2 \rangle = MSAD(\beta) = MSAD(\beta)_0 + \frac{2k_B T}{\kappa_R} \left[ 1 - \exp\left(-\frac{\kappa_R \Delta t}{\zeta_R}\right) \right], \quad (5.1)$$

where  $MSAD(\beta)_0$  represents a constant due to the noise of our image analysis and  $\kappa_R$  is the trap constant for the change of the particle orientation  $\beta$ . Note that the latter equation is equivalent to equation 4.2 with  $\kappa_R = 2\zeta_R \Gamma$ .

We first focus our attention on the plateau of  $MSAD(\beta)$ , which can be observed already at lag time = 0.04 s for partially engulfed Janus colloids. This plateau value corresponds to  $\frac{2k_B T}{\kappa_R}$ , see equation 5.1. Hence, we can estimate a characteristic angle



## 5.5 Particle rotational dynamics in the engulfment regime

$\beta^* = \sqrt{\frac{2k_B T}{\kappa_R}}$  describing the range of orientation  $\beta$  that can be explored by a Janus MF-Pt colloid partially engulfed by a membrane.  $\beta^*$  ranges between 1 and 2 degrees, which is very small but still measurable as shown in Figure 5.15.

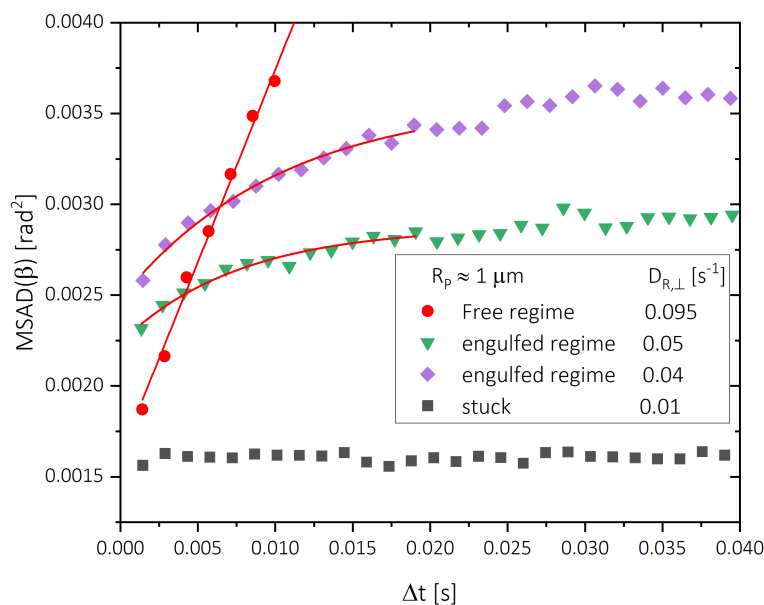


**Figure 5.15:**  $MSAD$  as a function of the lag time for MF-Pt Janus colloids in free, engulfed and stuck regimes. The plateau for the engulfed colloids signifies confinement due to engulfment.

We can discuss  $\beta^*$  assuming the partial engulfment geometry shown in Figure 5.16, where  $\beta^*$  leads to a rotation of the Janus colloid, which now exposes a Pt region originally in contact with the membrane (m) to the aqueous solution (aq) and an MF region from the aqueous solution to the membrane. This area region is simply  $2R_P^2\beta^*$  and the change in free energy between the initial and final Janus colloid orientation is  $\Delta E(\beta^*) = 2R_P^2\beta^*[(\sigma_{Pt,aq} - \sigma_{Pt,m}) + (\sigma_{MF,m} - \sigma_{MF,aq})]$ . This energy could be related to the adhesion cost to bring MF into contact with the membrane since  $w_{MF} = \sigma_{MF,m} - (\sigma_{MF,aq} + \sigma_{m,aq})$  is the contact energy of the MF. Assuming that in thermal equilibrium each degree of freedom possesses an energy of  $1/2k_B T$ , we can write  $\Delta E(\beta^*) = 1/2k_B T$  and estimate a contact energy of  $2-4 \cdot 10^{-8} \text{ N}\cdot\text{m}^{-1}$ , which is comparable to the membrane tension  $\sigma$  measured in our experiments.

## 5. JANUS COLLOID ENGULFMENT BY GUV MEMBRANES

---

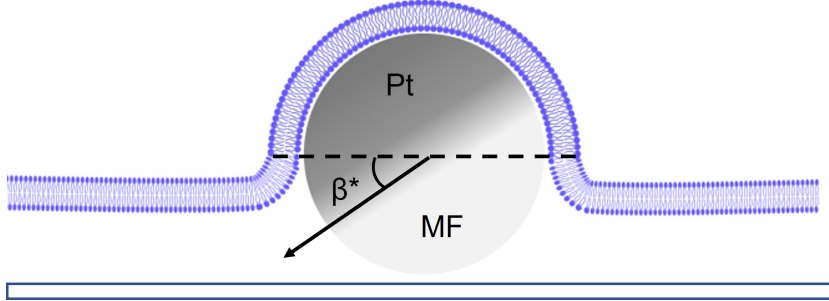


**Figure 5.16:** Schematic showing the partial engulfment of an MF-Pt colloid ( $R_P \approx 1 \mu\text{m}$ ) by a GUV, where  $\beta^*$  is a characteristic out-plane-rotation angle. For better visualisation the membrane thickness is not to scale, as the actual membrane thickness is only 5 - 6 nm.

### 5.5.2 $D_{R,\perp}$ and $D_{Tr,\parallel}$ in the engulfed regime

In this section, we focus our attention on the information given by the  $MSAD(\beta)$  in the short lag time limit, see Figure 5.15. For short lag times, equation 5.1 becomes  $MSAD(\beta) = MSAD(\beta)_0 + \frac{2k_B T}{\zeta_R} \Delta t = MSAD(\beta)_0 + 2D_{R,\perp} \Delta t$ , which provides the particle out-of-plane rotational diffusion coefficient.

Note that for each measurement of  $D_{R,\perp}$ , we can also measure the translational diffusion coefficient ( $D_{Tr,\parallel}$ ) of Janus MF-Pt colloids. In Figure 5.17 we plot the out-of-plane rotational diffusion coefficient ( $D_{R,\perp}$ ) as a function of the parallel translational diffusion ( $D_{Tr,\parallel}$ ) for colloids in the free and partially engulfed regimes. As observed in section 3.1.3 the data for passive Janus colloids in the free regime (close to a solid wall) lie within the range of theoretical predictions [98, 99]. However, as can be seen (apart from a few points) the data for the partially engulfed Janus colloids lie outside of the frame of theoretical predictions for the diffusion close to a single solid wall. Slowing down of both rotational and translational diffusion can be observed for partially engulfed Janus colloids. The limit of the resolution of  $D_{R,\perp}$  in our analysis was considered in relation to the rotational diffusion value that one could extract by analysing the reference data of a Janus colloid stuck on the substrate. This lower limit is  $D_{R,\perp} \approx 0.012 \text{ s}^{-1}$ . Hence, the data point below this limiting value can not be resolved.

## 5.5 Particle rotational dynamics in the engulfment regime

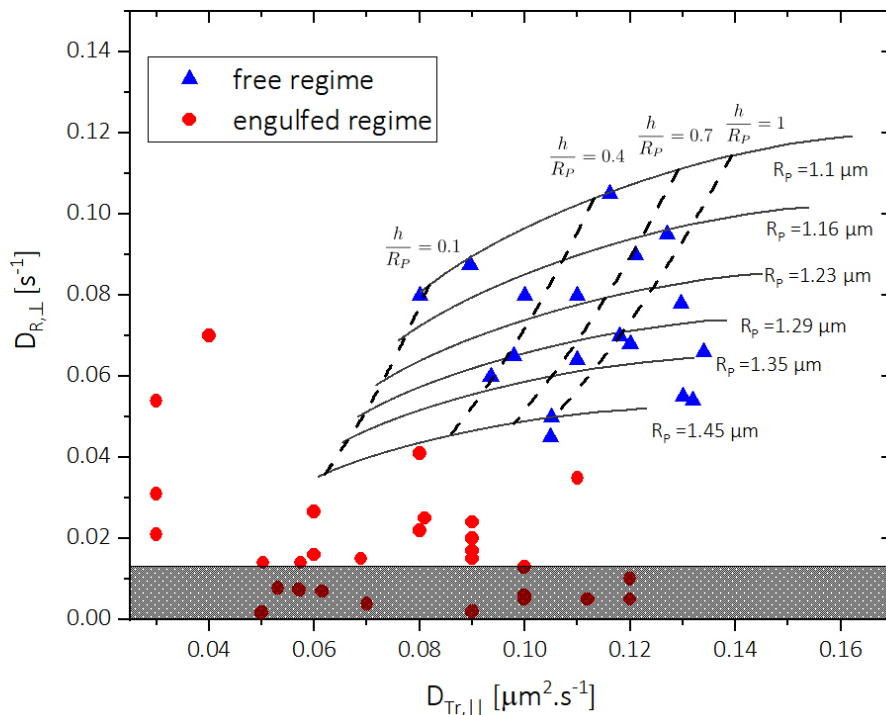


**Figure 5.17:**  $D_{R,\perp}$  as a function of  $D_{T,\parallel}$  for MF-Pt colloids in free and engulfed regimes. The gray area is the limit of  $D_{R,\perp}$  measurement.

To the best of our knowledge, no models exist in the literature to describe the change in rotational drag ( $\zeta_R$ ) experienced by a colloid that is partially engulfed by a membrane. The closest model we found in the literature related to such a confined geometry was proposed by Landau and Lifshitz [128], which consider the slow motion in the fluid contained in the gap between two concentric spheres. We consider the case when the inner sphere rotates while the outer sphere stays at rest. Actually, when a colloid is engulfed by a GUV it creates a bud ( $R_{bud}$ ) which wraps around the colloid (e.g. see Figures 5.5 and 5.16) separated from the main GUV bilayer, whose radius can be given by  $R_{bud} = R_P + d_g$ , where  $d_g$  is the gap distance between the colloid and the membrane (this gap is composed of the aqueous solution). In this engulfed regime,  $R_{bud}$  can be considered as the radius of the outer sphere while the engulfed Janus colloid ( $R_P \approx 1 \mu\text{m}$ ) can be considered as the inner sphere. Hence, the rotational drag  $\zeta_{R,S}$  felt by

## 5. JANUS COLLOID ENGULFMENT BY GUV MEMBRANES

---

the inner spherical particle in this spherical confinement geometry can be written as:

$$\zeta_{R,S} = \frac{8\pi\eta R_p^3}{1 - (R_p/R_{bud})^3} = \frac{\zeta_{R,b}}{1 - (R_p/R_{bud})^3}. \quad (5.2)$$

From equation [5.2](#), we found that for a rotational diffusion showing a slowing down of 1 order of magnitude compared to the free motion ( $D_{R,\perp}/D_{R,b}=1/10$ ), the gap distance between the lipid bilayer and the particles  $d_g \approx 50$  nm. Note that the range of experimental values of  $D_{R,\perp}$  is very large and different gap distances could be evaluated by using the previous equation. Still, a gap distance of 50 nm (assuming the rotational dynamics of a spherical particle inside a solid immobile sphere) is comparable to the gap distance measured between a giant vesicle and a solid substrate  $\approx 50 - 200$  nm [\[129, 130\]](#) but it is significantly larger than the water gap between a substrate and a supported bilayer  $\approx 1$  nm [\[131\]](#).

We can now discuss  $D_{Tr,\parallel}$  results for Janus particle partially engulfed by a GUV membrane. Thomas Fischer *et al.* [\[99\]](#) developed a model on the translational drag felt by a particle immersed in an incompressible planar membrane between two identical fluids. Although the model does not exactly correspond to the wrapping situation studied here, it has been invoked previously [\[132, 133, 134\]](#) as providing order of magnitude estimates. This model considers that the membrane possesses only a surface shear viscosity  $\eta_s$ , and the interface flow is incompressible. In this geometry, the membrane forms a hole to accommodate the particle. A no-slip condition on the solid particle surface leads to an infinite particle rotational if the particle is immersed in the membrane. The translational drag for a particle immersed with its equatorial plane in the membrane can be written as [\[99\]](#):

$$\zeta_{Tr,\parallel,Fischer} = 23.56\eta R_P + 7.5\eta_s \quad (5.3)$$

Comparing to the bulk translation drag  $\zeta_{Tr,b} = 6\pi\eta R_P$ , the bulk viscous drag contribution increases of 25% in this geometry and the membrane drag contribution is not a function of the particle size. Considering the average value of the experimental translational diffusion  $\bar{D}_{Tr,\parallel,free} = 0.12 \pm 0.01 \mu\text{m.s}^{-1}$  for Janus colloids in the free regime and  $\bar{D}_{Tr,\parallel,eng} = 0.07 \pm 0.02 \mu\text{m.s}^{-1}$  in the partially engulfed regime, we estimate an increase of the translational drag of a factor of  $\approx 2$ . Hence, we can evaluate a surface viscosity of  $\eta_s = 4 \times 10^{-9}$  Pa.s.m, assuming that the drag increase with respect to the bulk described in the Fischer model corresponds to the drag increase in our experiments

performed close to a solid wall. A membrane three-dimensional viscosity can be calculated as  $\eta_s/h_m = 1$  Pa.s ( $h_m = 4$  nm being the membrane thickness). Danov *et al.* [82] considered a similar model for the drag experienced by a particle moving parallel to a spherical membrane. In this model, it is assumed that the particle contact line is pinned, restricting any rotational motion. The perturbations caused by particle motion on the interface were found to be governed by the immersion depth of the colloidal particle, which gives rise to the re-circulation effect inside the spherical membrane (the more immersed the particle, the higher is the re-circulation). Our experiments showing  $R_{GUV}/R_P = 3 - 10$  correspond to  $\frac{\eta_s}{R_P\eta} = 2 - 30$  in the model. Hence, a surface shear viscosity  $\eta_s \approx 2.5 - 38.7 \times 10^{-9}$  Pa.s.m can be evaluated, which is similar as the one obtained using the model of Fischer *et al.* [99] and are comparable to other experimental results [135].

## 5.6 Conclusion

In this chapter, we investigated the effect of external forces on the partial or complete engulfment of Janus colloids by GUVs utilizing centrifugation and optical tweezer techniques.

Using external forces, we were able to observe partial and complete engulfment of Janus colloids by POPC and DOPC GUVs. Complete engulfment of Janus colloids was only observed for SiO<sub>2</sub> bare colloids, floppy GUVs and  $F \approx 10^{-12}$  N (by optical tweezers); while bare MF colloids did not exhibit engulfment. These results point to the importance of the particle surface properties to trigger engulfment. Partial engulfment was observed in centrifugation experiments for moderate force (up to  $10^{-10}$  N) while at higher forces the membrane rupture/splitting was observed.

Particle engulfment was found to occur for low membrane tensions  $\sigma < 10^{-8}$  N.m<sup>-1</sup> (floppy GUVs) when  $E_{tension}$  vanishes. The process of engulfment was found to be irreversible and manipulating an engulfed colloid with an optical trap resulted in membrane displacement.

In the partial engulfed regime for MF-Pt Janus colloids, the rotational dynamics was found to be severely confined and slowed down by *ca.* 1 order of magnitude compared to Janus particles in the free regime. Slowing down of both  $D_{R,\perp}$  and the translational diffusion  $D_{Tr,\parallel}$  were observed for partially engulfed particles. We discussed both the

## 5. JANUS COLLOID ENGULFMENT BY GUV MEMBRANES

---

confinement effect and the slowing down of the diffusion and evaluate contact energy (or adhesion strength) of  $\approx 10^{-8}$  N/m and surface shear viscosity of the membrane  $\eta_S \approx 10^{-8}$  Pa.s.m.

## Chapter 6

# Towards active dynamics of engulfed Janus colloids by GUVs

## 6. TOWARDS ACTIVE DYNAMICS OF ENGULFED JANUS COLLOIDS BY GUVS

---

### 6.1 Overview

In the previous chapter, we described the engulfment of Janus colloids by GUVs in the absence of  $\text{H}_2\text{O}_2$ , which is the catalytic fuel for the active motion of the Janus particles. In this chapter, we report some experimental results obtained for Janus colloids partially engulfed by GUVs after the addition of  $\text{H}_2\text{O}_2$  in the system. Hence, we have investigated the effect of the particle active motion in isolated Janus colloid-GUV systems showing a Janus particle already partially engulfed by a GUV [5, 6, 8, 136]. These promising results are described together with a plan for future investigations. General conclusions of this PhD work are finally drawn.

### 6.2 Transport of GUVs by engulfed active Janus colloids

In this section, we describe how an active Janus colloid in the engulfed regime is able to transport a GUV over very long distances. As described in Chapter 5, partial engulfment of Janus colloids by GUVs was obtained after the application of an external force via centrifugation. After the addition of a  $\text{H}_2\text{O}_2$  solution to reach a final concentration of 2% in the cell, we expected to observe active GUV transportation, where particle engulfment facilitates a continuous momentum transfer between the Janus colloid and the GUV. However, in our experiments, active GUV transport remains an extremely rare event. An example of one such event is shown in Figure 6.1. A  $\text{SiO}_2\text{-Pt}$  Janus colloid ( $R_P \approx 2 \mu\text{m}$ ) is partially engulfed by the GUV on a small region of the Pt face. The self-propelled particle is able to drag a POPC GUV of  $R_{GUV} \approx 6 \mu\text{m}$  with the platinum face persistently attached to the GUV. The particle trajectory during the GUV transportation is shown in yellow and it can be compared to the one of a free active trajectory as shown in Figure 2.14. Calculating the VACF of the particle, we measure the active velocity  $V = 1.6 \mu\text{m}\cdot\text{s}^{-1}$ , which is within the range of the active speeds measured in the free regime (see section 3.2.1).



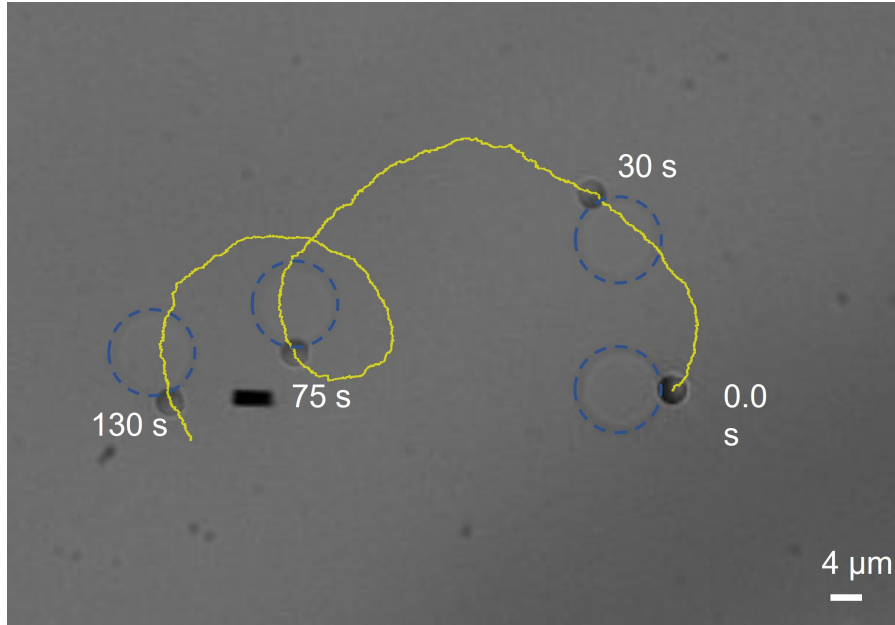


**Figure 6.1:** SiO<sub>2</sub>-Pt Janus colloid actively transporting a POPC GUV. In yellow is the trajectory of the colloid and the GUV is highlighted in blue (dashed). Note that particle-GUV at 30, 75, and 130 s are superimposed images for visualisation purpose.

For MF-Pt Janus colloids ( $R_P \approx 1 \mu\text{m}$ ) partially engulfed by GUVs, we also observed rare events of GUV transportation in the presence of H<sub>2</sub>O<sub>2</sub>. In this system, Janus colloid seems to "push" the GUV instead of dragging it. Figure 6.2 shows the active transport of a DOPC GUV by an engulfed MF-Pt Janus colloid. By VACF analysis, we measure  $V = 1 \mu\text{m}\cdot\text{s}^{-1}$  and a negligible rotational diffusion  $D_{R,\parallel}$ . In such cases of GUV transport, it seems that the particles in-plane rotational diffusion  $D_{R,\parallel}$  was hindered by the presence of membrane buds or tubes, which act as obstacles for the change of particle orientation to circumvent the GUV.

## 6. TOWARDS ACTIVE DYNAMICS OF ENGULFED JANUS COLLOIDS BY GUVS

---

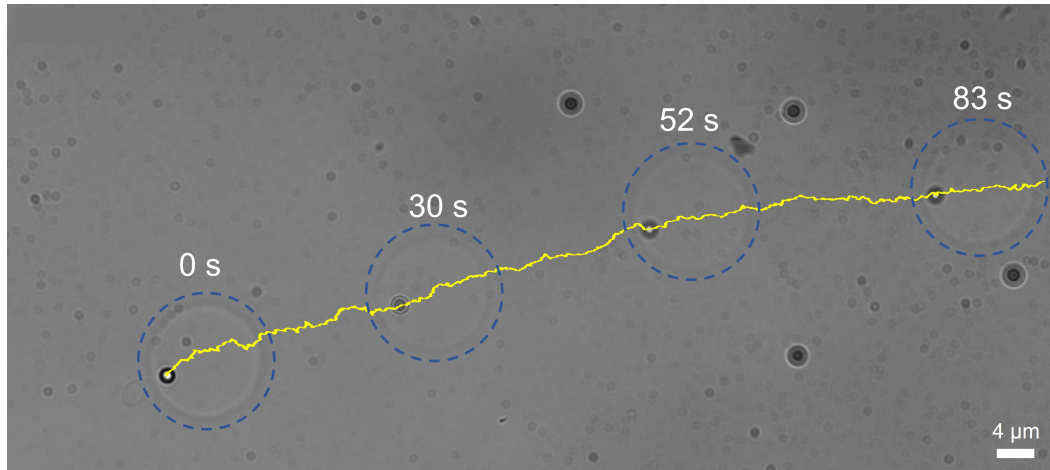


**Figure 6.2:** MF-Pt Janus colloid actively transporting a DOPC GUV. In yellow is the trajectory of the colloid and the GUV is highlighted in blue (dashed). Note that particle-GUV at 30, 52, and 83 s are superimposed images for visualisation purpose.

### 6.3 Quenching of active motion due to the partial engulfment state

In general, unlike in the free regime and the rare events described in the previous section, the activity of Janus colloids in engulfed conditions was observed to be severely quenched. Active MF-Pt Janus particles were observed to remain engulfed but did not show any persistent active motion,  $V = 0$ . In Fluorescence microscopy, engulfed Janus particles in active conditions show similar orientation, translational and rotational diffusion as when in passive conditions. They are oriented with the MF region facing down and the Janus boundary can be hardly observed.

The quenching of active motion in the engulfed regime could be associated to effects due to the partial engulfment of Janus colloids possessing only one adhesive face, as recently predicted by Agudo-Canalejo and Lipowsky [85]. The partial engulfment of a colloid by a GUV leads to a variation of the energy landscape of the GUV since the membrane curvature has to change close to the particle region. For asymmetrical shaped GUVs, a gradient of the membrane curvature may exist already before the particle engulfment. Hence, as a consequence of both the particle engulfment and the membrane curvature gradient, a force can act on the particle. The particle in fact may experience a curvature-induced force towards the region of the GUV with the lowest

### 6.3 Quenching of active motion due to the partial engulfment state

---

membrane curvature, which represents the minimum of the global free energy in the system [85].

Due to gravity, GUV membranes exhibit a flat geometry close to the substrate as measured by RICM microscopy and shown in Figure 6.4. Hence, a gradient of membrane curvature exists in our experimental system. Thus, the flat GUV membrane region of zero curvature is able to pull the colloid from its initial position towards the bottom of the GUV. For a Janus MF-Pt colloid partially engulfed by a GUV and located in the bottom region, the MF face of the colloid is facing downward. Such particle orientation can not give rise to self-propulsion in the X and Y directions.

The migration of a Janus colloid towards the bottom of the GUV was observed during the experiment as shown in Figure 6.3 for a partially engulfed MF-Pt colloid, which could be monitored before and after the addition of  $\text{H}_2\text{O}_2$ . At the beginning ( $t = 0$  s), in absence of  $\text{H}_2\text{O}_2$ , the MF colloid can be observed facing downwards and appearing fully bright in Fluorescence microscopy. However, almost instantaneously after the addition of  $\text{H}_2\text{O}_2$ , GUV transportation was observed up to 40 s, with the Janus colloid changing its orientation. The GUVs and Janus colloid, first drift to the left of the field of view due to perturbations caused by the  $\text{H}_2\text{O}_2$  addition. As Seen in Figure 6.3(A), in Fluorescence microscopy, the Janus colloid switches from bright (0 s) to dark (6-18 s) and progressively shows a bright region (42 s) on the front until becoming again fully bright. During this transition, the active Janus colloid is located in the periphery of the GUV and drags the GUV for a few  $\mu\text{m}$ . Once the particle orientation comes back to the initial state and the bright MF face (facing downwards) reappears, the particle migrates back to a central position at the bottom of the GUV (see Figure 6.3(A)). Because of the perturbations due to the addition of  $\text{H}_2\text{O}_2$ , the Janus particle is able to quickly change its orientation and show self-propulsion. However, when the GUV changes its curvature due to the active motion of the engulfed colloid, it slowly reacts by exerting a curvature induce force on the particle, which pulls the particle back to the bottom.

We sketched a scenario for this transient active GUV transport dynamics in Figure 6.3(B), showing the change of GUV shape and the membrane curvature due to the particle.

## 6. TOWARDS ACTIVE DYNAMICS OF ENGULFED JANUS COLLOIDS BY GUVS

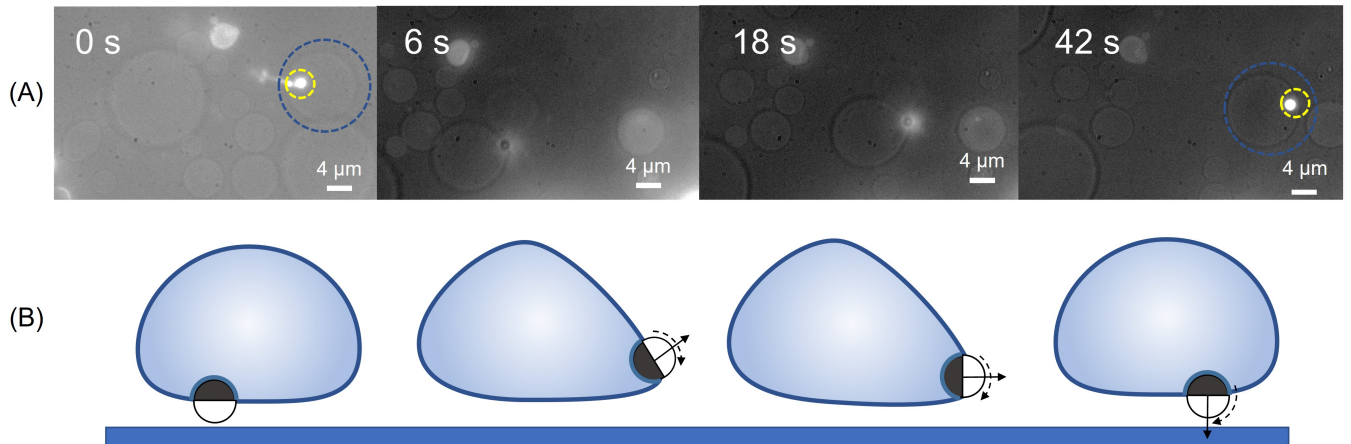


**Figure 6.3:** (A) Images showing an engulfed MF-Pt colloid changing orientation for  $t > 0$  due to the addition of  $\text{H}_2\text{O}_2$ , pulling the GUV membrane and returning to the bottom of the GUV. The colloid is highlighted in yellow and the GUV in blue. (B) Schematic representation of the transient behaviour for the colloid migration shown in (A). The solid arrow denotes the propulsion direction while the dashed arrow denoted the rotational direction. Images after the addition of  $\text{H}_2\text{O}_2$  ( $t > 0$ ) appear darker due to the formation of Oxygen bubbles in the cell.

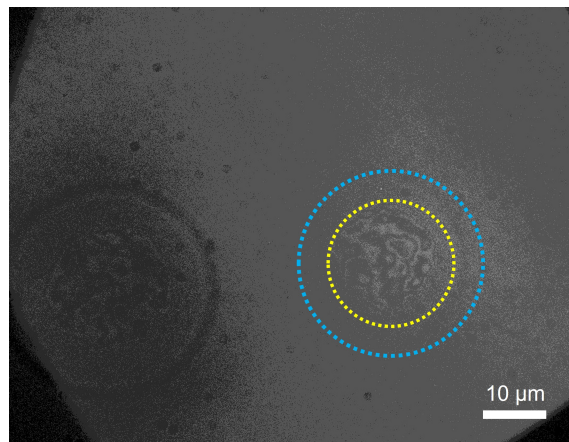


**Figure 6.4:** RICM + brightfield microscopy image of a floppy POPC vesicle where the blue (dashed) line represents the periphery of the vesicle while the yellow (dashed) line signifies the segment of the membrane touching the substrate. For a floppy membrane the footprint radius of the vesicle was observed to be up to  $3/4R_{GUV}$ .

In order to corroborate the scenario described before, a simple experiment was conducted where a partially engulfed MF-Pt Janus colloid was subjected to a repulsive optical trapping force. Unlike bare colloids, partially metallic Janus colloids [137, 138] are repelled by the optical trap resulting in a ballistic motion directed away from the

## 6.4 Future experimental investigations

trapping region. As depicted in Figure 6.5, when a partially engulfed MF-Pt colloid was subjected to this optical force, the colloid moves away from the trap towards the membrane equator, displacing the GUV along with itself. The Janus colloid however remains engulfed and quickly returns back to the bottom of the GUV. As seen in Figure 6.5, for the particle to reach at the bottom of the membrane after being displaced towards the equator took 0.6 s. For a moment, if we only account for gravity assisted particle sedimentation, the minimum time required by an MF-Pt colloid ( $R_P \approx 1 \mu\text{m}$ ) to reach the bottom is 3-4 s (considering particle sediments from the GUV equator  $R_P \approx 10 \mu\text{m}$ ). This accelerated migration of the colloid towards the bottom can be associated with the curvature induced force due to a gradient of membrane curvature, which tends to push back the particle to the flat membrane region near the substrate. Note that the position of the trap was not manipulated during the experiment and the displacement of the colloid/vesicle is purely due to the Janus repulsion of the optical trap.

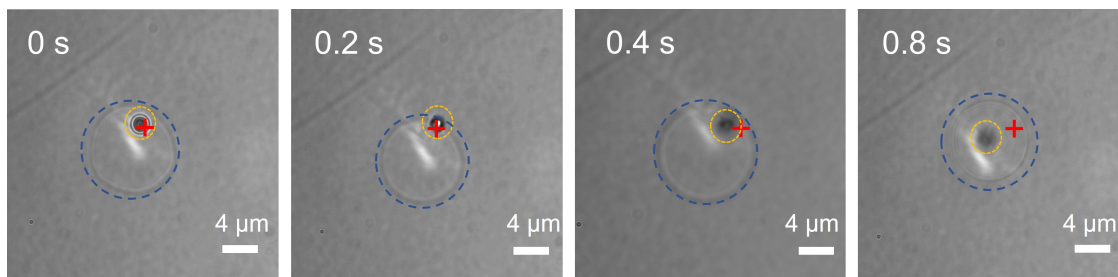


**Figure 6.5:** MF-Pt Janus colloid engulfed by POPC GUV resulting in a ballistic motion of the colloid repelling optical the trap, colloid migrating back to the bottom region of lower membrane tension. The position of the trap is indicated a red plus, the colloid is highlighted in dashed yellow and the GUV is highlighted in dashed blue.

## 6.4 Future experimental investigations

For future investigations, there is a need for a certain enhancement in the system to promote active dynamics of Janus colloids in the engulfed regime as well as to facilitate spontaneous engulfment of Janus colloids by GUVs. As discussed in the previous section, partial engulfment of the Janus colloids leads to a change in the membrane curvature to accommodate the colloid. The extent of this region of the membrane might be controlled by changing the Janus balance of a colloid: the area of the adhesive face of the Janus

## 6. TOWARDS ACTIVE DYNAMICS OF ENGULFED JANUS COLLOIDS BY GUVS

---

particle (e.g. dot Janus colloids [139]). As only the Pt face of the colloid shows affinity for the membranes, modifying the area fraction of Pt on the Janus can lead to lower variations of membrane curvature in the engulfment regime, lowering the curvature-induced force and allowing the Janus colloid to change its orientation to perform active GUV transport.

Another strategy that can be investigated to lower the membrane curvature gradient is to reduce the mismatch of densities in the interior and exterior of the GUV. The gradient of membrane curvature that exists due to the flat geometry of the GUV close to the interface can be avoided as a result of the reduced density mismatch. By avoiding the sedimentation of the GUVs and restricting the formation of a flat membrane region of zero curvature, the migration of the Janus colloids towards the bottom of the GUV can be curbed.

As mentioned in Chapter 5, the engulfment regimes were observed only after introduction of external force to drive the membrane GUV contact. Unlike the recent observations from Spank *et al.* [83], no spontaneous wrapping of the Janus colloids by the GUVs was observed in our system. As the membrane tension ( $\sigma$ ) was found to govern the engulfment of colloids, there is a need for consistently higher adhesion energies to drive the engulfment. In future experiments, the change in such energy landscape can be facilitated by varying the concentrations of salts in the exterior solution to generate asymmetric ionic conditions, giving rise to a negative spontaneous membrane curvature which favours membrane bending inwards [140]. Introduction of spontaneous membrane curvature leading to lower membrane tensions can be the key to observing the spontaneous engulfment regime.

### 6.5 Final Conclusions

In this thesis, the interaction dynamics of Janus colloids with GUV were thoroughly investigated in both active and passive conditions. Janus colloids used here are SiO<sub>2</sub> and MF colloids partially coated with Platinum and the activity was generated by the catalytic reaction on the Pt face of the colloid transforming H<sub>2</sub>O<sub>2</sub> into water and oxygen. POPC and DOPC GUVs were fabricated and investigated in interaction with Janus colloids.

For an isolated Janus colloid in passive conditions, the gap distance  $h$  between the Janus colloid and the bottom wall in thermal equilibrium was evaluated in between 300 nm and 1.5  $\mu\text{m}$ , which reflects the heterogeneous surface properties of the Janus colloids. The in-of-plane rotational diffusion  $D_{R,\parallel}$  was measured both in passive and active conditions and is very similar to the theoretical bulk value  $D_{R,b}$  and in agreement with the hydrodynamic prediction. The out-of-plane rotational diffusion  $D_{R,\perp}$  in passive conditions is significantly slowed down. In active conditions, a strong confinement of the out-of-plane particle rotational dynamics was observed. The highest active velocity obtained (at 2%  $\text{H}_2\text{O}_2$ ) at 4.5 - 5  $\mu\text{m}\cdot\text{s}^{-1}$  for both colloidal sizes and decreases with observation time. In this experimental condition, we could measure both the dynamics governed by thermal Brownian motion and the out-of-equilibrium active motion.

During the spontaneous interaction between a GUV and a Janus colloid in active condition, a persistent orbital motion of the active Janus colloids around the GUV was observed, which was independent on the GUV and particle size. Force and torque transfers between the particle and GUV were also observed (in the range of fN). Far-field hydrodynamics could explain the origin of the orbital motion, which is due to the fluid flow generated by the active particle and pointing towards the particle Janus boundary. The escape dynamics from the orbital trajectory displays a linear dependence on particle size, suggesting a role for the colloid translational friction in the escaping mechanism

Using external forces by centrifugation and optical tweezers, force-driven engulfment of Janus colloids by GUVs was realised. The engulfment of the colloids was found to be impacted by the surface properties of the colloid where platinum as well as silica show adhesion towards GUVs. Centrifugation experiments revealed partial engulfment of the colloids with forces up to  $10^{-10}$  N, while higher forces revealed membrane rupture/splitting. Particle engulfment was found to be closely related to the membrane tension and engulfment of bare Silica colloids was achieved only in floppy GUVs showing low membrane tensions. MF-Pt Janus colloids are partially engulfed by the GUV membranes with the MF face showing no affinity towards the membrane. The partial engulfment of MF-Pt colloids was confirmed by the confined out-of-plane particle rotational dynamics. A slowing down of the rotational diffusion ( $D_{R,\perp}$ ) by an order of magnitude in the engulfed regime compared to the free regime was also measured. Translational diffusion ( $D_{Tr,\parallel}$ ) of Janus colloids is also slowed down in the engulfed regime. Theoretical models

## 6. TOWARDS ACTIVE DYNAMICS OF ENGULFED JANUS COLLOIDS BY GUVS

---

were used to explain the slowing down of  $D_{Tr,\parallel}$  in terms of a membrane shear viscosity  $\eta_s \approx 10^{-9}$  Pa.s.m.

The activity of Janus colloids in the partially engulfed state was found to be severely suppressed with some rare exceptions of GUV membrane transportation. The quenching of the active motion was associated to the partial engulfed geometry of the particle and the curvature induced force of the GUV membrane, which leads to a change in the particle orientation with the active velocity vector pointing towards the solid wall, resulting in the quenching of X and Y translational active motion.



# References

- [1] SRIRAM RAMASWAMY. **The mechanics and statistics of active matter.** *Annual Review of Condensed Matter Physics*, **1**:323–345, 2010. [2](#)
- [2] YASUHIRO SHIRAI, ANDREW J. OSGOOD, YUMING ZHAO, KEVIN F. KELLY, AND JAMES M. TOUR. **Directional control in thermally driven single-molecule nanocars.** *Nano Letters*, **5**(11):2330–2334, 2005. [2](#) [121](#)
- [3] WALTER F. PAXTON, KEVIN C. KISTLER, CHRISTINE C. OLMEDA, AYUSMAN SEN, SARAH K. ST. ANGELO, YANYAN CAO, THOMAS E. MALLOUK, PAUL E. LAMMERT, AND VINCENT H. CRESPI. **Catalytic nanomotors: Autonomous movement of striped nanorods.** *Journal of the American Chemical Society*, **126**(41):13424–13431, 2004. [2](#) [6](#) [121](#)
- [4] RAMIN GOLESTANIAN AND SRIRAM RAMASWAMY. **Active matter.** *The European physical journal. E, Soft matter*, **36**(6):67, 2013. [2](#) [121](#)
- [5] XING MA, KERSTEN HAHN, AND SAMUEL SANCHEZ. **Catalytic mesoporous janus nanomotors for active cargo delivery.** *Journal of the American Chemical Society*, **137**(15):4976–4979, 2015. [2](#) [5](#) [106](#)
- [6] AHMET F. DEMIRÖRS, MEHMET TOLGA AKAN, ERIK POLONI, AND ANDRÉ R. STUDART. **Active cargo transport with Janus colloidal shuttles using electric and magnetic fields.** *Soft Matter*, **14**(23):4741–4749, 2018. [2](#) [106](#)
- [7] DANDAN XU, YONG WANG, CHUNYAN LIANG, YONGQIANG YOU, SAMUEL SANCHEZ, AND XING MA. **Self-Propelled Micro/Nanomotors for On-Demand Biomedical Cargo Transportation.** *Small*, **1902464**:1–22, 2019. [2](#)
- [8] L. BARABAN, M. TASINKEVYCH, M. N. POPESCU, S. SANCHEZ, S. DIETRICH, AND O. G. SCHMIDT. **Transport of cargo by catalytic Janus micro-motors.** *Soft Matter*, **8**(1):48–52, 2012. [2](#) [106](#)
- [9] JAIME AGUDO-CANALEJO AND REINHARD LIPOWSKY. **Critical particle sizes for the engulfment of nanoparticles by membranes and vesicles with bilayer asymmetry.** *ACS Nano*, **9**(4):3704–3720, 2015. [2](#) [16](#) [68](#)
- [10] SULIN ZHANG, HUAJIAN GAO, AND GANG BAO. **Physical Principles of Nanoparticle Cellular Endocytosis.** *ACS Nano*, **9**(9):8655–8671, 2015. [2](#)
- [11] WILSON C.K. POON, AIDAN T. BROWN, SUSANA O.L. DIREITO, DANIEL J.M. HODGSON, LUCAS LE NAGARD, ALEX LIPS, CAIT E. MACPHEE, DAVIDE MARENDUZZO, JOHN R. ROYER, ANDREA F. SILVA, JOB H.J. THIJSEN, AND SIMON TITMUSS. **Soft matter science and the COVID-19 pandemic.** *Soft Matter*, **16**(36):8310–8324, 2020. [2](#)
- [12] RUMIANA DIMOVA. **Giant Vesicles and Their Use in Assays for Assessing Membrane Phase State, Curvature, Mechanics, and Electrical Properties.** *Annual Review of Biophysics*, **48**(1):93–119, 2019. [2](#) [3](#) [6](#) [7](#) [121](#)
- [13] RUMIANA DIMOVA, SAID ARANDA, NATALYA BEZLYEPKINA, VESSELIN NIKOLOV, KARIN A. RISKE, AND REINHARD LIPOWSKY. **A practical guide to giant vesicles. Probing the membrane nanoregime via optical microscopy.** *Journal of Physics Condensed Matter*, **18**(28):1151–1176, 2006. [3](#)
- [14] CARLOS M. MARQUES AND RUMIANA DIMOVA. *The Giant Vesicle Book*. 2019. [3](#) [7](#)
- [15] SUSANNE F FENZ AND KHEYA SENGUPTA. **Giant vesicles as cell models.** *Integrative biology : quantitative biosciences from nano to macro*, **4**(9):982–995, 9 2012. [3](#)
- [16] F M MENDER AND J S KEIPER. **Chemistry and physics of giant vesicles as biomembrane models.** *Current opinion in chemical biology*, **2**(6):726–732, 12 1998. [3](#)
- [17] PETER WALDE, KATIA COSENTINO, HELEN ENGEL, AND PASQUALE STANO. **Giant vesicles: preparations and applications.** *Chembiochem : a European journal of chemical biology*, **11**(7):848–865, 5 2010. [3](#)
- [18] RUMIANA DIMOVA. **Chapter One - Giant Vesicles: A Biomimetic Tool for Membrane Characterization.** **16** of *Advances in Planar Lipid Bilayers and Liposomes*, pages 1–50. Academic Press, 2012. [3](#)
- [19] C. CASAGRANDE, P. FABRE, E. RAPHAËL, AND M. VEYSSIÉ. **«Janus beads»: Realization and behaviour at water/oil interfaces.** *Epl*, **9**(3):251–255, 1989. [3](#)
- [20] HONG LIANG, ANGELO CACCIUTO, ERIK LUIJTER, AND STEVE GRANICK. **Clusters of charged janus spheres.** *Nano Letters*, **6**(11):2510–2514, 2006. [3](#)
- [21] QIAN CHEN, JONATHAN K. WHITMER, SHAN JIANG, SUNG CHUL BAE, ERIK LUIJTER, AND STEVE GRANICK. **Supracolloidal reaction kinetics of janus spheres.** *Science*, **331**(6014):199–202, 2011. [3](#)
- [22] FEDERICO TOSCHI AND SEGA MARCELLO. *Flowing matter*. 2019. [ix](#) [3](#) [4](#)
- [23] NICOLE GLASER, DAVE J. ADAMS, ALEXANDER BÖKER, AND GEORG KRAUSCH. **Janus particles at liquid-liquid interfaces.** *Langmuir*, **22**(12):5227–5229, 2006. [3](#)

## REFERENCES

- [24] MIGUEL ANGEL FERNANDEZ-RODRIGUEZ, YANG SONG, MIGUEL ÁNGEL RODRÍGUEZ-VALVERDE, SHAOWEI CHEN, MIGUEL ANGEL CABRERIZO-VILCHEZ, AND ROQUE HIDALGO-ÁLVAREZ. **Comparison of the interfacial activity between homogeneous and Janus gold nanoparticles by pendant drop tensiometry.** *Langmuir*, **30**(7):1799–1804, 2014. [3](#)
- [25] HUI MIN GAO, ZHONG YUAN LU, HONG LIU, ZHAO YAN SUN, AND LI JIA AN. **Orientation and surface activity of Janus particles at fluid-fluid interfaces.** *Journal of Chemical Physics*, **141**(13), 2014. [3](#)
- [26] XIAOSHAN FAN, JING YANG, XIAN JUN LOH, AND ZIBIAO LI. **Polymeric Janus Nanoparticles: Recent Advances in Synthetic Strategies, Materials Properties, and Applications.** *Macromolecular Rapid Communications*, **40**(5):1–19, 2019. [4](#)
- [27] YI YI, LUCERO SANCHEZ, YUAN GAO, AND YAN YU. **Janus particles for biological imaging and sensing.** *Analyst*, **141**(12):3526–3539, 2016. [4](#)
- [28] ANDREAS WALTHER AND AXEL H.E. MÜLLER. **Janus particles: Synthesis, self-assembly, physical properties, and applications.** *Chemical Reviews*, **113**(7):5194–5261, 2013. [4](#)
- [29] P. YÁNEZ-SEDEÑO, S. CAMPUZANO, AND J. M. PINGARÓN. **Janus particles for (bio)sensing.** *Applied Materials Today*, **9**:276–288, 2017. [4](#)
- [30] YONGDONG JIN AND XIAOHU GAO. **Plasmonic fluorescent quantum dots.** *Nature Nanotechnology*, **4**(9):571–576, 2009. [4](#)
- [31] FUXIN LIANG, CHENGLIANG ZHANG, AND ZHENZHONG YANG. **Rational design and synthesis of Janus composites.** *Advanced Materials*, **26**(40):6944–6949, 2014. [4](#)
- [32] JUN BING FAN, YONGYANG SONG, HONG LIU, ZHONGYUAN LU, FEILONG ZHANG, HONGLIANG LIU, JINGXIN MENG, LIN GU, SHUTAO WANG, AND LEI JIANG. **A general strategy to synthesize chemically and topologically anisotropic Janus particles.** *Science Advances*, **3**(6):1–9, 2017. [4](#)
- [33] STOYAN K. SMOUKOV, SUMIT GANGWAL, MANUEL MARQUEZ, AND ORLIN D. VELEV. **Reconfigurable responsive structures assembled from magnetic Janus particles.** *Soft Matter*, **5**(6):1285–1292, 2009. [5](#)
- [34] J LYKLEMA. **Fundamentals of Interface and Colloid Science.** pages 3–302. Academic Press, 1995. [5](#)
- [35] SO AIZAWA, KEISUKE SETO, AND ELJI TOKUNAGA. **External field response and applications of metal coated hemispherical Janus particles.** *Applied Sciences (Switzerland)*, **8**(4), 2018. [5](#)
- [36] ANNA EICHLER-VOLF, YARA ALSAADAWI, FERNANDO VAZQUEZ LUNA, QAISER ALI KHAN, SIMON STIERLE, CHI XU, MICHAEL HEIGL, ZAHRA FEKRI, SHENGQIANG ZHOU, PETER ZAHN, MANFRED ALBRECHT, MARTIN STEINHART, AND ARTUR ERBE. **Sensitivity of PS/CoPd Janus particles to an external magnetic field.** *RSC Advances*, **11**(28):17051–17057, 2021. [5](#)
- [37] HONG REN JIANG, NATSUHIKO YOSHINAGA, AND MASAKI SANO. **Active motion of a Janus particle by self-thermophoresis in a defocused laser beam.** *Physical Review Letters*, **105**(26):1–4, 2010. [5](#)
- [38] LARYSA BARABAN, DENYS MAKAROV, ROBERT STREUBEL, INGOLF MÖNCH, DANIEL GRIMM, SAMUEL SANCHEZ, AND OLIVER G SCHMIDT. **Catalytic Janus Motors on Microfluidic Chip: Deterministic Motion for Targeted Cargo Delivery.** *ACS Nano*, **6**(4):3383–3389, 4 2012. [5](#)
- [39] BIAN QIAN, DANIEL MONTIEL, ANDREAS BREGULLA, FRANK CICHOS, AND HAW YANG. **Harnessing thermal fluctuations for purposeful activities: the manipulation of single micro-swimmers by adaptive photon nudging.** *Chem. Sci.*, **4**(4):1420–1429, 2013. [5](#)
- [40] SÉBASTIEN FAYOLLE, THOMAS BICKEL, AND ALOIS WÜRGER. **Thermophoresis of charged colloidal particles.** *Physical Review E - Statistical, Nonlinear, and Soft Matter Physics*, **77**(4):1–8, 2008. [5](#)
- [41] RUMIANA DIMOVA. **Recent developments in the field of bending rigidity measurements on membranes.** *Advances in Colloid and Interface Science*, **208**:225–234, 2014. [5](#) [90](#)
- [42] WEI GAO, ALLEN PEI, RENFENG DONG, AND JOSEPH WANG. **Catalytic Iridium-Based Janus Micromotors Powered by Ultralow Levels of Chemical Fuels.** *Journal of the American Chemical Society*, **136**(6):2276–2279, 2 2014. [5](#)
- [43] WEI GAO, ALLEN PEI, XIAOMIAO FENG, CAMILLE HENNESSY, AND JOSEPH WANG. **Organized Self-Assembly of Janus Micromotors with Hydrophobic Hemispheres.** *Journal of the American Chemical Society*, **135**(3):998–1001, 1 2013. [5](#)
- [44] SHANG YIK REIGH, MU JIE HUANG, HARTMUT LÖWEN, ERIC LAUGA, AND RAYMOND KAPRAL. **Active rotational dynamics of a self-diffusiophoretic colloidal motor.** *Soft Matter*, **16**(5):1236–1245, 2020. [5](#)
- [45] JOHN F BRADY. **Particle motion driven by solute gradients with application to autonomous motion: continuum and colloidal perspectives.** *Journal of Fluid Mechanics*, **667**:216–259, 2011. [5](#)
- [46] RAMIN GOLESTANIAN, TANNIEMOLA B. LIVERPOOL, AND ARMAND AJDARI. **Propulsion of a molecular machine by asymmetric distribution of reaction products.** *Physical Review Letters*, **94**(22):1–4, 2005. [5](#)
- [47] J. G. GIBBS AND Y. P. ZHAO. **Autonomously motile catalytic nanomotors by bubble propulsion.** *Applied Physics Letters*, **94**(16):3–6, 2009. [6](#) [56](#) [64](#)
- [48] WALTER F. PAXTON, AYUSMAN SEN, AND THOMAS E. MALLOW. **Motility of catalytic nanoparticles through self-generated forces.** *Chemistry - A European Journal*, **11**(22):6462–6470, 2005. [6](#)
- [49] SÉBASTIEN FOURNIER-BIDOZ, ANDRÉ C ARSENAULT, IAN MANNERS, AND GEOFFREY A OZIN. **Synthetic self-propelled nanomotors.** *Chem. Commun.*, (4):441–443, 2005. [6](#)

## REFERENCES

- [50] AIDAN BROWN AND WILSON POON. [Ionic effects in self-propelled Pt-coated Janus swimmers](#). *Soft Matter*, 10(22):4016–4027, 2014. [6](#) [11](#)
- [51] OLE G. MOURITSEN AND LUIS A. BAGATOLLI. *LIFE – AS A MATTER OF FAT Lipids in a Membrane Biophysics Perspective*, 56. 2016. [6](#)
- [52] GERRIT VAN MEER. **Cellular lipidomics**. *The EMBO journal*, 24(18):3159–3165, 9 2005. [7](#)
- [53] DEREK MARSH. *Handbook of Lipid Bilayers*. 2013. [7](#)
- [54] A. J. GOLDMAN, R. G. COX, AND H. BRENNER. **Slow viscous motion of a sphere parallel to a plane wall-II Couette flow**. *Chemical Engineering Science*, 22(4):653–660, 1967. [8](#)
- [55] C. K. CHOI, C. H. MARGRAVES, AND K. D. KIHM. **Examination of near-wall hindered Brownian diffusion of nanoparticles: Experimental comparison to theories by Brenner (1961) and Goldman et al. (1967)**. *Physics of Fluids*, 19(10), 2007. [8](#)
- [56] MAURICIO D. CARBAJAL-TINOCO, RICARDO LOPEZ-FERNANDEZ, AND JOSÉ LUIS ARAUZ-LARA. **Asymmetry in colloidal diffusion near a rigid wall**. *Physical Review Letters*, 99(13):1–4, 2007. [8](#)
- [57] PETER HOLMQUIST, JAN K.G. DHONT, AND PETER R. LANG. **Colloidal dynamics near a wall studied by evanescent wave light scattering: Experimental and theoretical improvements and methodological limitations**. *Journal of Chemical Physics*, 126(4), 2007. [8](#)
- [58] MICHAEL A. BEVAN AND DENNIS C. PRIEVE. **Hindered diffusion of colloidal particles very near to a wall: revisited**. *Journal of Chemical Physics*, 113(3):1228–1236, 2000. [8](#)
- [59] ALBERT EINSTEIN. [On the Movement of Small Particles Suspended in Stationary Liquids Required by the Molecular-Kinetic Theory of Heat](#). *Annalen der Physik*, 1905. [8](#) [42](#)
- [60] HILDING FAXÉN. **Der Widerstand gegen die Bewegung einer starren Kugel in einer zähen Flüssigkeit, die zwischen zwei parallelen ebenen Wänden eingeschlossen ist**. *Annalen der Physik*, 373(10):89–119, 1922. [xii](#) [8](#) [46](#)
- [61] J. HAPPEL AND H. BRENNER. *Low Reynolds number hydrodynamics*. 1973. [8](#)
- [62] A. J. GOLDMAN, R. G. COX, AND H. BRENNER. **Slow viscous motion of a sphere parallel to a plane wall-I Motion through a quiescent fluid**. *Chemical Engineering Science*, 22(4):637–651, 1967. [ix](#) [8](#) [9](#) [44](#) [51](#) [58](#) [125](#)
- [63] STEFANIA KETZETZI, JOOST DE GRAAF, AND DANIELA J. KRAFT. [Diffusion-based height analysis reveals robust microswimmer-wall separation](#), pages 1–7, 2020. [ix](#) [9](#) [10](#) [44](#) [45](#) [55](#) [62](#)
- [64] AIDIN RASHIDI AND CHRISTOPHER L. WIRTH. [Motion of a Janus particle very near a wall](#). *Journal of Chemical Physics*, 147(22), 2017. [ix](#) [10](#)
- [65] SCOTT G FLICKER AND STACY G BIKE. [Measuring double layer repulsion using total internal reflection microscopy](#). *Langmuir*, 9(1):257–262, 1 1993. [ix](#) [10](#)
- [66] SAMBEETA DAS, ASTHA GARG, ANDREW I. CAMPBELL, JONATHAN HOWSE, AYUSMAN SEN, DARRELL VELEGOL, RAMIN GOLESTANIAN, AND STEPHEN J. EBBENS. **Boundaries can steer active Janus spheres**. *Nature Communications*, 6:1–10, 2015. [ix](#) [10](#) [11](#) [58](#) [59](#) [71](#) [76](#)
- [67] A. M. ROBERTS. **Mechanisms of gravitaxis in Chlamydomonas**. *Biological Bulletin*, 210(2):78–80, 2006. [11](#)
- [68] ANDREW I CAMPBELL AND STEPHEN J EBBENS. [Gravitaxis in Spherical Janus Swimming Devices](#). *Langmuir*, 29(46):14066–14073, 11 2013. [11](#)
- [69] XIAOLU WANG, MARTIN IN, CHRISTOPHE BLANC, MAURIZIO NOBILI, AND ANTONIO STOCO. **Enhanced active motion of Janus colloids at the water surface**. *Soft Matter*, 11(37):7376–7384, 2015. [11](#) [43](#) [74](#)
- [70] DAISUKE TAKAGI, JÉRÉMIE PALACCI, ADAM B. BRAUNSCHWEIG, MICHAEL J. SHELLEY, AND JUN ZHANG. **Hydrodynamic capture of microswimmers into sphere-bound orbits**. *Soft Matter*, 10(11):1784–1789, 2014. [11](#) [66](#) [71](#) [75](#) [79](#)
- [71] AT BROWN, ID VLADESCU, A DAWSON, JANA SCHWARZLINEK, JS LINTUVUORI, AND WILSON C K POON. **Swimming in a crystal**. *Soft matter*, 12:131, 2016. [11](#) [66](#) [71](#)
- [72] SAVERIO E. SPAGNOLIE AND ERIC LAUGA. **Hydrodynamics of self-propulsion near a boundary: predictions and accuracy of far-field approximations**. *Journal of Fluid Mechanics*, 700:105–147, 2012. [11](#) [12](#) [58](#) [79](#)
- [73] NIKHIL DESAI, VASEEM A. SHAIK, AND AREZOO M. ARDEKANI. [Hydrodynamics-mediated trapping of micro-swimmers near drops](#). *Soft Matter*, 14(2):264–278, 2018. [11](#) [12](#) [79](#)
- [74] SAVERIO E. SPAGNOLIE, GREGORIO R. MORENO-FLORES, DENIS BARTOLO, AND ERIC LAUGA. [Geometric capture and escape of a microswimmer colliding with an obstacle](#). *Soft Matter*, 11(17):3396–3411, 2015. [12](#) [76](#)
- [75] SAVERIO E. SPAGNOLIE, GREGORIO R. MORENO-FLORES, DENIS BARTOLO, AND ERIC LAUGA. [Geometric capture and escape of a microswimmer colliding with an obstacle](#). *Soft Matter*, 11(17):3396–3411, 2015. [8](#) [13](#) [71](#) [72](#) [79](#)
- [76] MATTEO PAOLUZZI, ROBERTO DI LEONARDO, M. CRISTINA MARCHETTI, AND LUCA ANGELANI. **Shape and displacement fluctuations in soft vesicles filled by active particles**. *Scientific Reports*, 6(September):1–10, 2016. [13](#)
- [77] ABDALLAH DADDI-MOUSSA-IDER, SEGUN GOH, BENNO LIEBCHEN, CHRISTIAN HOELL, ARNOLD J.T.M. MATHIJSEN, FRANCISCA GUZMÁN-LASTRA, CHRISTIAN SCHOLZ, ANDREAS M. MENZEL, AND HARTMUT LÖWEN. [Membrane penetration and trapping of an active particle](#). *Journal of Chemical Physics*, 150(6), 2019. [13](#)

## REFERENCES

- [78] HANUMANATHA RAO VUTUKURI, MASOUD HOORE, CLARA ABAURREA-VELASCO, LENNARD VAN BUREN, ALESSANDRO DUTTO, THORSTEN AUTH, DMITRY A. FEDOSOV, GERHARD GOMPPER, AND JAN VERMANT. **Active particles induce large shape deformations in giant lipid vesicles.** *Nature*, **586**(7827):52–56, 2020. [14](#)
- [79] CHRISTIAN DIETRICH, MIGLENA ANGELOVA, AND BERNARD POULIGNY. **Adhesion of Latex spheres to giant phospholipid vesicles: Statics and dynamics.** *Journal de physique. II*, **7**(11):1651–1682, 1997. [14](#)
- [80] KAZUKI SHIGYOU, KEN H. NAGAI, AND TSUTOMU HAMADA. **Lateral Diffusion of a Submicrometer Particle on a Lipid Bilayer Membrane.** *Langmuir*, **32**(51):13771–13777, 2016. [14](#) [31](#) [84](#)
- [81] K. D. DANOV, R. AUST, F. DURST, AND U. LANGE. **Slow motions of a solid spherical particle close to a viscous interface.** *International Journal of Multiphase Flow*, **21**(6):1169–1189, 1995. [14](#)
- [82] KRASSIMIR D. DANOV, RUMIANA DIMOVA, AND BERNARD POULIGNY. **Viscous drag of a solid sphere straddling a spherical or flat surface.** *Physics of Fluids*, **12**(11):2711–2722, 2000. [14](#) [103](#) [130](#)
- [83] HENDRIK T. SPANKE, ROBERT W. STYLE, CLAIRE FRANÇOIS-MARTIN, MARIA FEOFILOVA, MANUEL EISENTRAUT, HOLGER KRESS, JAIME AGUDO-CANALEJO, AND ERIC R. DUFRESNE. **Wrapping of Microparticles by Floppy Lipid Vesicles.** *Physical Review Letters*, **125**(19):1–10, 2020. [3](#) [14](#) [15](#) [64](#) [82](#) [83](#) [89](#) [90](#) [112](#)
- [84] M. DESERNO AND T. BICKEL. **Wrapping of a spherical colloid by a fluid membrane.** *Europhysics Letters*, **62**(5):767–773, 2003. [16](#)
- [85] JAIME AGUDO-CANALEJO AND REINHARD LIPOWSKY. **Uniform and Janus-like nanoparticles in contact with vesicles: energy landscapes and curvature-induced forces.** *Soft Matter*, **13**(11):2155–2173, 2017. [16](#) [108](#) [109](#)
- [86] J. CHRISTOPHER LOVE, BYRON D. GATES, DANIEL B. WOLFE, KATERI E. PAUL, AND GEORGE M. WHITESIDES. **Fabrication and Wetting Properties of Metallic Half-Shells with Submicron Diameters.** *Nano Letters*, **2**(8):891–894, 2002. [18](#) [123](#)
- [87] B. H. KEMMENOE AND G. R. BULLOCK. **Structure analysis of sputter-coated and ion-beam sputter-coated films: a comparative study.** *Journal of Microscopy*, **132**(2):153–163, 1983. [22](#)
- [88] TANSEL KARABACAK. **Thin-film growth dynamics with shadowing and re-emission effects.** *Journal of Nanophotonics*, **5**(1):052501, 2011. [23](#)
- [89] ROBERT D. DEEGAN, OLGICA BAKAJIN, TODD F. DUPONT, GREG HUBER, SIDNEY R. NAGEL, AND THOMAS A. WITTEN. **Capillary flow as the cause of ring stains from dried liquid drops.** *Nature*, **389**(6653):827–829, 1997. [23](#)
- [90] JOHN P. REEVES AND ROBERT M. DOWBEN. **Formation and properties of thin-walled phospholipid vesicles.** *Journal of Cellular Physiology*, **73**(1):49–60, 1969. [24](#)
- [91] KANTA TSUMOTO, HIDEKI MATSUI, MASAHIRO TOMITA, AND TETSURO YOSHIMURA. **Efficient formation of giant liposomes through the gentle hydration of phosphatidylcholine films doped with sugar.** *Colloids and Surfaces B: Biointerfaces*, **68**(1):98–105, 2009. [24](#)
- [92] ANDREAS WEINBERGER, FENG CHING TSAI, GIJSJE H. KOENDERINK, THAIS F. SCHMIDT, ROSÁNGELA ITRI, WOLFGANG MEIER, TATIANA SCHMATKO, ANDRÉ SCHRÖDER, AND CARLOS MARQUES. **Gel-assisted formation of giant unilamellar vesicles.** *Biophysical Journal*, **105**(1):154–164, 2013. [25](#) [124](#)
- [93] M. ANGELOVA AND D. S. DIMITROV. **A mechanism of liposome electroformation.** *Trends in Colloid and Interface Science II*, **67**:59–67, 2007. [28](#)
- [94] VAIBHAV SHARMA, ELISE AZAR, ANDRÉ SCHRÖDER, CARLOS M. MARQUES, AND ANTONIO STOCCO. **Active colloids orbiting giant vesicles.** *Soft Matter*, 2020. [30](#) [126](#)
- [95] BRUCE D. LUCAS AND TAKEO KANADE. **Iterative Image Registration Technique With an Application To Stereo Vision.** **2**(April 1981):674–679, 1981. [32](#)
- [96] J. ILLINGWORTH AND J. KITTLER. **The Adaptive Hough Transform.** *IEEE Transactions on Pattern Analysis and Machine Intelligence*, **PAMI-9**(5):690–698, 1987. [36](#)
- [97] JÉRÉMIE PALACCI, CÉCILE COTTIN-BIZONNE, CHRISTOPHE YBERT, AND LYDÉRIC BOCQUET. **Sedimentation and effective temperature of active colloidal suspensions.** *Physical Review Letters*, **105**(8):1–4, 2010. [43](#)
- [98] J. LEACH, H. MUSHFIQUE, S. KEEN, R. DI LEONARDO, G. RUOCCO, J. M. COOPER, AND M. J. PADGETT. **Comparison of Faxén’s correction for a microsphere translating or rotating near a surface.** *Physical Review E - Statistical, Nonlinear, and Soft Matter Physics*, **79**(2), 2009. [44](#) [46](#) [100](#)
- [99] TH. M. FISCHER, P. DHAR, AND P. HEINIG. **The viscous drag of spheres and filaments moving in membranes or monolayers.** *Journal of Fluid Mechanics*, **558**:451–475, 2006. [44](#) [46](#) [51](#) [100](#) [102](#) [103](#) [125](#) [130](#)
- [100] HOWARD BRENNER. **The slow motion of a sphere through a viscous fluid towards a plane surface.** *Chemical Engineering Science*, **16**(3-4):242–251, 1961. [45](#) [47](#)
- [101] MOJDEH HEIDARI, ANDREAS BREGULLA, SANTIAGO MUINOS LANDIN, FRANK CICHOS, AND REGINE VON KLITZING. **Self-Propulsion of Janus Particles near a Brush-Functionalized Substrate.** *Langmuir*, **36**(27):7775–7780, 2020. [45](#)
- [102] JACOB N. ISRAELACHVILI. **Intermolecular and Surface Forces: Third Edition.** *Intermolecular and Surface Forces: Third Edition*, pages 1–676, 2011. [45](#)
- [103] STEFANO VILLA, ANTONIO STOCCO, CHRISTOPHE BLANC, AND MAURIZIO NOBILI. **Multistable interaction between a spherical Brownian particle and an air-water interface.** *Soft Matter*, **16**(4):960–969, 2020. [45](#)

- [104] RUBEN W. VERWEIJ, STEFANIA KETZETZI, JOOST DE GRAAF, AND DANIELA J. KRAFT. **Height distribution and orientation of colloidal dumbbells near a wall.** *Physical Review E*, **102**(6):1–15, 2020. [xii](#) [46](#)
- [105] ANTONIO STOCO, BENJAMIN CHOLLET, XIAOLU WANG, CHRISTOPHE BLANC, AND MAURIZIO NOBILI. **Rotational diffusion of partially wetted colloids at fluid interfaces.** *Journal of Colloid and Interface Science*, **542**:363–369, 2019. [46](#) [49](#)
- [106] S. H. LEE AND L. G. LEAL. **Motion of a sphere in the presence of a plane interface. Part 2. An exact solution in bipolar co-ordinates.** *Journal of Fluid Mechanics*, **98**(1):193–224, 1980. [48](#) [62](#)
- [107] S. A. ROGERS, M. LISICKI, B. CICHOCKI, J. K.G. DHONT, AND P. R. LANG. **Rotational diffusion of spherical colloids close to a wall.** *Physical Review Letters*, **109**(9), 2012. [50](#)
- [108] J. HAPPEL AND H. BRENNER. *Low Reynolds number hydrodynamics*. Springer Netherlands. [50](#)
- [109] BOGDAN CICHOCKI, MARIA L. EKIEL-JEZEWSKA, AND ELIGIUSZ WAJNRYB. **Communication: Translational Brownian motion for particles of arbitrary shape.** *Journal of Chemical Physics*, **136**(7), 2012. [50](#)
- [110] M. E. O’NEILL, K. B. RANGER, AND H. BRENNER. **Slip at the surface of a translating–rotating sphere bisected by a free surface bounding a semi-infinite viscous fluid: Removal of the contact-line singularity.** *Physics of Fluids*, **29**(4):913, 1986. [51](#) [125](#)
- [111] ANDERS TJELL AND KRISTOFFER ALMDAL. **Diffusion rate of hydrogen peroxide through water-swelled polyurethane membranes.** *Sensing and Bio-Sensing Research*, **21**(October):35–39, 2018. [53](#)
- [112] STEPHEN EBBENS, RICHARD A.L. JONES, ANTHONY J. RYAN, RAMIN GOLESTANIAN, AND JONATHAN R. HOWSE. **Self-assembled autonomous runners and tumblers.** *Physical Review E - Statistical, Nonlinear, and Soft Matter Physics*, **82**(1):6–9, 2010. [53](#) [54](#)
- [113] S. DAS AND A. CACCIUTO. **Colloidal swimmers near curved and structured walls.** *Soft Matter*, **15**(41):8290–8301, 2019. [58](#) [61](#)
- [114] JONATHAN R. HOWSE, RICHARD A.L. JONES, ANTHONY J. RYAN, TIM GOUGH, REZA VAFABAKHSH, AND RAMIN GOLESTANIAN. **Self-Motile Colloidal Particles: From Directed Propulsion to Random Walk.** *Physical Review Letters*, **99**(4):8–11, 2007. [64](#)
- [115] T. BICKEL. **Brownian motion near a liquid-like membrane.** *European Physical Journal E*, **20**(4):379–385, 2006. [65](#)
- [116] XIAOLU WANG, MARTIN IN, CHRISTOPHE BLANC, ALOIS WÜRGER, MAURIZIO NOBILI, AND ANTONIO STOCO. **Janus Colloids Actively Rotating on the Surface of Water.** *Langmuir*, **33**(48):13766–13773, 2017. [75](#)
- [117] STEFANO VILLA, GIUSEPPE BONIELLO, ANTONIO STOCO, AND MAURIZIO NOBILI. **Motion of micro- and nanoparticles interacting with a fluid interface.** *Advances in Colloid and Interface Science*, **284**:102262, 2020. [76](#)
- [118] JULIANE SIMMCHEN, JAIDEEP KATURI, WILLIAM E. USPAL, MIHAIL N. POPESCU, MYKOLA TASINKEVYCH, AND SAMUEL SÁNCHEZ. **Topographical pathways guide chemical microswimmers.** *Nature Communications*, **7**(May 2015):1–9, 2016. [80](#)
- [119] ANTOINE LAGARDE, NOÉMIE DAGÈS, TAKAHIRO NEMOTO, VINCENT DÉMERY, DENIS BAROLO, AND THOMAS GIBAUD. **Colloidal transport in bacteria suspensions: From bacteria collision to anomalous and enhanced diffusion.** *Soft Matter*, **16**(32):7503–7512, 2020. [80](#)
- [120] HANUMANTHA RAO VUTUKURI, MACIEJ LISICKI, ERIC LAUGA, AND JAN VERMANT. **Light-switchable propulsion of active particles with reversible interactions.** *Nature Communications*, **11**(1):1–9, 2020. [80](#)
- [121] MARKUS DESERNO. **Elastic deformation of a fluid membrane upon colloid binding.** *Physical Review E - Statistical, Nonlinear, and Soft Matter Physics*, **69**(3 1):1–14, 2004. [xv](#) [83](#) [84](#)
- [122] FELIX CAMPELO, CLEMENT ARNAEZ, SIEWERT J. MARRINK, AND MICHAEL M. KOZLOV. **Helfrich model of membrane bending: From Gibbs theory of liquid interfaces to membranes as thick anisotropic elastic layers.** *Advances in Colloid and Interface Science*, **208**:25–33, 2014. [83](#)
- [123] AMIR H. BAHRAMI, MICHAEL RAATZ, JAIME AGUDO-CANALEJO, RAPHAEL MICHEL, EMILY M. CURTIS, CAROL K. HALL, MICHAEL GRADZIELSKI, REINHARD LIPOWSKY, AND THOMAS R. WEIKL. **Wrapping of nanoparticles by membranes.** *Advances in Colloid and Interface Science*, **208**:214–224, 2014. [84](#)
- [124] C. MONZEL AND K. SENGUPTA. **Measuring shape fluctuations in biological membranes.** *Journal of Physics D: Applied Physics*, **49**(24):243002, 2016. [87](#) [88](#)
- [125] HÉLÈNE BOUVRAIS, MARTIN HOLMSTRUP, PETER WESTH, AND JOHN H. IPSEN. **Analysis of the shape fluctuations of reconstituted membranes using GUVs made from lipid extracts of invertebrates.** *Biology Open*, **2**(4):373–378, 2013. [87](#) [88](#)
- [126] FLORENT FESSLER. **STUDY OF MEMBRANE-PARTICLE INTERACTION BY MEANS OF OPTICAL TWEEZERS.** Technical Report June, 2021. [88](#)
- [127] M. DOKTOROVA, D. HARRIES, AND G. KHELASHVILI. *Determination of bending rigidity and tilt modulus of lipid membranes from real-space fluctuation analysis of molecular dynamics simulations*, **19**. 2017. [90](#) [94](#)
- [128] L.D LANDAU AND E.M LIFSHITZ. *Fluid Mechanics*. Addison Wesley, second edi edition, 1959. [101](#)
- [129] IVÁN REY SUÁREZ, CHAD LEIDY, GABRIEL TÉLLEZ, GUILAUME GAY, AND ANDRES GONZALEZ-MANCERA. **Slow Sedimentation and Deformability of Charged Lipid Vesicles.** *PLoS ONE*, **8**(7), 2013. [102](#) [130](#)

## REFERENCES

---

- [130] MARCELINA CARDOSO DOS SANTOS, CYRILLE VÉZY, AND RODOLPHE JAFFIOL. [Nanoscale characterization of vesicle adhesion by normalized total internal reflection fluorescence microscopy](#). *Biochimica et Biophysica Acta - Biomembranes*, **1858**(6):1244–1253, 2016. [102](#) [130](#)
- [131] T. CHARITAT, E. BELLET-AMALRIC, G. FRAGNETO, AND F. GRANER. [Adsorbed and free lipid bilayers at the solid-liquid interface](#). *European Physical Journal B*, **8**(4):583–593, 1999. [102](#) [130](#)
- [132] JAVED ALLY AND A. AMIRFAZLI. [Magnetophoretic measurement of the drag force on partially immersed microparticles at air-liquid interfaces](#). *Colloids and Surfaces A: Physicochemical and Engineering Aspects*, **360**(1):120–128, 2010. [102](#)
- [133] FRANCISCO ORTEGA, HERNÁN RITACCO, AND RAMÓN G RUBIO. [Interfacial microrheology: Particle tracking and related techniques](#). *Current Opinion in Colloid & Interface Science*, **15**(4):237–245, 2010. [102](#)
- [134] M SICKERT, F RONDELEZ, AND H A STONE. [Single-particle Brownian dynamics for characterizing the rheology of fluid Langmuir monolayers](#). **79**(6):66005, 8 2007. [102](#)
- [135] PIETRO CICUTA, SARAH L. KELLER, AND SARAH L. VEATCH. [Diffusion of liquid domains in lipid bilayer membranes](#). *Journal of Physical Chemistry B*, **111**(13):3328–3331, 2007. [103](#) [130](#)
- [136] JILIANG CHEN, HONGYAN ZHANG, XU ZHENG, AND HAIHANG CUI. [Janus particle microshuttle: 1D directional self-propulsion modulated by AC electrical field](#). *AIP Advances*, **4**(3), 2014. [106](#)
- [137] YUQUAN ZHANG, XIUJIE DOU, YANMENG DAI, XIANYOU WANG, CHANGJUN MIN, AND XIAOCONG YUAN. [All-optical manipulation of micrometer-sized metallic particles](#). *Photonics Research*, **6**(2):66, 2018. [110](#)
- [138] S HUOSHUO Z HANG, Y UQUAN Z HANG, Y F U ANAN, Z HENG, Z HU, Z HONGSHENG M AN, J B U ING, H U I F ANG, C HANGJUN M IN, AND X IAOCONG Y UAN. [Nonlinearity-modulated single molecule trapping and Raman scattering analysis](#). **29**(20):32285–32295, 2021. [110](#)
- [139] RANDALL M. ERB, NATHAN J. JENNESS, ROBERT L. CLARK, AND BENJAMIN B. YELLEN. [Towards holo-nomic control of Janus particles in optomagnetic traps](#). *Advanced Materials*, **21**(47):4825–4829, 2009. [112](#)
- [140] MARZIEH KARIMI, JAN STEINKÜHLER, DEBJIT ROY, RAKTIM DASGUPTA, REINHARD LIPOWSKY, AND RUMIANA DIMOVA. [Asymmetric Ionic Conditions Generate Large Membrane Curvatures](#). *Nano Letters*, **18**(12):7816–7821, 2018. [112](#)
- [141] C. K. CHOI, C. H. MARGRAVES, AND K. D. KIHM. [Examination of near-wall hindered Brownian diffusion of nanoparticles: Experimental comparison to theories by Brenner \(1961\) and Goldman et al. \(1967\)](#). *Physics of Fluids*, **19**(10), 2007. [125](#)



# Resumé en Français

## Introduction

Beaucoup de processus importants tels que les infections microbiennes, la distribution de médicaments par voie interne et la toxicité des nanomatériaux dépendent de l'interaction entre des systèmes actifs et les membranes biologiques. L'étude de la matière active est une nouvelle discipline dans laquelle la physique de la matière molle est en lien avec l'étude des particules qui peuvent utiliser de l'énergie de leur environnement pour générer un mouvement systématique et autonome [4]. Beaucoup de systèmes biologiques et vivants dont les bactéries, les oiseaux ou les humains, constituent un bon exemple de ces systèmes actifs. En s'inspirant des systèmes biologiques, divers nageurs artificiels ont été synthétisés, produisant des exemples de "nanomoteurs" [2] et micronageurs [3], qui par extension à différentes échelles sont capables d'imiter les fonctionnalités des systèmes vivants actifs.

Les mécanismes d'interaction entre les colloïdes actifs et les membranes biologiques sont encore loin d'être parfaitement compris comme le prouve la récente pandémie de Covid-19. Pour étudier des membrane biologique, il serait très intéressant de concevoir une cellule vivante vides en son intérieur [12], résultant en une capsule de lipides qui pourrait mener à une meilleure compréhension de la biophysique. Même s'il n'est pas encore possible de concevoir une cellule biologique "vide", les vésicules de lipides géantes qui sont d'un ordre de taille typique allant de 10 à 100  $\mu\text{m}$  suivent le paradigme biologique d'une cellule vivante. Elles peuvent être synthétisés et utilisés pour arriver à une compréhension plus avancée des comportements des cellules biologiques en interaction avec des particules actives.

Dans cette étude nous essayons de mettre en lumière l'interaction entre des colloïdes de Janus "Janus colloids", au niveau d'une particule seule, avec des vésicules de

## Resumé en Français

---

lipides géantes ou vésicules unilamellaires géantes, en anglais "GUVs". Les colloïdes de Janus sont une classe émergente de systèmes de matière molle qui présentent deux faces distinctes avec deux propriétés de surface différentes, leur permettant de réaliser une propulsion autonome sans aucune intervention extérieure. Dans notre système, les colloïdes sont partiellement recouverts de platine, ce qui permet une propulsion catalytique en présence de  $H_2O_2$ . Les GUVs et les colloïdes de Janus peuvent être observés en microscopie optique, mais la microscopie électronique à balayage (MEB) a également été utilisée pour obtenir une vue plus détaillée des colloïdes de Janus. La fabrication des colloïdes de Janus et la préparation des GUVs sont brièvement abordées dans la section ci-dessous, suivi de certains résultats majeurs présentés dans les sections suivantes.

## Matériaux et méthodes

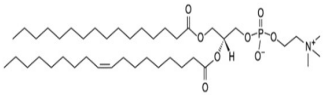
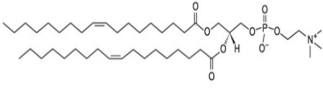
Nous avons utilisé deux tailles différentes de colloïdes sphériques une de silice ( $SiO_2$ -R) d'un rayon de  $R_P \approx 2 \mu m$  et une de résine de mélamine fluorescente (MF-FluoOrange) d'un rayon de  $R_P \approx 1 \mu m$ , avec des longueurs d'ondes d'excitation et d'émission de 560 nm et 584 nm respectivement. Les propriétés des colloïdes  $SiO_2$  et MF sont présentées dans le tableau ci-dessous.

Particule	Rayon Moyen $\mu m$	déviatiion standard	Densité $g/cm^3$	Indice de réfraction
$SiO_2$ -R	2.15	0.065	1.85	1.47
MF-R	1.245	0.05	1.51	1.68

**Table 1:** Propriétés physiques des colloïdes de  $SiO_2$  et de MF

Les principaux phospholipides utilisés dans cette étape de préparation des GUVs étaient le POPC (1-palmitoyl-2-oleoyl-sn-glycero-3-phosphocholine) et le DOPC (1,2-dioleoyl-sn-glycero-3-phosphocholine) acquis auprès de Avanti polar lipids-USA et ont été reçus sous forme sèche. Les propriétés des phospholipides sont présentées dans le tableau ci-dessous.



Lipid	Nom complet	Mw g/mol	Température de transition (°C)	Formule chimique
POPC (16:0-18:1)	1-palmitoyl-2-oleoyl-sn -glycero-3 -phosphocholine	760	-3.5	
DOPC(18:1)	1,2-dioleoyl-sn -glycero-3- phosphocholine	785.6	-17	

**Table 2:** Structure et propriétés des phospholipides POPC et POPC.

La microscopie en champ clair a été utilisée pour les observations et la microscopie de fluorescence pour caractériser la vésicule, les lipides étant marqués par fluorescence à l'aide du nitrobenzoxadiazole (NBD) (voir Figure 1).

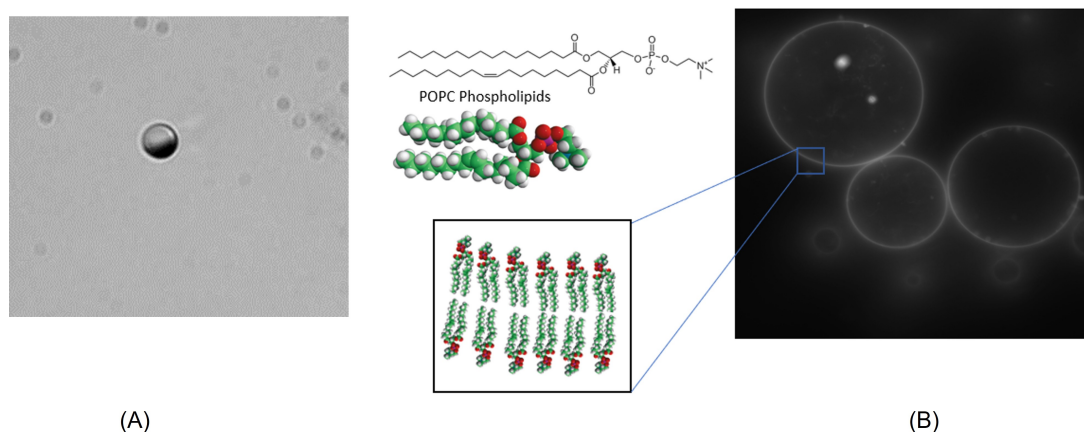


**Figure 1:** (a) Image de microscopie en champ clair de colloïde SiO<sub>2</sub>-Pt (b) Image de GUVs en microscopie de fluorescence (à gauche- illustration lipidique individuelle de POPC.)

### Fabrication de colloïdes de Janus et préparation de GUVs

Pour fabriquer les colloïdes de Janus, nous créons une monocouche de colloïdes sphériques (SiO<sub>2</sub> et MF) qui sont ensuite recouverts d'une fine couche de platine à l'aide d'un dispositif de pulvérisation métallique [86]. Cela donne un hémisphère de platine sur les colloïdes d'une épaisseur d'environ  $6 \pm 1$  nm . La Figure 2 montre le schéma de la préparation de colloïde Janus.

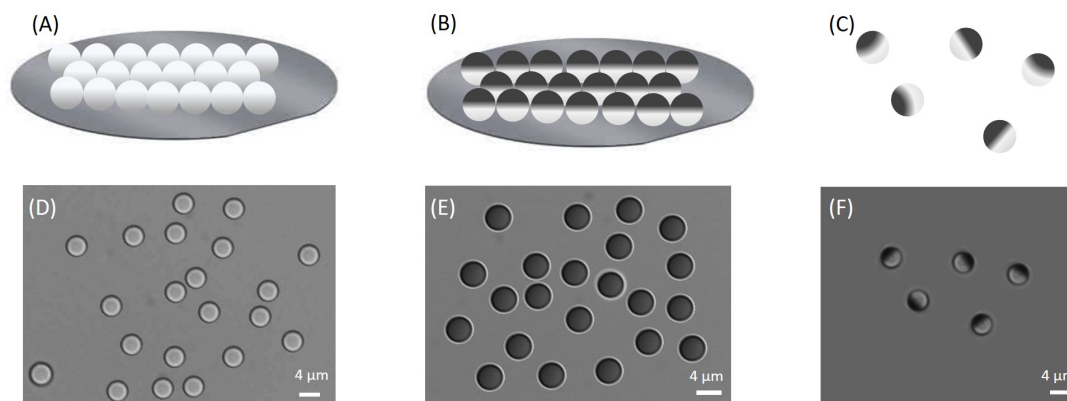


**Figure 2:** Rangée supérieure : Schéma montrant la fabrication des colloïdes de Janus  $\text{SiO}_2\text{-Pt}$ . (A)(B) Monocouche de colloïdes de  $\text{SiO}_2$  sur une tranche de silicium avant et après le dépôt de platine. (C) Colloïdes en solution, avec frontière de Janus perpendiculaire au substrat. Rangée inférieure : images de microscopie en champ clair pour les colloïdes dans une solution (D) Colloïdes nus (E) après dépôt de platine (F) Particules de  $\text{SiO}_2\text{-Pt}$  dans une solution après avoir été détachées du substrat.

Pour la préparation des GUVs, les lipides secs sont d'abord étalés sur un gel PVA qui est ensuite hydraté à l'aide d'une solution de saccharose à 150 millimolaire, puis laissé gonfler pendant 3 heures. Ensuite, les vésicules sont extraites et sédimentées dans un tube de centrifugation avec 1 mL de solution de glucose de concentration 150 millimoles [92]. La Figure 3 montre le schéma du gonflement et du détachement de la GUV de la bicouche lipidique.

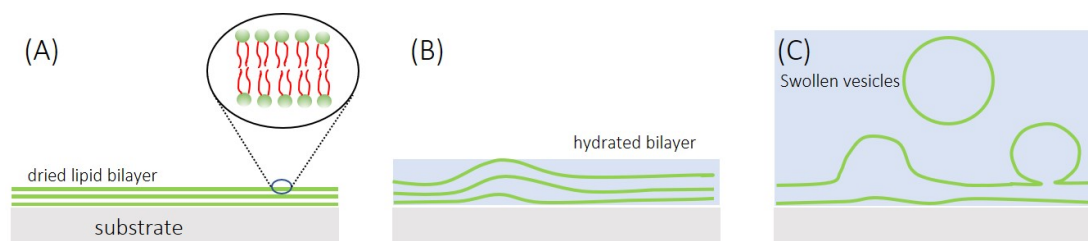


**Figure 3:** Schéma illustrant les étapes du gonflement d'une bicouche lipidique (A) Bicouches lipidiques séchées sur un substrat, (B) Début de l'hydratation et de l'auto-assemblage des vésicules, (C) Vésicules gonflées se détachant de la bicouche.

Le mouvement actif des particules est obtenu en utilisant une solution à 2% de peroxyde d'hydrogène ( $\text{H}_2\text{O}_2$ ). Nous utilisons le logiciel open source *Blender* pour suivre

le centre de masse (COM) du colloïde en microscopie en champ clair afin d'extraire le mouvement de translation des colloïdes. Les colloïdes fluorescents peuvent également être utilisés et sont plus efficaces pour obtenir des informations de rotation.

## Résultats

Comme les colloïdes en suspension dans un liquide possèdent un mouvement brownien aléatoire à la fois en translation et en rotation, il était intéressant de voir l'effet de l'interface solide-liquide sur la diffusion brownienne du colloïde lorsque celui-ci se trouve sur le fond près du substrat. Pour le colloïde MF-Pt ( $R_P \approx 1 \mu\text{m}$ ) on a constaté que la diffusion en rotation ( $D_{R,\perp}$ ) et en translation ( $D_{Tr,\parallel}$ ) était ralentie par rapport aux valeurs en volume. Les coefficients de diffusion expérimentaux peuvent être comparés aux prédictions théoriques de la diffusion en présence d'une interface solide, comme le montre la Figure 4 [99, 141]. Les coefficients de diffusion par rotation et translation parallèle près d'une interface solide-liquide peuvent s'écrire comme suit [62, 99, 110];  $D_{R,\perp} = \frac{k_B T}{k_{(R,\perp)} \eta R_P^3}$ ;  $D_{Tr,\parallel} = \frac{k_B T}{k_{(Tr,\parallel)} \eta R_P}$ , où  $k_{(R,\perp)}$  et  $k_{(Tr,\parallel)}$  sont des fonctions de distance d'espacement ( $h/R_P$ ). Selon Faxen,  $k_{(R,\perp)}$  varie de  $12\pi$  à  $\frac{h}{R_P} = 0,1$  près de l'interface à  $8\pi$  dans le volume. De même,  $k_{(Tr,\parallel)}$  varie de  $14\pi$  à  $\frac{h}{R_P} = 0,1$  et s'approche de  $6\pi$  pour les grandes distances d'espacement. Ainsi,  $D_{R,\perp}$ ,  $D_{Tr,\parallel}$  sont les plus lents pour les plus gros colloïdes les plus proches de l'interface et les plus rapides pour les plus petits colloïdes les plus éloignés de l'interface. Pour un colloïde de Janus (MF-Pt) isolé dans des conditions passives, la distance d'espacement  $h$  entre le colloïde de Janus et la paroi de la lamme de verre en équilibre thermique a été évaluée entre 300 nm et  $1,5 \mu\text{m}$ , ce qui reflète les propriétés de surface hétérogènes des colloïdes de Janus. La diffusion rotationnelle dans le plan  $D_{R,\parallel}$  a été mesurée à la fois dans des conditions passives et actives et est très similaire à la valeur théorique dans le volume  $D_{R,b}$  et en accord avec la prédiction hydrodynamique.

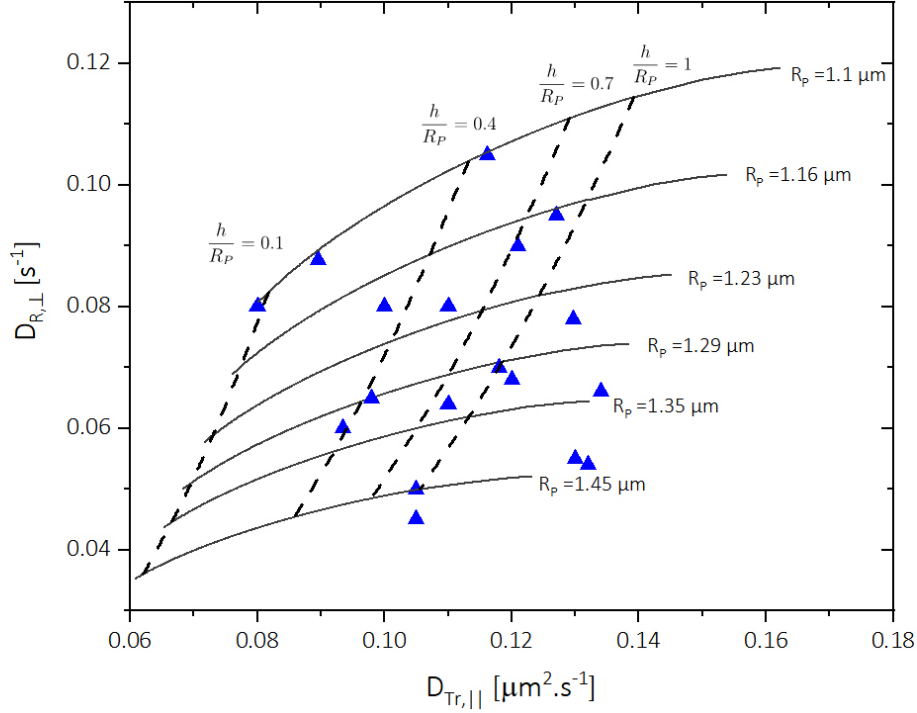


**Figure 4:** Coefficient de diffusion rotationnelle ( $D_{R,\perp}$ ) en fonction du coefficient de diffusion translationnelle ( $D_{Tr,\parallel}$ ). Comparaison entre les résultats expérimentaux et la prédiction théorique pour les colloïdes MF-Pt proches d'une paroi unique. Les lignes pleines montrent les prédictions théoriques pour les coefficients de diffusion à différents  $R_P$ , tandis que les lignes en pointillées représentent les prédictions pour la distance normalisée de l'espace ( $\frac{h}{R_P}$ ).

En ce qui concerne le mouvement actif des colloïdes, la particule et la vésicule sont observées ensemble dans une dispersion préparée par simple sédimentation. Lorsque les particules se déplacent activement et se trouvent près d'une vésicule, il a été observé que les particules sont piégées dans un mouvement orbital persistant, ce qui était vrai pour les deux particules (SiO<sub>2</sub>-Pt and MF-Pt). La Figure 5 montre le mouvement du colloïde Janus d'une vésicule à l'autre ainsi que le tracé d'autocorrélation de la vitesse [94]. On a également observé que la vitesse des colloïdes actifs reste la même dans le mouvement orbital. Cependant, il a été découvert que la particule peut transférer une certaine force ou un certain couple sur la vésicule sans déformer la vésicule. Pour un colloïde actif possédant à la fois une vitesse active ( $V$ ) et une vitesse angulaire ( $\omega$ ), la

décroissance de la fonction d'autocorrélation de la vitesse  $\langle \bar{v}(t + \Delta t) \cdot \bar{v}(t) \rangle$  pendant le mouvement libre en raison de la diffusion rotationnelle dans le plan ( $D_{R,\parallel}$ ) pourrait être ajustée par l'équation suivante :

$$\langle \bar{v}(t + \Delta t) \cdot \bar{v}(t) \rangle = V^2 \cos(\omega \Delta t) f_r + V_d^2 \quad (1)$$

où  $V_d$  est la vitesse de dérive. Une vitesse angulaire nulle (sans mouvement orbital) fournit  $f_r = \exp(-D_R \Delta t)$  et conduit à la diffusion rotationnelle dans le mouvement "libre". Cependant, le mouvement orbital de la particule autour d'une GUV n'est en général pas décrit par l'équation (1) car les interactions de la particule avec la vésicule introduisent un certain nombre d'autres sources de force. Il est facile de montrer que pour un mouvement orbital parfaitement circulaire à fréquence orbitale constante  $\omega$ , la fonction d'autocorrélation aurait la forme de l'équation (1) avec  $f_r = 1$ , fournissant ainsi une manière pratique d'extraire directement les vitesses orbitales à partir des seules données de trajectoire des particules.

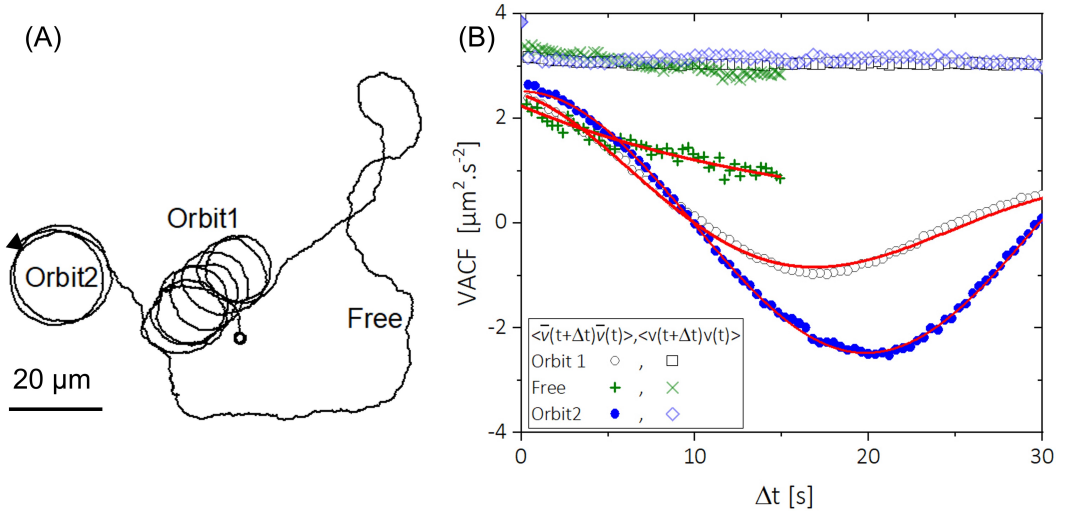


**Figure 5:** (A) Trajectoire d'un colloïde actif  $R_P \approx 2 \mu\text{m}$  en orbite autour de deux GUV et effectuant un mouvement "libre" entre les deux. (B) Fonctions d'autocorrélation de la vitesse en fonction du temps de latence  $\Delta t$  pour la trajectoire représentée en (A).

Au lieu d'un simple mélange, l'interaction entre les particules et les vésicules peut également être guidée par une force, et cette force peut être appliquée en utilisant soit la centrifugation, soit des pinces optiques. En utilisant des pinces optiques, les expériences ont été limitées aux colloïdes nus, car le décalage des propriétés diélectriques d'un

## Resumé en Français

---

système Janus rend impossible le piégeage optique de colloïdes de Janus partiellement platinés. L'engloutissement complet de  $\text{SiO}_2$  ( $R_P \approx 2 \mu\text{m}$ ) a été observé comme le montre la Figure 6. Les colloïdes MF ( $R_P \approx 1 \mu\text{m}$ ) au contraire n'ont montré aucune affinité avec la membrane, ce qui laisse supposer une sélectivité de l'enveloppement de la membrane en fonction des propriétés de surface d'une particule. En termes de propriétés des vésicules, l'engloutissement a été limité aux GUVs présentant des fluctuations continues dans le contour de la membrane, appelées vésicules "souples" et possédant une tension de membrane  $\sigma < 10^{-8} \text{ N.m}^{-1}$ . Dans le cas des vésicules souples, la résistance à la flexion joue un rôle majeur dans l'engloutissement, tandis que dans le cas des vésicules tendues ( $\sigma > 10^{-8} \text{ N.m}^{-1}$ ), l'énergie  $E_{tension}$  doit également être prise en compte.

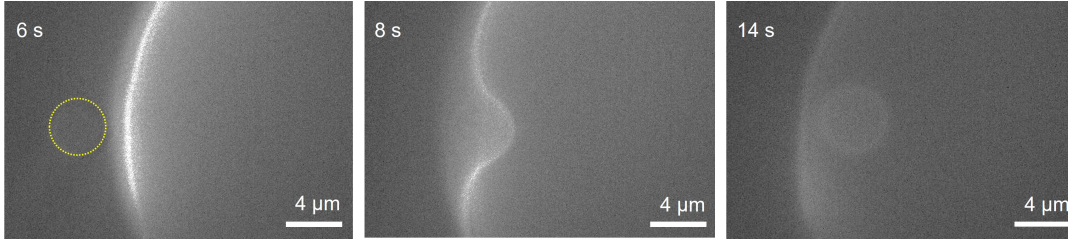


**Figure 6:** (de gauche à droite) Régimes de contact de  $\text{SiO}_2$  ( $R_P \approx 2 \mu\text{m}$ ) représentés en jaune pointillé s'approchant d'une GUV souple, déforme la vésicule avec la force fournie par la pince optique, puis est entièrement englouti par la vésicule.

L'engloutissement actif des colloïdes de Janus a été réalisé par centrifugation. Il est à noter que cette méthode n'a permis d'observer qu'un engloutissement partiel pour les deux tailles de colloïdes. Pour les colloïdes  $\text{SiO}_2\text{-Pt}$  ( $R_P \approx 2 \mu\text{m}$ ), très peu de cas d'engloutissement ont été observés, limités à des forces de niveau modéré (jusqu'à  $10^{-10} \text{ N}$ ). Pour une force supérieure à  $10^{-10} \text{ N}$ , les particules colloïdales ont détruit les vésicules. L'engloutissement partiel pour les colloïdes MF-Pt était significativement plus élevé pour la même gamme de forces de centrifugation ( $10^{-9}$  à  $10^{-11} \text{ N}$ ). Cependant, comme pour les colloïdes  $\text{SiO}_2\text{-Pt}$ , une centrifugation plus importante a entraîné la rupture des membranes. Pour les colloïdes MF-Pt partiellement engloutis, on a observé un ralentissement de la diffusion rotationnelle (perpendiculaire à la surface) et translationnelle (parallèle à la surface).

Dans la figure 7, nous traçons le coefficient de diffusion rotationnelle hors du plan ( $D_{R,\perp}$ ) en fonction de la diffusion translationnelle parallèle ( $D_{Tr,\parallel}$ ) pour les colloïdes en régime libre et partiellement englouti. A l'exception de quelques points, les données pour

les colloïdes partiellement engoutis s'éloignent des prédictions théoriques à proximité d'une paroi solide unique. La zone grise englobant les points expérimentaux qui se situent en dessous de la résolution de notre analyse ( $D_{R,\perp} \approx 0.012 \text{ s}^{-1}$ ) ne peuvent être résolus.

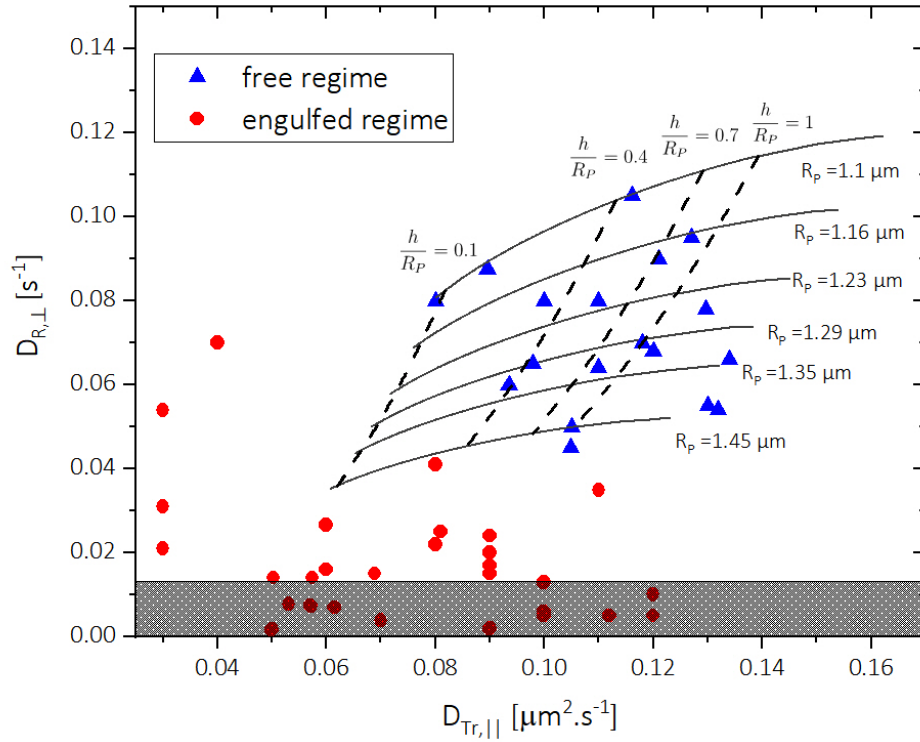


**Figure 7:**  $D_{R,\perp}$  en fonction de  $D_{T,\parallel}$  pour les colloïdes MF-Pt en régime libre et engouti. La zone grise représente la limite de la mesure de  $D_{R,\perp}$ .

À notre connaissance, aucun modèle n'existe dans la littérature pour décrire la variation du coefficient la traînée rotationnelle ( $\zeta_R$ ) subie par un colloïde qui est partiellement engouti par une membrane. Le modèle le plus proche d'une telle géométrie discuté dans la littérature est celui de Landau et Lifshitz qui considère le mouvement lent dans le fluide contenu dans l'espace entre deux sphères concentriques. En considérant la GUV comme une sphère extérieure (rotation nulle) et le colloïde engouti comme une sphère intérieure, la résistance à la rotation  $\zeta_{R,S}$  ressentie par la particule sphérique intérieure

dans une telle géométrie confinée peut s'écrire comme suit :

$$\zeta_{R,S} = \frac{8\pi\eta R_p^3}{1 - (R_P/R_{bud})^3} = \frac{\zeta_{R,b}}{1 - (R_P/R_{bud})^3}. \quad (2)$$

A partir de l'équation (2), nous avons trouvé que pour que  $D_{R,\perp}$  ralentisse d'un ordre de grandeur (évalué à partir des données expérimentales,  $D_{R,\perp}/D_{R,b} = 1/10$ ), la distance d'espacement entre la particule et la bicouche serait de  $d_g \approx 50$  nm, ce qui est comparable à la distance d'espacement mesurée entre une GUV et un substrat solide [129, 130] mais nettement moins grande que l'espacement de l'eau entre un substrat et une bicouche supportée ( $d_g \approx 1$  nm) [131]. D'autres modèles existant dans la littérature ne considèrent que le ralentissement de  $D_{Tr,\parallel}$  mais ne correspondent toujours pas à la géométrie complexe en régime englobé près d'une frontière solide. Thomas Fischer et al. ont décrit la viscosité de cisaillement de surface ( $\eta_s$ ) d'une membrane où la membrane forme un trou pour accueillir le colloïde. La résistance à la translation d'un colloïde immergé jusqu'à son plan équatorial dans une membrane peut s'écrire comme suit :

$$\zeta_{Tr,\parallel,Fischer} = 23.56\eta R_P + 7.5\eta_s. \quad (3)$$

En considérant la valeur moyenne de la diffusion translationnelle expérimentale  $\bar{D}_{Tr,\parallel,free} = 0.12 \pm 0,01 \mu\text{m}\cdot\text{s}^{-1}$  pour le colloïde de Janus en régime libre et  $\bar{D}_{Tr,\parallel,eng} = 0.07 \pm 0.02 \mu\text{m}\cdot\text{s}^{-1}$  en régime englobé, nous estimons une augmentation du coefficient de traînée en translation d'un facteur  $\approx 2$ , ce qui donne une viscosité de surface de  $\eta_s = 4 \times 10^{-9}$  Pa.s.m. La viscosité tridimensionnelle de la membrane peut être calculée comme  $\eta_s/h_m = 1$  Pa.s ( $h_m = 4$  nm étant l'épaisseur de la membrane).

Danov et al. [82] ont considéré un modèle similaire pour le coefficient de traînée subie par une particule se déplaçant parallèlement à une membrane sphérique. Nos expériences montrant  $R_{GUV}/R_P = 3-10$  correspondent à  $\frac{\eta_s}{R_P\eta} = 2 - 30$  dans le modèle. Par conséquent, une viscosité de cisaillement de surface  $\eta_s \approx 2.5-38.7 \cdot 10^{-9}$  Pa.s.m peut être évaluée, et est similaire à celle obtenue en utilisant le modèle de Fischer et al. [99] et d'autres résultats expérimentaux [135].

L'introduction d'une activité dans les colloïdes de Janus en régime d'englobement a donné lieu à de très rares observations de transport actif de GUV. Ces cas rares ont été observés pour les deux tailles de particules où une particule poussait ou tirait activement une GUV. Un exemple de transport membranaire est montré dans la figure 8 où la



vitesse active mesurée est  $V = 1.6 \mu\text{m.s}^{-1}$  et dont la trajectoire est comparable à un colloïde actif en régime libre. En général, à l'exception de quelques rares événements, l'activité d'un colloïde partiellement englouti s'est avérée être sévèrement atténuée, et n'a pas montré de mouvement actif persistant ( $V = 0$ ). L'extinction du mouvement actif dans le régime englouti pourrait être associée aux effets qui se produisent lors de l'engloutissement. Prédit par Agudo-Canalejo et Lipowsky, l'engloutissement partiel d'un colloïde conduit à une variation du paysage énergétique d'une GUV. Pour une GUV asymétrique, un gradient de la courbure de la membrane existe avant l'engloutissement de la particule, en raison de la géométrie plate (courbure nulle, vérifiée avec RICM) d'une GUV souple ( $\sigma < 10^{-8} \text{ N.m}^{-1}$ ). Ainsi, la région de courbure nulle de la membrane de la GUV est capable de tirer le colloïde de sa position initiale vers le bas de la GUV. La migration du colloïde vers le bas donne une orientation de la particule où la face MF du colloïde est orientée vers le bas et ne peut pas donner lieu à une auto-propulsion dans les directions X et Y. La migration colloïdale rapide due à la courbure de la membrane GUV est un facteur important de la migration. La migration colloïdale rapide due aux forces induites par la courbure a été déduite en utilisant des pinces optiques où un colloïde englouti a été repoussé avec le piège optique pour atteindre le bas de la GUV depuis la région équatoriale en moins de 0,8 s, alors qu'avec la gravité seule il faudrait plus de 3-4 s.

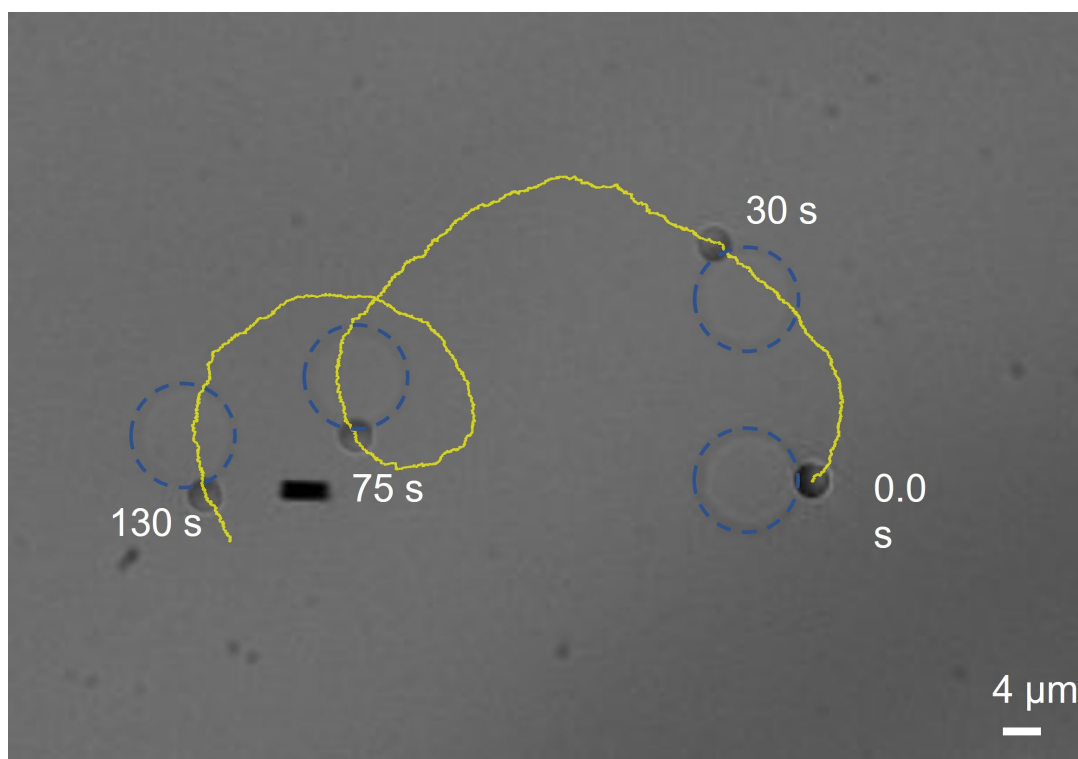


**Figure 8:** Colloïde de Janus  $\text{SiO}_2\text{-Pt}$  transportant activement une GUV de POPC. La trajectoire du colloïde est en jaune et la GUV est mis en évidence en bleu (pointillé). Notez que les images de la particule et de la GUV à 30, 75 et 130 s sont superposées à des fins de visualisation.

Pour des recherches futures, certaines stratégies peuvent être mises en œuvre pour limiter l'effet des forces de gradient induites par la courbure, comme l'introduction de colloïdes de Janus avec une surface de revêtement Pt plus faible, ainsi que la réduction du décalage de densité à l'intérieur et à l'extérieur de la vésicule pour éviter une courbure plate près du substrat.

## Conclusion

Dans cette étude, la dynamique d'interaction du colloïde de Janus avec la GUV a été étudiée de manière approfondie dans des conditions actives et passives. Pour un colloïde de Janus isolé dans des conditions passives, la distance d'espacement  $h$  a été évaluée entre 300 nm et 1.5  $\mu\text{m}$ . La  $D_{R,\parallel}$  mesurée dans des conditions actives et passives s'est avérée être très similaire à la valeur en volume et en accord avec les prédictions

théoriques précédentes. Cependant,  $D_{R,\perp}$  en conditions passives est significativement ralentie. La vitesse active la plus élevée mesurée pour les deux tailles de colloïdes (à 2%  $\text{H}_2\text{O}_2$ ) a été évaluée à  $4.5 - 5 \mu\text{m}\cdot\text{s}^{-1}$ . Pendant l'interaction spontanée d'un colloïde de Janus actif avec une GUV, un mouvement orbital indépendant de la taille des particules et de la GUV a été observé. On a également constaté que les colloïdes exerçaient une force et un couple sur une GUV de l'ordre du fN. En utilisant une force externe de centrifugation ou une pince optique, l'engloutissement colloïdal par une GUV peut être réalisé. On a constaté que l'engloutissement des colloïdes de Janus est influencé par les propriétés de surface du colloïde, le platine et la silice présentant une adhérence aux GUV. Dans le cas des colloïdes de Janus MF-Pt, un ralentissement important de  $D_{R,\perp}$  a été observé dans le cas de engloutissement. L'activité du colloïde Janus à l'état partiellement englouti s'est avérée être sévèrement ralentie avec quelques rares exceptions pour le transport de la GUV.



# List of Symbols

- $V$  : Active velocity
- $\Delta t$  : Lag time
- $T$  : Temperature
- $k_B$  : Boltzman constant
- $R_P$  : Particle radius
- $R_{GUV}$  : Vesicle radius
- $\sigma$  : Membrane tension
- $\kappa_b$  : Bending modulus
- $m$  : Spontaneous curvature
- $D_R$  : Rotational diffusion
- $D_{Tr}$  : Translational diffusion
- $\zeta_R$  : Rotational drag
- $\zeta_{Tr}$  : Traslational drag
- $h$  : Gap distance
- $\eta$  : Viscosity
- $\varphi$  : In-plane rotation angle
- $\beta$  : Out-of-plane rotation angle
- $\tau_R$  : Rotational diffusion time
- $\omega$  : Angular velocity
- $\Gamma$  : Effective elastic coefficient
- $R_O$  : Orbital radius
- $E_{adhesion}$  : Adhesion energy
- $E_{bending}$  : Bending energy
- $E_{adhesion}$  : Energy cost to pull excess membrane
- $A_{contact}$  : Contact area
- $z_p$  : Degree of penetration
- $F_c$  : Centrifugation force
- $\eta_s$  : Membrane surface viscosity
- $\sigma_{MF,m}$  : MF-membrane interfacial tension
- $\sigma_{aq,m}$  : Aqueous-membrane interfacial tension
- $\sigma_{Pt,m}$  : Platinum-membrane interfacial tension

## List of Symbols

---

- $\sigma_{MF,aq}$  : MF-Aqueous interfacial tension
- $\sigma_{t,aq}$  : Platinum-Aqueous interfacial tension

# Appendix

### A.1 Export Center of Mass coordinates from Blender

```
import bpy
import os

D = bpy.data

if not os.path.exists(bpy.path.abspath('//') + 'data'):
    os.makedirs(bpy.path.abspath('//') + 'data')

for clip in D.movieclips:
    for track in clip.tracking.tracks:
        name = '\\tr_{0}_{1}.csv'.format(clip.name.split('.')[0], track.
            ↪ name)
        fn=bpy.path.abspath('//')+ 'data\\' + name
        with open(fn, 'w') as f:
            f.write('Frame,x,y\n')
            for marker in track.markers:
                coords = marker.co.xy
                frameno = marker.frame
                f.write('{0},{1},{2}\n'.format(frameno, coords[0]*clip.
                    ↪ size[0],
                    coords[1]*clip.size[1]))
```



## A.2 ImageJ routine for Rotation tracking

```
function action(input, output, filename) {
    open(input + filename);
    run("Duplicate...", "duplicate");
        setMinAndMax(1, 2);
        run("Apply LUT", "stack");
        setThreshold(2, 255);
        setOption("BlackBackground", true);
        run("Convert to Mask", "method=Default background=Dark
            ↪ black");
    saveAs("AVI", output + filename);
    close();
    for (i = 0; i < nSlices; i++) {
        run("Create Selection");
        run("Fit Ellipse");
        //setTool("dropper");
        setForegroundColor(0, 0, 0);
        setForegroundColor(0, 0, 0);
        run("Fill", "slice");
        run("Measure");
        run("Next Slice [>]");}

    selectWindow("Results");
    saveAs("Results", path + name + "result.csv");
    run("Clear Results");
    close("*");
}

input = getDirectory("input Directory");
output = getDirectory("output directory");
list = getFileList(input);
for (i = 0; i < list.length; i++)
    action(input, output, list[i]);
```

### A.3 Tracking GUV size and center of mass

```
#!/usr/bin/env python3

#import the necessary packages
import numpy as np
import argparse
import cv2
import os
import sys

file_name = [f for f in os.listdir('.') if f.endswith('.tif')]
print(file_name )

radi = np.ndarray()
coordinates = np.array(coordinates)

for fn in file_name :
    # load the image, clone it for output, and then convert it to
    ↪ grayscale
    image = cv2.imread(fn)
    output = image.copy()
    gray = cv2.cvtColor(image, cv2.COLOR_BGR2GRAY)
    # detect circles in the image
    circles = cv2.HoughCircles(gray,cv2.HOUGH_GRADIENT,1.5,100,param1
        ↪ =22,param2=28,minRadius=5,maxRadius=100)

    # ensure at least some circles were found
    if circles is not None:
        # convert the (x, y) coordinates and radius of the circles
        ↪ to integers
        circles = np.round(circles[0, :]).astype("int")
        radi = np.append(radi,circles[:,0:2])

    # loop over the (x, y) coordinates and radius of the
```

---

```
↪ circles
for (x, y, r) in circles:
    # draw the circle in the output image, then draw a
    ↪ rectangle
    # corresponding to the center of the circle
    cv2.circle(output, (x, y), r, (0, 255, 0), 4)
    cv2.rectangle(output, (x - 5, y - 5), (x + 5, y +
    ↪ 5), (0, 128, 255), -1)

# show the output image
cv2.imshow("output", np.hstack([image, output]))
cv2.waitKey(0)
coordinates.append(coordinates)

np.savetxt("measurements.csv", radi)
coordinates = pd.DataFrame(coordinates)
coordinates.to_csv("coordinates.csv", coordinates)
```

## A.4 Orbital motion around vesicle

Figure A4 shows the orbital time as a function of the orbital radius ( $R_O$ ) for all experiments where we could detect both the approach and escape time of an active particle interacting with an isolated vesicle. As already discussed in the main text, no critical orbital radius or vesicle radius was observed. Data shown in Figure A4 roughly follows the same statistics of the  $GUV$  size distribution as is shown in Figure 4.3

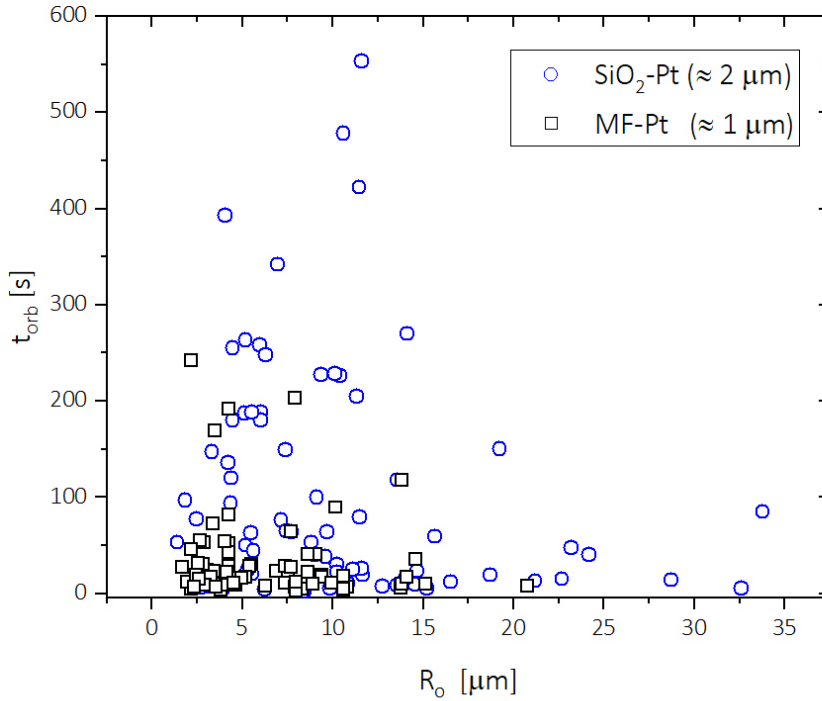


**Figure A4:** Orbital time versus orbital radius for  $R_P \approx 1$  and  $2 \mu m$  active colloids.

## A.5 RICM images of GUVs

Figure A5 shows the RICM + brightfield microscopy image of a tense POPC vesicle sedimented on the substrate. The footprint of the vesicle touching the substrate which is very small compared to the vesicle size. On the other hand, the footprint for a less tense (floppy vesicle) is comparable to its size as shown in the main text (see Figure 6.4).

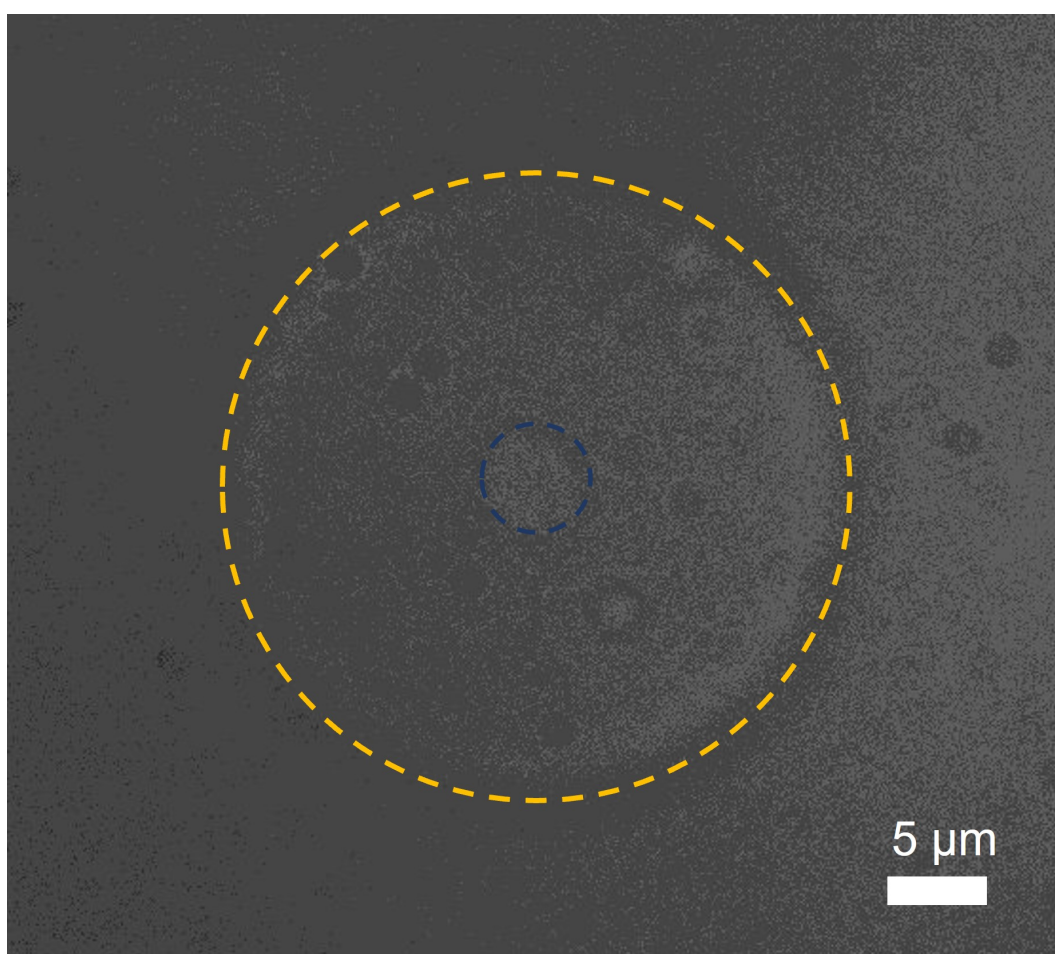


**Figure A5:** RICM image of a POPC vesicle where the dashed yellow is the equator of the vesicle while the dashed blue line shows the area in contact with the substrate.

**Dynamique des colloïdes de Janus interagissant avec des vésicules lipidiques géantes**

## Résumé

L'interaction d'une entité artificielle ou biologique autopropulsée avec la membrane cellulaire joue un rôle crucial dans la gestion de divers processus importants tels que les infections microbiennes, l'administration de médicaments et la toxicité des nanomatériaux. Dans cette thèse, le comportement des colloïdes artificiels autopropulsés de Janus dans et hors des conditions d'équilibre thermique lors de la rencontre avec une Vésicule Unilamellaire Géante a été étudié. De même, la dynamique d'interaction des colloïdes de Janus a été observée en utilisant des conditions d'interactions spontanées et forcées. Des centrifugations et des méthodes de pinces optiques ont été utilisées pour obtenir un englobement activé, ce qui a permis de mieux comprendre les facteurs qui régissent l'englobement d'un colloïde sphérique par une GUV.

La diffusion de la rotation et de la translation pour un colloïde brownien de Janus près d'une surface solide unique ainsi que dans l'interaction spontanée avec un GUV a été étudiée et les résultats se sont avérés en accord avec les prédictions théoriques. Un mouvement orbital a été observé lorsqu'un colloïde de Janus actif rencontre un GUV sur son chemin. L'englobement activé de colloïdes de Janus sphériques ou nus, déclenché par une force externe, a montré un effet de confinement important et un ralentissement significatif de la diffusion rotationnelle et translationnelle des colloïdes. L'activité d'un colloïde de Janus est également sévèrement entravée dans des conditions d'englobement.

Mots clés : *Colloïdes de Janus, phospholipide, GUV, Pince optique, auto-propulsion, englobement.*

## Résumé en anglais

Interaction of a self-propelling artificial or biological entity, with cell membrane plays a crucial role in governing various important processes like microbial infections, drug delivery, and nanomaterial toxicity. In this thesis, the behaviour of self-propelling artificial Janus colloids in- and out-of thermal equilibrium conditions on encountering a Giant Unilamellar Vesicle was investigated. Also, the interaction dynamics for Janus colloids in active and passive conditions were observed by utilizing spontaneous and force driven interactions conditions. Centrifugations and Optical tweezer methods were employed to achieve activated engulfment which helped in gaining a deeper understanding on the factors that govern engulfment of a spherical colloid by GUV.

The rotation and translation diffusion for a Brownian Janus colloid near a single solid boundary as well as in spontaneous interaction with a GUV were investigated and the results were found in tune with the previous theoretical prediction. A striking orbital motion was observed when an active Janus colloid encountered a GUV in its path. Activated engulfment of spherical Janus/bare colloids, triggered by external force showed a severe confinement effect and significant slowing down in the rotational and translational diffusion of the colloids. The activity of a Janus colloid was also found to be severely hampered in engulfed conditions.

Keywords : *Janus colloids, phospholipid, GUV, Optical Tweezers, self-propulsion, engulfment*